

**KfK 4339
EUR 10539e
Dezember 1987**

**Nuclear Fusion Project
Semi-annual Report of the
Association KfK/EURATOM**

April - September 1987

Projekt Kernfusion

Kernforschungszentrum Karlsruhe

KERNFORSCHUNGSZENTRUM KARLSRUHE

Projekt Kernfusion

KfK 4339
EUR 10539e

Nuclear Fusion Project

Semi-annual Report
of the Association KfK/EURATOM

April 1987 - September 1987

compiled by
G. Kast

Kernforschungszentrum Karlsruhe GmbH, Karlsruhe

Als Manuskript vervielfältigt
Für diesen Bericht behalten wir uns alle Rechte vor

Kernforschungszentrum Karlsruhe GmbH
Postfach 3640, 7500 Karlsruhe 1

ISSN 0303-4003

Contents

	page
Report on Technology Tasks	
B1	Blanket Design Studies 1
B 2	Development of Computational Tools for Neutronics 5
B6	Corrosion of Structural Materials in Flowing Pb-17Li 7
B 6.3	Fatigue of Structural Material in Pb-17Li 7
B9	Tritium Extraction from Liquid Pb-17Li by the Use of Solid Getters 8
B 11-16	Development of Ceramic Breeder Materials 10
M1	The Large Coil Task 16
M 3	Development of High Field Composite Conductors 19
M 4	Superconducting Poloidal Field Coil Development 21
M 8	Design and Construction of a Poloidal Field Coil for TORE Supra as NET-Prototype Coil 23
M 9	Structural Materials Fatigue Characterization at 4 K 24
M 12	Low Electrical Conductivity Structures Development 25
MAT 1.6	Development and Qualification of Type 1.4914 Base metal Properties 26
MAT 1.9	Pre- and Post-Irradiation Fatigue Properties of 1.4914 Martensitic Steel 27
MAT 1.11	Post-Irradiation Fracture Toughness of Type 1.4914 Martensitic Steel 30
MAT 2.2	In-Pile Creep-Fatigue Testing of Type 316 and 1.4914 Steels 31
MAT 6/ MAT 13	Ceramics for First-Wall Protection and for RF Windows 32
Mat 9.2	Investigation of Fatigue Under Dual Beam Irradiation 34
MAT 18	Development of Low Activation Ferritic-Martensitic Steels 36
N1	Design Study of Plasma Facing Components 37
N2	Shield Design Studies 38
N3	Development of Procedures and Tools for Structural Design Evaluation 39
N5	Development of Theory and Tools for Evaluation of Magnetic Field Effects on Liquid-Metal Breeder Blankets 40
N6	Studies of Pebble Beds of Ceramic Compounds 42
RM1	Background Studies on Remote Maintenance 43

RM2	Mechanical Components Assembly	45
RM 3	Handling Equipment for In-Vessel Components	46
S+ E 4.1.2	Safety Aspects of the Cryosystem	50
S+ E 4.1.3	Safety Aspects of Superconducting Magnets	52
S+ E 5.2.2	Behaviour of Gaseous Tritium in the System Plant/Soil	53
S+ E 5.4	Overall Plant Accident Scenarios for NET	54
S+ E 5.5	Development of Safety Guidelines for the Design of NET	55
T 6	Industrial Development of Large Components for Plasma Exhaust Pumping	56
T 10 A	Plasma Exhaust Purification by Means of Cryosorption on Molecular-Sieves or Alternative Adsorbents ...	58
T 10 C	Plasma Exhaust Gas Purification by Use of Hot-Metal Getters	59
T 10 E	Adsorption of DT on Heated Metal Beds other than Uranium	61
T 10 H	Catalyst Development Exhaust Purification Process	62
	Development of ECRH Power Sources at 150 GHz	63
	Report on NET Study Contracts	64
	Availability of the LCT Plant	64
	Study on the NET Pancake Test	64
	Investigation of the Vacuum and Exhaust Performance of NET	65
	Development of Helium Cryopumping Materials and Preliminary Design Concept of Cryocompound Pumps for NET	65
	Engineering Problems of NET Blanket Testing and Blanket Insertion Strategy	66
	Evaluation of Crack Growth Delay in Multilayer Sheets	68
	Design Study of Plasma Facing Components	68
	CAD Data Exchange between NET and KfK	69
Appendix I:	Table of Fusion Technology Contracts	70
Appendix II:	Table of NET Study Contracts	72
Appendix III:	KfK Departments contributing to the Fusion Projekt	73
Appendix IV:	Fusion Project Management Staff (PKF-PL)	74

B1 Blanket Design Studies

Two design concepts are studied by KfK: a helium-cooled ceramic blanket and a blanket with Pb-17Li eutectic as breeder material and coolant. The study includes small scale experiments and collaboration with industry for special feasibility problems. The studies are coordinated with efforts of CEA and UKAEA in a common working group.

1. **Helium-Cooled Ceramic Breeder Blanket (includes N6 Pebble Bed Studies)**

More detailed investigations on critical design issues were made for this blanket concept.

To calculate the impact of electro-magnetic forces during disruptions the 3d code CARIDDI was implemented and improved at KfK and first calculations were performed. They indicate that the circumferential currents around a segment generate quite large forces and bending moments and that 2d calculations may be totally misleading. To avoid an electrical contact of toroidally bending segments insulating pads on the side walls are considered as an alternative to a fixing pin at the bottom part.

Calculations with the computer code ABAQUS showed that the stresses due to temperature differences between first wall (average temperature = 390°C) and the backplate (average temperature = 270°C) are relatively low (30 MPa von Mises). The primary stresses in the segment vessel due to blanket weight and a conservatively assumed maximum pressure inside the vessel of 0.1 MPa amount to 90 MPa (von Mises).

The impact of canister pressurisation as a consequence of a pressure tube rupture also was investigated by calculations and experiments [1]. Calculations show that for pressures up to 0.6 MPa the stresses in the canister walls remain in the elastic region. If one allows plastic deformation the canisters can even withstand the pressure of 6 MPa, which is the maximum pressure which could occur in the canister due to the failure of a cooling tube. Recent experiments confirm the calculations and show that the canisters fail at 9 MPa. Of course excessive pressurisation of the helium purge flow system and plastic deformation of the canisters during an accident should be avoided, thus a pressure limitation system, for instance a burst membrane acting at about 0.4-0.5 MPa, should be provided. However, the calculations and experiments show that even a complete pressurisation of the canisters at the maximum pressure of 6 MPa does not produce a catastrophic failure of the blanket.

Detailed neutronics and thermohydraulics analyses were performed for the modified blanket design as described in the last progress report (KfK 4276). Fig. 1 shows a radial-toroidal section of a canister edge with temperature values at certain

points. From the temperature distribution in the whole blanket the tritium inventory was estimated. The estimate

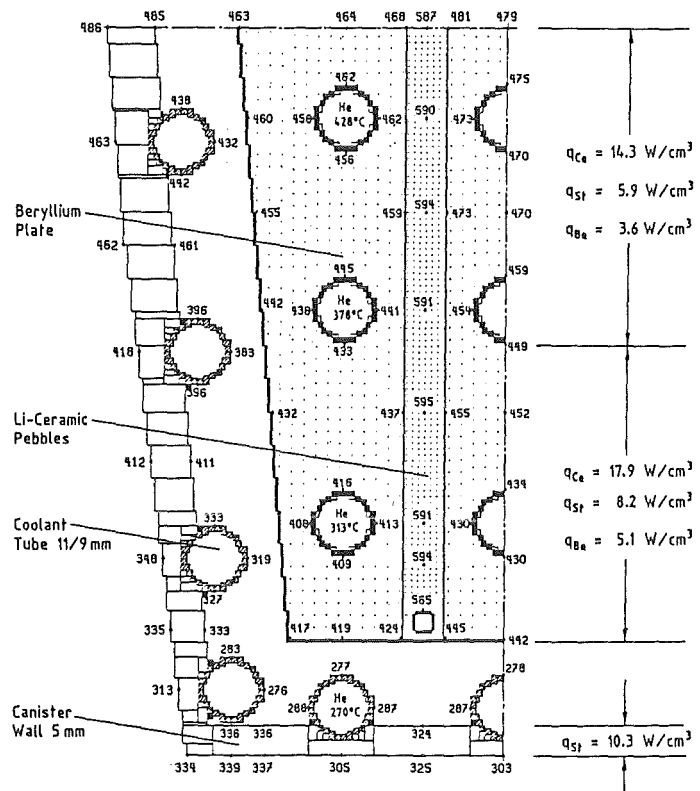


Fig. 1 Radial-toroidal section of the outboard canister edge showing the results of the temperature calculations for the highest-rated canister in the HEATING5 code geometry representation.

was based on the recent LISA2 results on the tritium residence time as a function of temperature. For a complete blanket of this kind a total tritium inventory of 250g was found.

As already mentioned in the last but one progress report the behaviour of the pebble bed under thermal cyclic load conditions was investigated by experiments.

Fig. 2 shows the test apparatus: a small steel container filled with pebbles. The filling operation is performed at 600°C and the bed is vibrated until the bed packing factor reaches the statistical value of 62-63%, which is the design value for the blanket. The container is closed by a plug, having care that it is completely filled by the pebbles. Afterwards the container is subjected to temperature cycles. During the immersion of the container in a water bath the temperature in the center of the bed is about 500°C higher than that of the steel container. This is a very severe test, as for the blanket operation the

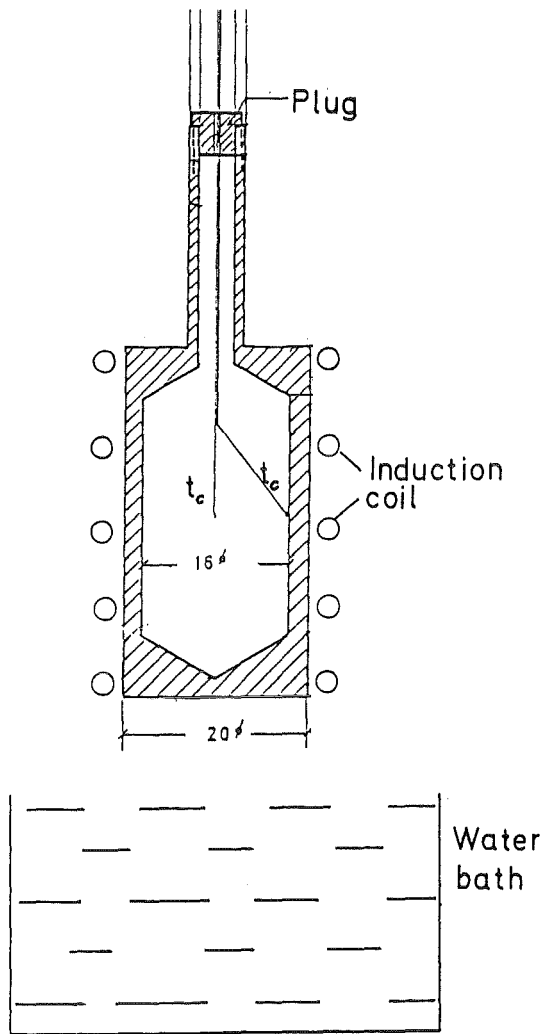


Fig. 2 Test apparatus for pebble thermal cycling tests (dimensions in mm)

maximum temperature difference between bed center and steel container for beryllium and pebble bed is about 170-180°C. After this test of the pebbles as received, about 11% of the pebbles were found to be broken. For pebbles which were annealed for two hours at 1000°C before the test only 2% were broken and the resulting pieces were rather large.

A comprehensive report on the KfK pebble bed canister blanket concept was written and is submitted for publication in Fusion Technology, special issue on NET /2/.

Staff:

- L. Boccaccini
- E. Bojarsky
- M. Dalle Donne
- U. Fischer
- R. Krieg
- M. Küchle
- H. Reiser
- S. Schneider
- G. Schumacher
- E. Wehner

2. Liquid Metal-Cooled Blanket

The development of a blanket concept where the eutectic lithium-lead alloy Pb-17Li serves both as breeder material and as coolant has been continued. One important feature of the present design is the arrangement of a beryllium layer in the front part of the blanket serving as neutron multiplier. Another novel feature is the use of laminated flow channel inserts in all poloidal ducts in order to reduce the MHD pressure drop. The work has been concentrated on three subjects:

- Three-dimensional neutronics calculation,
- Calculation of the temperature field in the first wall and the multiplier region,
- Development of fabrication and testing procedures for flow channel inserts.

The neutronic performance of the liquid metal blanket has been studied in a complete three-dimensional analysis of one torus sector of 7.5° in the double null divertor configuration of NET.

The main objective of the neutronics analysis has been the assessment of the global tritium breeding ratio and a detailed calculation of the spatial distribution of the power density.

Due to the spatial restriction of the breeding blanket to the outboard side of the torus, the blanket coverage is only 52 percent. At the inboard side a simple helium-cooled steel reflector has been used in the neutronics analysis. Nevertheless, a global tritium breeding ratio (TBR) of 0.83 can be achieved using 90% enriched Pb-17Li as breeding and coolant material. This is mainly due to the presence of beryllium in the front channel ensuring a high neutron multiplication. It has also been shown that the global TBR is at the same level if liquid lithium (natural or slightly enriched) is used as breeding and cooling material instead of Pb-17Li.

The spatial power distribution has also been calculated by means of a three-dimensional Monte Carlo calculation. The front part of the radial power distribution is shown in Fig.3 together with the geometry of the first wall and the multiplier region.

There are graphite protection tiles arranged transferring heat to the corrugated steel wall by thermal radiation. Liquid metal cools the region by flowing in parallel through the first wall channels and through holes in the beryllium blocks. There is a surface heat flux of 40 W/cm² and a volumetric heat generation caused by neutrons and γ -radiation. The finite difference program RELAX has been used to calculate the 3-dimensional temperature profile in the front part of the blanket. It is assumed that the liquid metal enters the parallel toroidal coolant channels with uniform temperature. The flow rate in the different cooling channels has been adjusted with the goal to minimize the maximum

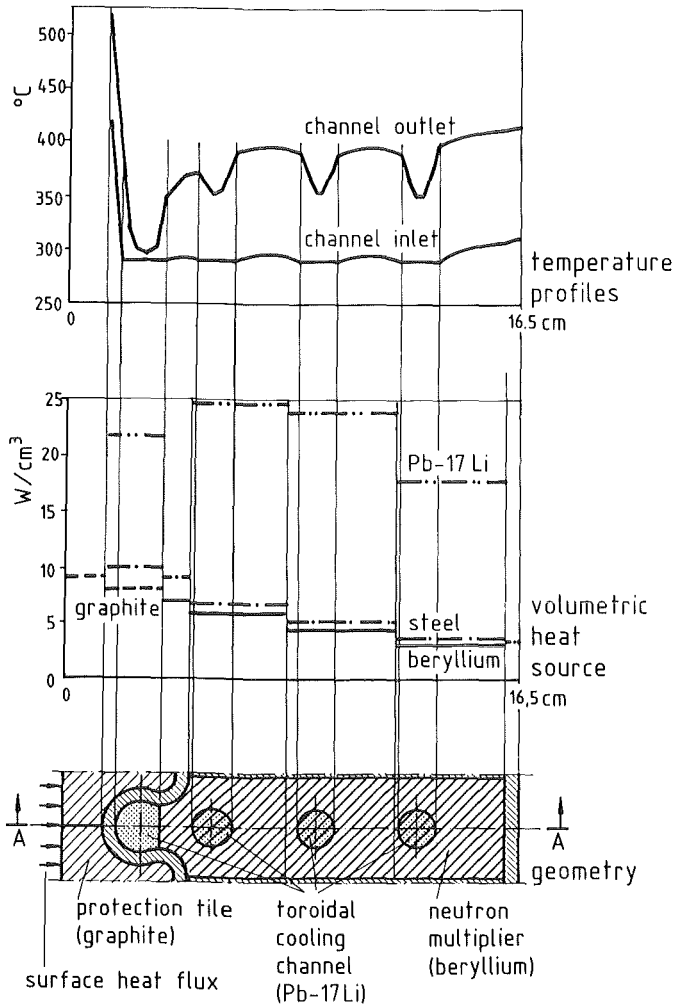


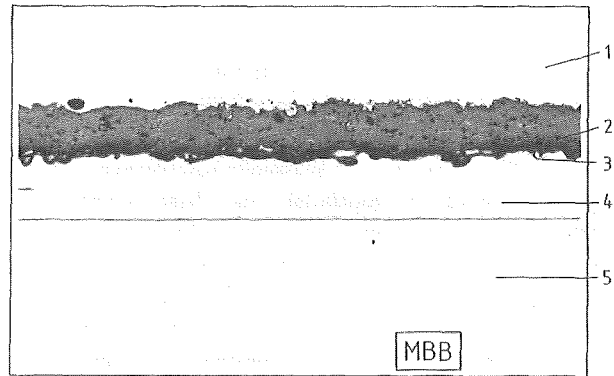
Fig.3 Liquid metal-cooled blanket first wall and multiplier region

temperature at the liquid metal/wall interface in order to limit corrosion problems.

Coolant temperatures for the blanket segment are 275°C at the inlet and 350°C at the outlet. About 2/3 of the total blanket power is generated in the first-wall and multiplier region, where the coolant flows in toroidal direction; in the poloidal channels the heat-up rate is only 25 K. This temperature rise does not shift the maximum interface temperature to the upper end of the blanket segment because it is outweighed by the larger power density at the torus midplane compared to the one at the upper and lower end of the blanket. A temperature profile across the first wall and multiplier region at the torus midplane can be seen in Fig.3, which shows a maximum temperature at the liquid metal/wall interface of 390°C and a maximum steel temperature of 520°C. Both values are in the allowable range for austenitic steel.

To avoid prohibitively high MHD-pressure drop in the poloidal channels of a liquid metal-cooled blanket, the use of

"flow channel inserts" (FCI) is provided. The FCI consists of a laminated wall with two thin metal sheets separated from each other by a ceramic layer. The prefabricated laminated element is welded together at all edges to protect the ceramic from the liquid metal. The welded laminated sheet is formed to fit loosely into the flow channel; a longitudinal slot provides pressure equalization. Voltage induced by the motion of liquid metal perpendicular to the magnetic field then caused only an electric short circuit in the inner sheet of the laminated element.



- ① steel sheet
- ② plasmasprayed $Al_2O_3+TiO_2$
- ③ plasma sprayed cermet
- ④ Inconel brazing foil
- ⑤ steel sheet

Fig.4 Metallurgical cut through a FCI

A program has been initiated to develop and test such flow channel inserts. The development of the fabrication procedures is carried out by MBB. The following fabrication process has been selected:

- plasma spraying of a stainless steel sheet with a mixture of $Al_2O_3 + TiO_2$.
- possibly plasma spraying of a metallic layer on the ceramic (Ni)
- diffusion brazing of the second metallic sheet on the metallized or nonmetallized ceramic with or without a brazing foil (Cu or InCuAg or TiCuNi) under pressure

well below the liquidus temperature of the brazing material. With several pairings good diffusion brazing has been achieved. Fig. 4 shows a photograph of a metallurgical cut through a laminated element.

Staff:

K. Arheidt
V. Casal
U. Fischer
C. Günther
W. Hartmann
S. Malang
K. Rust

3. Tritium Removal by Cold Trapping in an Intermediate NaK-Loop

For a self-cooled Pb-17 Li blanket with an intermediate NaK loop (or a double-walled heat exchanger with NaK flowing in the gap), the following tritium removal technique is investigated: The bred tritium permeates through the heat exchanger walls into the NaK and precipitates as tritide in a cold trap. For tritium recovery, the tritide is decomposed by heating up the cold trap and vacuum pumping.

The WAWIK program (= Wasserstoff-Abtrennung und Wiedergewinnung in Kaltfallen) has been started to investigate the questions related to the kinetics of precipitation and decomposition as a function of hydrogen concentration, temperatures and impurities. Tritium is simulated by hydrogen (protium). The test loop to investigate the precipitation is presently designed including two experimental cold traps, a hydrogen injection device, and a concentration measurement system. Another test facility to decompose hydride has started operation. NaH powder was decomposed at various temperatures. The results agree well with values from literature. To obtain more relevant specific surfaces of the NaH compared to NaH powder, a third test loop was built to produce in a simple way NaH crystals. This facility will be used until the first facility will operate.

Staff

G. Eisele
H. John
J. Reimann

Publications

1. E. Wehner, R. Krieg, B. Dolensky
"Load carrying capacity of canister type blanket elements for NET under accident conditions" SMIRT 1987
2. M. Dalle Donne et al.
"Pebble Bed Canister: The Karlsruhe Ceramic Breeder Blanket Design for NET" submitted for publication in Fusion Technology

B 2 Development of Computational Tools for Neutronics

The KfK activities within the B2-frame comprise the evaluation and processing of relevant nuclear data, the development of new techniques, as well as the adoption and application of existing methods and codes for use in fusion neutronics.

The efforts to develop a general transport code system for a rigorous treatment of the anisotropic neutron scattering have been continued. The establishment of the one-dimensional module in cylindrical geometry has been completed now. At present it is documented. The one-dimensional transport module ANTRA1 therefore is available now in plane, spherical and cylindrical geometry. Both homogeneous and inhomogeneous problems can be treated. There is also an option to choose between the rigorous treatment of the neutron scattering and the approximative one by applying the conventional Legendre expansion of the scattering kernel.

The study on the multiplication of 14 MeV neutrons in lead has been completed. The essential of this study is the analysis of the neutron multiplication using the new nuclear data evaluation of lead contained on the European Fusion File EFF-1 and the newly developed transport programme ANTRA1. It is shown, however, that for lead there is no significant difference in the total neutron multiplication when using different procedures and data. There is an improvement in so far as the EFF-1 data in general produce the same spectral distribution of the leakage neutrons as it is observed in the experiments (see e.g. fig. 5), whereas the neutron spectra based on the ENDF/B-IV data are much too "soft".

There is however still an underestimation of the experimentally observed total neutron multiplication by ca. 10 %. Therefore a higher $(n, 2n)$ - cross section at 14 MeV is suggested for lead. This conclusion is in agreement with a very recent, yet unpublished lead evaluation of H. Vonach (IRK, Wien) recommending a $(n, 2n)$ - cross section of 2.2 ± 0.06 b at 14 MeV. This value is 5 % higher than the one currently contained in the nuclear data files (ENDF/B-IV, -V, EFF-1).

The Monte Carlo code MCNP is in routine use for fusion neutronics applications at KfK. The main subject of its application is the geometrical modelling of a fusion reactor blanket in three dimensions in order to assess the global tritium breeding ratio, to treat spatial heterogeneities and to evaluate the spatial distribution of the power density $/l/$. By the use of sophisticated variance reduction schemes it is even possible to treat deep penetration problems with MCNP.

MCNP has been used to assess the efficiency of a shielding blanket of the NET-reactor (see task N2). Using the same geometrical model, it has been shown by means of MCNP calculations that the most relevant radiation dose on the electrical insulator of the superconducting magnet is underestimated by the ONETRAN multigroup calculation by a factor of 2 (fig. 6). This discrepancy can mainly be attributed to the use of a single group constant set that is inadequate for this purpose (the main features are: there are very broad energy groups; so the group constants are very sensitive to the weighting function; the neutron spectrum, on the other hand, varies strongly through the blanket; furthermore, no resonance shielding is taken into account). MCNP uses the continuous energy representation of the nuclear data and avoids these problems in this way. To achieve a low statistical error of course long computing times are needed; typically two hours CPU-time are needed for a one-dimensional shielding problem.

The group constant generation programme NJOY is in use for the calculation of group constants from ENDF/B-formatted nuclear data files (EFF, JEF, ENDF/B) at KfK. The present status of the KfK version of NJOY has been documented in an internal report. The corrections and modifications performed at KfK so far started from the American version 6/83 of NJOY and mainly concern the neutron interaction cross sections. An error in the calculation of the total photon KERMA factor also has been removed.

At present the calculation of photon production cross sections by NJOY is being studied. The generation of a coupled neutron-photon library in the KfK standard group constant format GRUBA is being discussed. This would require the extension of the KfK group constant testing and formatting programmes (e.g. JOYFOR, MITRA) and of the GRUBA library itself to include photon production and photon interaction cross sections.

Staff:

I. Broeders
U. Fischer
B. Krieg
H. Küsters
A. Schwenk-Ferrero
E. Stein
E. Wiegner

Publications:

1. U. Fischer: Blanket Modelling in a Tokamak Reactor, Int. AMSE Conf. "Modelling and Simulation", Karlsruhe, 20 - 22 July, 1987.

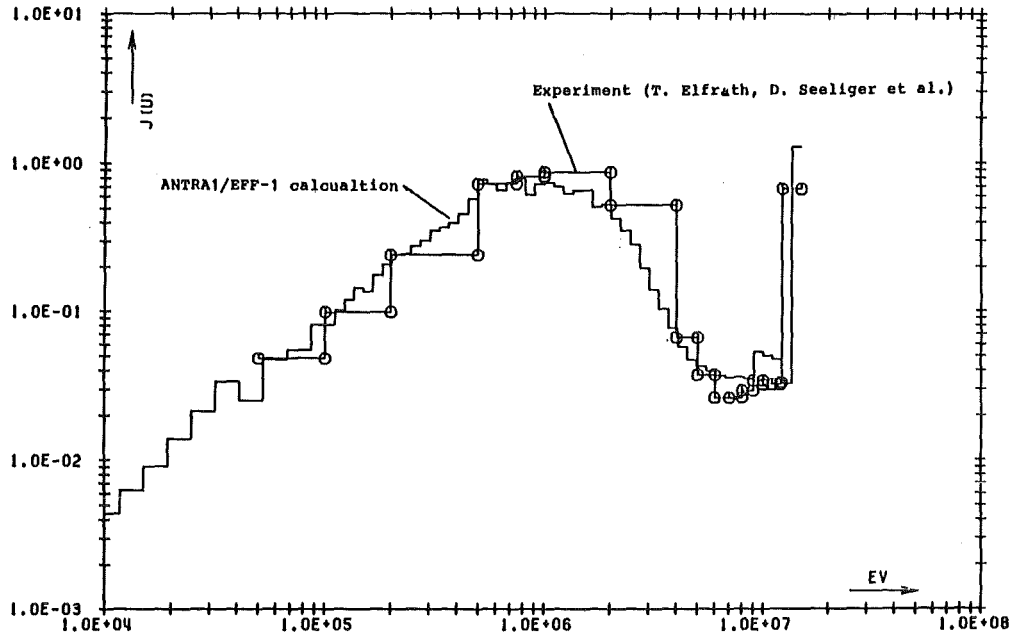


Fig.5 Leakage spectra of a 14 MeV neutron source surrounded by a 22.5 cm thick spherical lead shell.

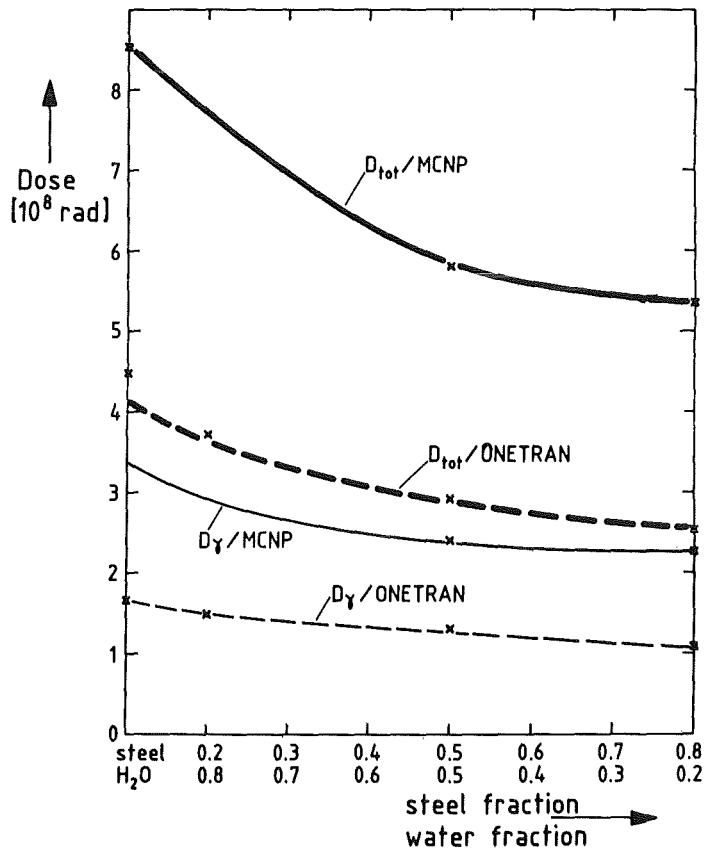


Fig.6 Radiation dose on the Epoxy insulator of the superconducting toroidal field magnet for different steel/water fractions of a shielding blanket of NET: Comparison between ONETRAN multigroup calculations and MCNP calculations using a continuous energy representation (a neutron wall load of 1.4 MW/m^2 and an operation time of 1 year is assumed).

B6 Corrosion of Structural Materials in Flowing Pb-17Li

The PICOLO loop has been operated for 3700 hours with specimens of steel 1.4914 (X18 CrMoVNb 12 1), NET batch, at 550°C test temperature and a flow velocity of $V = 0.3$ m/s in the test section. The Reynold's number in the test section is $R_e = 20950$, the ΔT of the loop has a value of ~ 250 K.

As is shown in the Table 1, the specimens lose weight and are reduced in their diameters. Metallographic examination shows that the material losses are not uniform (see Fig. 7). The unequal attack of the steel by the liquid metal Pb-17Li is also seen by scanning microscopy. Further examinations are under way.

Spec. no.	Position	Exposure time (h)	Change of diameter (mm)	Change of weight	
				(mg)	(mg/cm ²)
1	1	1058	0.040	+92.19*	+7.33
3	3	2983	0.170	-1046.74	-83.29
5	7	2983	0.185	-895.35	-71.25

* value influenced by adhering Pb

Table 1: Corrosion effects in the PICOLO loop at 550°C

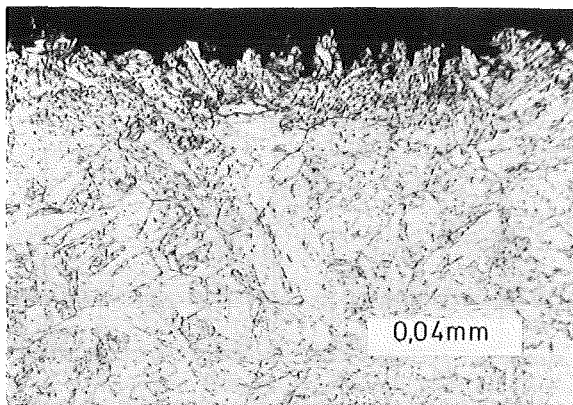


Fig. 7. Micrograph (500:1) of specimen no. 3, corroded 2983 h in flowing Pb-17Li at 550°C

The chemical analysis of the eutectic alloy shows that the composition is nearly unchanged during the first operation period. Compared to earlier analyses of material taken from the old loop, the contents of Cr and Ni are remarkably higher (see Table 2).

Sample	Li-content (wt-%)	Fe-content (µg/g)	Cr-content (µg/g)	Ni-content (µg/g)
Initial	0.75 ± 0.005	8.6 ± 1.6	1	2
1058 h	0.74 ± 0.005	0.8 ± 3.0	1	6.2 ± 0.6

Table 2: Chemical composition of Pb-17Li

Staff:

- Ch. Adelhelm
- H.U. Borgstedt
- G. Drechsler
- G. Frees
- Z. Perić
- G. Streib
- S. Winkler

B 6.3

Fatigue of Structural Material in Pb-17Li

The low cycle fatigue behaviour of the martensitic steel 1.4914 (X 18 CrMoVNb 12 1) will be tested at 550°C in the liquid alloy Pb-17Li. First cold tests with this materials have been made. Reference tests are under way, the programme can be started in October 1987.

Staff:

- H.U. Borgstedt
- M. Grundmann
- Z. Perić
- B. Seith

Publication:

H.U. Borgstedt, M. Grundmann: Trans. of the 9th Internat. Conf. on Structural Mechanics in Reactor Technology, Ed. F.H. Wittmann, A.A. Balkema, Rotterdam 1987, Vol. N, 145-150.

B 9 Tritium Extraction from Liquid Pb-17Li by the Use of Solid Getters

Several methods were proposed to extract tritium from the liquid Pb-17Li blanket material. Task 9 will study the use of solid getters. In static capsule experiments, compatibility tests were performed with five possible getter metals at temperatures up to 600°C and run-times up to 2500 hours.

All preparation was done in an argon atmosphere with less than 1 ppm oxygen. 50 to 60 grams of Pb-17Li were used in Mo-crucibles, the metal sheets fixed by Mo-stripes. Degassing and annealing of samples and capsules was done at 700°C at 10⁻⁵ mbar.

Any contact between the samples and the Mo-crucible was avoided.

Otherwise problems occurred because of reactions between the sample and molybdenum below the Pb-17Li surface.

Up to 6 crucibles were heated together in one capsule. Fig. 8 shows the arrangement. The cover gas in the capsules was slowly flowing purified Ar-6.0. Below the radiation shields the temperature was constant in all parts of the capsule within ± 2°C.

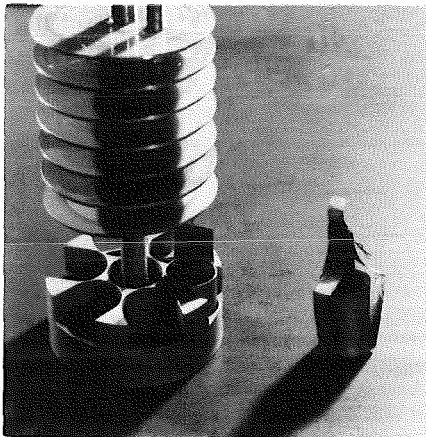


Fig. 8: Arrangement of samples in a capsule

After an experiment the capsules were opened in the glove box and the samples removed from the Pb-17Li. All the Pb-17Li was dissolved, using a special extraction technique with nearly the stoichiometric amounts on nitric acid. Dissolved materials were determined by ICP-AES analysis. Remaining Pb-17Li in the Mo-crucibles was dissolved in acetic acid/H₂O₂, the samples cleaned by an electrolytic and prepared for metallographic and microprobe investigations.

Results

The following getter metals were studied:

Y, U, Zr, Ti, Ti-alloy BETA 3

Wetting problems with Pb-17Li determined the lower temperature limit for the experiments.

YTTRIUM, URANIUM

Even below 400°C the samples were completely dissolved in liquid Pb-17Li within the week.

ZIRCONIUM:

Fig. 9 shows dissolution rates as a function of temperature. 600°C is a limiting temperature because the metal becomes very brittle. Larger concentrations of lead were found in the zirconium and are probably responsible for this effect.

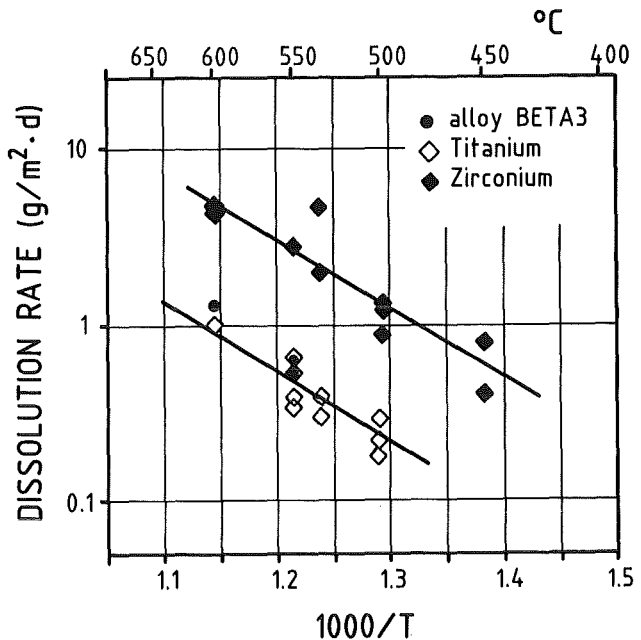


Fig. 9: Dissolution rates of getter metals in liquid Pb-17Li

TITANIUM, ALLOY BETA 3:

The dissolution rates are about three times lower compared to zirconium. The alloy BETA 3 (12% Mo, 6% Zr, 4.5% Sn) shows the same behavior as the pure metal (Fig. 9).

The limiting temperature will be at ~ 500°C. At higher temperatures crystals of an intermetallic compound grow on the sample surface, consisting of about 23% titanium + 77% lead, with very small concentrations of

other metals in case of the alloy also with some zirconium). Such crystals were also formed in pure lead, as observed in an experiment at 550°C. As in the case of zirconium lead was dissolved in titanium at higher temperatures and the metal becomes brittle. Probably because of stabilizing effects of the molybdenum, lead dissolution and embrittlement were smaller for the alloy.

Discussion

From the investigated getter metals Y and U cannot be used in liquid Pb-17Li at all.

Limiting temperatures were found for Ti and Zr, but it is doubtful whether these metals can be used without a coating as getters for the tritium extraction. The corrosion rates are too high. Also strong embrittlement, probably caused by lead dissolved in the metal, may limit the temperature for the use. Furthermore an intermetallic compound on Ti surfaces was observed.

Further investigations

So far, mainly tests in static Pb-17Li were performed. Experiments with stirred liquid metal are under way. The next static tests will be done with molybdenum-coating getter materials.

Metallographic and microprobe investigations have started.

Staff:

H. Feuerstein

H. Gräbner

J. Oschinski

B 11-16 Development of Ceramic Breeder Materials

The KfK contribution concentrates on the Li-Silicates and includes all the steps necessary to achieve a product to be used in the helium-cooled blanket design. The development starts with fabrication and characterization of pellets and pebbles. Physical, mechanical and chemical properties are measured before and after irradiation. The irradiation program makes use of several reactors within the European and the Beatrix Cooperation. Lithium-Orthosilicate has been proven to be the most promising candidate for the NET reference ceramic breeder material.

1. **Fabrication and Characterization of Ceramic Breeder Materials (B 11, B 12)**

The preparation and fabrication of lithium containing monosilicates, especially Li_2SiO_3 and Li_4SiO_4 , are under development to be used as breeder materials for fusion reactors within the European Fusion Program (Task B11 and B12). Samples of different breeder materials - LiAlO_2 , Li_2SiO_3 , Li_4SiO_4 , Li_2ZrO_3 , and Li_2O prepared by the cooperating European groups - have been assembled for the international irradiation experiment ELIMA-2. Progress in fabricating Li_4SiO_4 powders obtained from alcoholic suspensions has been made by fabricating a batch of about 75 kg spray-dried powder under industrial conditions.

Assembling of 72 Irradiation Test Tubes for ELIMA-2 and DELICE-03

The international irradiation experiments ELIMA-2 and DELICE-03 include 72 test pins with different samples of breeder materials to compare the irradiation behaviour under fast neutron and thermal neutron conditions (see Table 3). The different materials, delivered to KfK, were stored and handled under dry inert gas (helium) conditions in a glove-box, exclusively. All the materials, except the Li_2O , were dried under helium at temperatures of 300 to 350 °C and then filled into the stainless steel tubes. The tubes were closed with end-plugs, which had boreholes, by means of vacuum electron welding, then refilled with pure helium, and the boreholes closed and welded with stainless steel pins. The test tubes now are ready to be mounted for the irradiation experiment.

Characterization of Ceramic Breeder Materials

Comparative irradiation experiments for ceramic breeder materials have been proposed in a fast and a thermal neutron test bed. The objective is to find out if there are differences in the materials behaviour as a consequence of different damage rates by fast neutron scattering and the Li-6 (n, α)T reaction, respectively.

Laboratories of Saclay/CEA, Springfields/UKAEA, Mol/CEN, Casaccia/ENEA, and Karlsruhe/KfK participate in these experiments, which will be performed in the HFR of

Material	Number of Pins	Shape of Material	Co-operating Group
LiAlO_2	8 + 8	pellets	SACLAY/FRANCE
	6 + 6	pellets	CASACCIA/ITALY
Li_4SiO_4	2 + 2	pellets	KfK/GERMANY
	2 + 2	ceramic pebbles	KfK/GERMANY
	2 + 2	melted pebbles	KfK/GERMANY
Li_2SiO_3	2 + 2	pellets	KfK/GERMANY
	6 + 6	pellets	MOL/BELGIUM
Li_2ZrO_3	4 + 4	pellets	SPRINGFIELDS/U.K.
Li_2O	4 + 4	pellets	SPRINGFIELDS/U.K.

Table 3: Irradiation Test pins for ELIMA-2 and DELICE-03

Petten (ELIMA 2) and the OSIRIS reactor of Saclay (DELICE 03).

KfK has prepared lithium metasilicate and lithium orthosilicate samples for the two experiments. The samples comprise pellets, sintered granules and molten spheres. The pre-irradiation analysis of the pellets has been finished. Some results are compiled in Table 4.

		Li_2SiO_3	Li_4SiO_4
Mean diameter	(mm)	4.51	4.97
Geometric density	(g/cm ³)	2.35	2.09
Hg porosimeter density	(g/cm ³)	2.37	2.15
	(% T.D. *)	93.7	90.0
He pycnometer density	(g/cm ³)	2.51	2.38
Total porosity **)	(%)	6.3	10.0
Open porosity			
Hg porosimeter	(%)	2.4	2.8
He pycnometer	(%)	5.6	9.7
Effective channel diameters**	(μm)	< 0.4	< 3
Sound velocity	(km/s)	5.64	6.21
Specific surface area	(m ² /g)	0.67	1.54

*) $\rho_{\text{th}} = 2.39 \text{ g/cm}^3$

***) acc. to Hg porosimetry

Table 4: Geometric and structure data of Li_2SiO_3 and Li_4SiO_4 pellet specimens of the ELIMA 2/DELICE 03 experiment

Both pellet samples are of high density, about 94 and 90 % T.D.. The amounts of open porosity which were determined using Hg porosimetry were at the same level for the two pellet samples. But differences were observed for the shape of the cumulative distributions of the open porosity (Fig. 10).

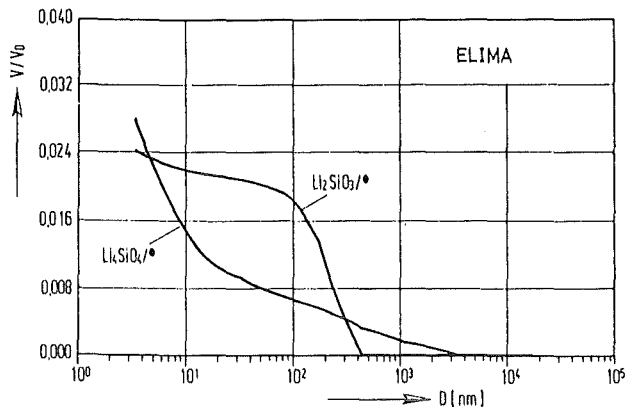


Fig. 10: Cumulative open porosity vs. intrusion channel diameter of Li_2SiO_3 and Li_4SiO_4 pellet specimens of the ELIMA 2/DELICE 03 experiments

The measurements which were carried out with a He pycnometer demonstrated that considerable volume of open porosity existed below the measuring limit of the Hg porosimeter. The sound velocities of the samples lay within the range which has been found for other high-dense lithium silicate samples. The specific surface area determined by applying the BET theory to volumetric nitrogen gas adsorption proved to be higher by a factor of about 2 for the orthosilicate sample in comparison to the metasilicate sample.

Industrial Fabrication of Li_4SiO_4 Powder

A batch of about 75 kg spray-dried Li_4SiO_4 powder was fabricated from an alcoholic suspension under industrial conditions to confirm the laboratory preparation method and to improve scaling-up. The main steps of the preparation technique already described in detail are fabrication of the suspension, spray-drying of the suspension, and calcination of the powder obtained. The total amount of the suspension was fabricated in two batches of about 400 l at Fa. Roth/Karlsruhe. Two samples of the suspension, 5 l each, were taken to the laboratory and the quality examined, showing no differences between the industrial and the laboratory preparation. The suspension was then transported to Fa. NIRO/Kopenhagen for spray-drying. Also this step shows no problems for a further industrial scaling-up. The calcination step will be carried-out in the next days at Fa. BUSS /Pratteln where the powder can be calcinated in a larger furnace under fluidizing conditions. The experience gained from these technological experiments shows that there are no larger problems for the production of Li_4SiO_4 powder by the suspension technique developed under laboratory conditions.

Staff:

- B. Dörzapf
- H. Elbel
- E. Günther
- R. Hanselmann
- J. Heger
- W. Jahraus
- E. Kaiser
- W. Laub
- H. Nagel
- R. Scherwinsky
- Dr. D. Vollath
- Dr. H. Wedemeyer
- M. Wittmann

Publication:

D. Vollath, H. Wedemeyer: American Ceramic Society Meeting 1987, 26.-30.4.1987, Pittsburgh, PA

"Techniques for Synthesizing Lithium Silicates and Lithium Aluminates"

2. Measurement of Physical, Mechanical and Chemical Properties (B 13)

Physical and Mechanical Properties

A review of physical and mechanical properties was presented at the Petten Workshop on Progress in Ceramic Tritium Breeding Materials Development (June 24 - 26,

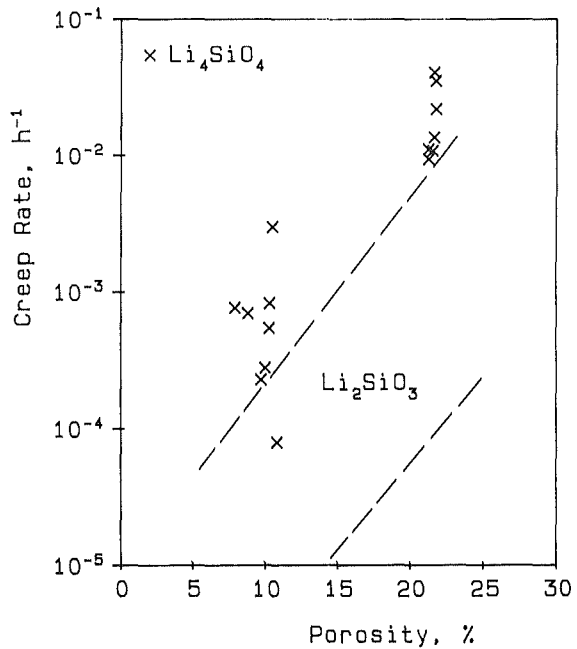


Fig. 11: Compressive creep rate of Li_4SiO_4 in 100 h at 900 °C and 10 MPa.

1987). Particular importance was given to the resistance to

thermal crack formation. It is predicted to be highest in LiAlO₂ and lowest in Li₄SiO₄, for the latter also in view of rather low values of compressive strength and thermal conductivity, which were newly measured.

The Young's modulus of the lithium silicates is comparatively low. The compressive strength of the different breeder materials appears rather unspecific, with a major dependence on the grain size, and does not suggest a definite ranking.

Recent compressive creep tests on Li₄SiO₄ resulted in creep rates much higher than those measured on Li₂SiO₃ (Fig. 11). Generally, creep rates indicate rough temperature limits (at about 10⁻⁶/h), below which the breeder materials can be considered virtually rigid (and probably stable in microstructure). LiAlO₂: 900 °C, Li₂SiO₃: 800 °C, Li₄SiO₄: 700 °C, Li₂O: 600 °C.

Staff:

M. Blumhofer

W. Dienst

H. Zimmermann

Interaction with Water Vapour

After having observed the formation of unidentified phases by long time annealing experiments with Li₄SiO₄ in humid atmosphere, further attempts were made to explain the questionable reactions by thermal analyses. DSC runs were conducted at different water vapour concentrations in flowing argon (< 1, 500 and 10000 vpm H₂O). Up to 800 °C no new effects were observed in addition to the well known peaks at 608, 665 and 724 °C. These peaks correspond to one crystallographic and two higher order transformations of Li₄SiO₄ and do not depend on the water vapour concentration. X-ray diffraction showed no other crystalline phases, and the weight changes were insignificant.

LiAlO₂ pellets were tested in order to simulate their storing and handling conditions. After 3 weeks at ambient temperature in air the weight increase was 3.6 %, X-ray diffraction showed no significant change compared to the starting material, and transient heating in Ar (< 1 vpm H₂O) up to 800 °C resulted in a peak of the H₂O release at 193 °C.

Staff:

V. Schauer

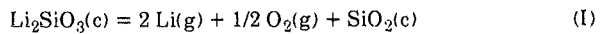
G. Schlickeiser

A. Skokan

The Thermochemistry of Solid Lithium Metasilicate

Lithium ceramics, such as lithium silicates, have been proposed as candidate materials for tritium breeding in fusion reactors. For their evaluation and selection knowledge of their high temperature properties is required. Therefore a thermochemical study of Li₂SiO₃ with emphasis on the properties of the solid ceramic was initiated employing mass spectrometric analysis of Knudsen effusates.

The partial pressures of lithium and - for the first time - those of oxygen were determined over Li₂SiO₃ below its melting point (1474 K) within a wide range of temperatures. In addition, one data point of gaseous Li₂O was obtained at a temperature just below the melting point. From the experimental findings it is concluded that the thermal decomposition process of solid Li₂SiO₃ can be described by the following equation:



Similar to the results obtained in the vaporization experiments with solid Li₂SiO₃, the Li and O₂ partial pressures over the liquid were found to be about two orders of magnitude higher than those of all other species. The experimental p_{Li}/p_{O₂} partial pressure ratio has an average value of ≈ 1.83 and is nearly independent of temperature. Also observed were the gaseous lithium oxides LiO, Li₂O and Li₃O. A small fraction of the liquid vaporizes without decomposition. A least square treatment was applied to the data obtained with the solid and the liquid material to calculate the coefficients of the Arrhenius equations of the examined species.

Equilibrium constants, K_{eq}, obtained from partial pressures were used to calculate reaction enthalpies employing Gibbs free energy functions Δ(G°_T - H°₂₉₈)/T from the JANAF thermochemical tables. The reaction enthalpy changes H°_{298,r} obtained for the various reactions are given in Table 5. The data show good thermodynamic consistency. The heat of fusion of Li₂SiO₃(c) was found to be 23.3 ± 10 kJ/mol, in satisfactory agreement with data from the literature (28.03 ± 2.1 kJ/mol). The standard enthalpies of formation of LiO and Li₂O were found to be

$$\Delta H_{f,298}^\circ(\text{Li}_2\text{O}) = (-130.7 \pm 10.5) \text{ kJ/mol}$$

$$\Delta H_{f,298}^\circ(\text{LiO}) = (93.8 \pm 3.6) \text{ kJ/mol}$$

The temperature dependence of p_{Li₂SiO₃} yields an enthalpy of vaporization for



$$\text{of } \Delta H_{\text{vap},1695}^\circ = (455.65 \pm 8.6) \text{ kJ/mol.}$$

No.	reaction	$\Delta H^{\circ}_{298,r}$ kJ/mol
solid Li_2SiO_3		
I	$\text{Li}_2\text{SiO}_3(c) = 2 \text{Li}(g) + 1/2 \text{O}_2(g) + \text{SiO}_2(c)$	1007.96 ± 4.13
II	$\text{Li}_2\text{SiO}_3(c) = \text{Li}_2\text{O}(g) + \text{SiO}_2(c)$	540.36
III	$\text{Li}_2\text{O}(g) = 2 \text{Li}(g) + 1/2 \text{O}_2(g)$	453.00
liquid Li_2SiO_3		
IV	$\text{Li}_2\text{SiO}_3(c) = 2 \text{Li}(g) + 1/2 \text{O}_2(g) + \text{SiO}_2^*$	984.63 ± 5.54
V	$\text{Li}_2\text{SiO}_3(c) = \text{Li}_2\text{O}(g) + \text{SiO}_2$	531.56 ± 4.80
VI	$\text{Li}_2\text{O}(g) = 2 \text{Li}(g) + 1/2 \text{O}_2(g)$	452.14 ± 1.46
VII	$\text{Li}_2\text{O}(g) = \text{Li}(g) + 1/2 \text{O}_2(g)$	66.89 ± 3.59

* unknown state of SiO_2 in $\text{Li}_2\text{SiO}_3(1)$

Table 5: Standard reaction enthalpies for various equilibria obtained from partial pressure measurements.

Extrapolated data of the oxygen partial pressure obtained over the solid lithium metasilicate were used in combination with the equilibrium



to calculate the ratio $p_{\text{H}_2\text{O}}/p_{\text{H}_2}$ as a function of temperature under equilibrium conditions. Data of hydrogen were used instead of tritium because the isotope effects are small in comparison to the uncertainty of the estimate. The results, given by the expression

$$\log \frac{\text{H}_2\text{O}}{\text{H}_2} = \frac{1588}{T} + 0.979$$

illustrate that in the temperature range 500 - 1300 K water will be the predominant chemical form of the released tritium. This conclusion is of course only valid under quasi-equilibrium conditions and in the absence of structural materials with reducing properties.

Staff:

- H.R. Ihle
- R.-D. Penzhorn
- P. Schuster
- K. Zmbov (visiting scientist)

3. Compatibility with Metallic Materials (B 14)

Recent annealing experiments with Li_2SiO_3 and Li_4SiO_4 concentrated on the compatibility with metallic beryllium, which is of interest as a neutron multiplier. Results of a first test series with Li_2SiO_3 at 600, 750 and 900 °C are presented in Fig. 12. No observable attack could be found at 600 °C. The deep localized attack at 750 °C is believed to be due to the occurrence of a liquid lithium silicide phase in addition to the BeO reaction product on the Li_2SiO_3 surface (see micrographs in Fig. 12). According to the Li-Si binary phase diagram, lithium silicides are liquid at temperatures ≥ 750 °C.

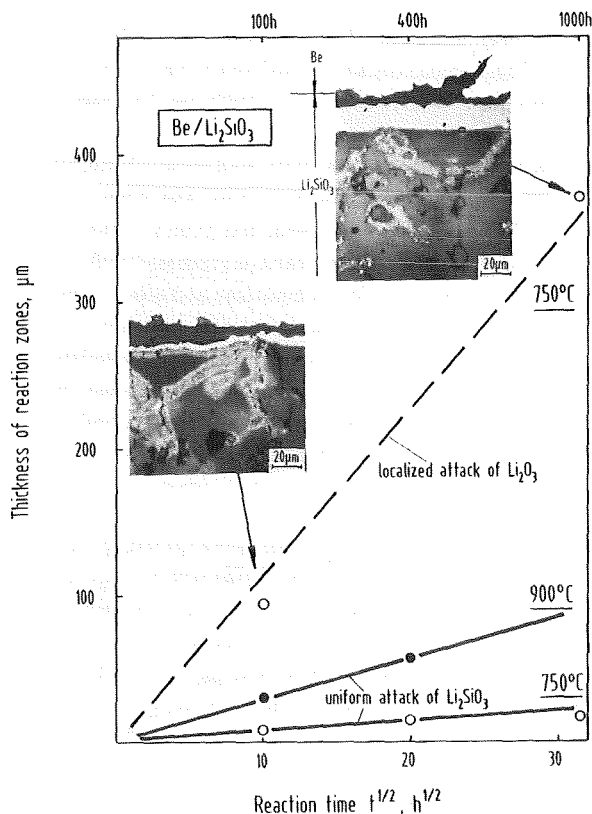


Fig. 12: Chemical reaction between Be and Li_2SiO_3 .

Further annealing tests, now including Li_4SiO_4 , have been conducted (but not yet evaluated) at 600, 650 and 750 °C. In the annealing tests, contact is also made between Be and AISI 316 as the capsule material. The extent of the Be/316 reaction seemed to be admissible at 600 °C, but no more at 750 °C (reaction layer thickness after 1000 h: about 25 µm at 600 °C, and 150 µm at 750 °C). AES and ion microprobe analytical examination of the specimens showed a diffusion of the Be into the stainless steel under the formation of BeNi. The stainless steel matrix was depleted in Ni within the reaction zone.

Staff:

- Ch. Adelhelm
- P. Hofmann
- K.-H. Kurz
- H. Metzger
- E. Nold

4. Irradiation Testing of Ceramic Breeder Materials (B15 and B15.3)

A number of lithium ceramics are considered as candidates for a solid breeder blanket of a fusion reactor. KfK concentrates on lithium silicates. In assessing the potential performance of solid breeders, tritium release rate and retention are important aspects. In addition to the in-pile tests (B16), tritium release is studied in out-of-pile annealing experiments.

Different types of meta- and orthosilicate samples, irradiated in the DIDO reactor at KFA Jülich and the meta- and orthosilicate pellets of the first in-pile test LISA-1 in the SILOE-reactor have been annealed. The annealing temperature has been varied systematically and the influence of purge gas and samples has been tested. In agreement with previous results, release from orthosilicate was found to be faster than from metasilicate. Release from both, meta- and orthosilicate, was found to be insensitive to type, flow rate and pressure of purge gas. The experimental release has been compared to theoretical predictions assuming various processes (diffusion, trapping, recombination). This comparison and other evidence indicate that in our tests tritium release, especially from orthosilicate below 450 °C, is controlled by water chemistry. The measured release is generally slower than diffusion prediction and can very well be described by OH/OT recombination and desorption /1/. Future work will concentrate on reducing the moisture in the samples and the purge gas.

Annealing of the high-activity samples from the first irradiation in the OSIRIS reactor at Saclay, DELICE 01, has been started. A first step of the ceramography work in the KfK hot cells has been the optimization of the preparation technique. The transport of the samples from the second irradiation, DELICE 02, from Saclay to Karlsruhe is planned for October 1987.

In a comparative irradiation B15.3 it is planned to study the influence exerted by different neutron spectra on breeder material samples furnished by five partner institutions (see table 6). With different spectra the contributions to damage originating in fast neutron scattering and $Li_6(n,\alpha)T$ reaction are greatly varied. Although the total rate of damage expressed in dpa remains the same, the contributions of the n,α reaction to damage are high under the DELICE 03 thermal irradiation conducted in the OSIRIS reactor whereas they are relatively low in a fast flux. On account of the temporary shutdown of the KNK II reactor, it is envisaged now to perform the ELIMA 2 irradiation in HFR Petten under a cadmium screen. For both irradiations, DELICE 03 and ELIMA 2, the sample materials have been provided by the partners and cladding was done at KfK under uniform conditions. Preparation of the irradiation rigs in Saclay and in Petten has advanced to a stage where they can be assembled by the end of the year and where irradiation can start in spring 1988. The irradiation time in OSIRIS will last about 80 full power days and that in HFR 175 full power days.

Staff:

E. Bojarsky
W. Breitung
T. Eberle
H. Elbel
H.E. Häfner
K. Heckert
J. Lebkücher
K. Philipp
G. Schumacher
H. Werle

References:

- /1/ W. Breitung et al., "Out-of-pile Tritium Extraction from Lithium Silicate", ICFRM-3, October 1987, paper R-70

5. Tritium Recovery from Ceramic Breeder Material (B16)

Tritium recovery from ceramic breeder material is important in assessing the potential performance of breeder blankets. The behaviour of lithium silicates is studied by KfK in the LISA-series of in-pile tests performed in the SILOE reactor at CEN Grenoble.

Because of the fast tritium release from orthosilicate observed in the first test LISA-1, the second test LISA-2 concentrated on this materials and, to meet the requirements of the KfK pebble bed design for a NET blanket, especially on high-density (97 % TD) spheres and low temperatures. Irradiation of LISA-2 started November 24 and was stopped December 2, 1986 because of a leak in the reactor tank. The test will be continued in the neighbouring MELUSINE reactor October 1987. Some results have already been discussed in the last report. A recent more detailed evaluation indicated that influx tritium release from the high-density orthosilicate samples is for temperatures above 500 °C consistent with the assumption that diffusion is one controlling process. At least one other process, probably related to residual moisture, is involved and gets dominant at lower temperatures /1/. The influence of residual moisture on tritium release from orthosilicate must be studied in detail and more effort is required to reduce and control the moisture in in-pile experiments.

Staff:

H. Elbel
H.E. Häfner
H. Werle

References:

- /1/ H. Werle et al., "The LISA-2 Experiment: In-situ Tritium Release from Lithium Orthosilicate", ICFRM-3, October 1987, paper R-69

	ELIMA 2/HFR-Petten		DELICE 03/OSIRIS-Saclay		Total of samples
	400 to 450 °C	650 to 700 °C	400 to 450 °C	650 to 700 °C	
CEA, Saclay	2 LiAlO ₂ 78 % Pellets *) 1 LiAlO ₂ 62 % Pellets 1 LiAlO ₂ 84 % Pellets	2 LiAlO ₂ 78 % Pellets 1 LiAlO ₂ 62 % Pellets 1 LiAlO ₂ 84 % Pellets	2 LiAlO ₂ 78 % Pellets 1 LiAlO ₂ 62 % Pellets 1 LiAlO ₂ 84 % Pellets	2 LiAlO ₂ 78 % Pellets 1 LiAlO ₂ 62 % Pellets 1 LiAlO ₂ 84 % Pellets	16
ENEA, Cassacia	3 LiAlO ₂ 80 % Pellets	12			
UKAEA, Springfield	2 Li ₂ O 83 % Pellets 79 % Pellets 2 Li ₂ ZrO ₃ 80 % Pellets	2 Li ₂ O 82 % Pellets 2 Li ₂ ZrO ₃ 80 % Pellets	2 Li ₂ O 79 % Pellets 81 % Pellets 2 Li ₂ ZrO ₃ 80 % Pellets	2 Li ₂ O 82 % Pellets 2 Li ₂ ZrO ₃ 80 % Pellets	8 8
CEN, Mol	2 Li ₂ SiO ₃ 82 % Pellets 1 Li ₂ SiO ₃ 75 % Pellets	1 Li ₂ SiO ₃ 82 % Pellets 1 Li ₂ SiO ₃ 75 % Pellets 1 Li ₂ ZrO ₃ 80 % Pellets	2 Li ₂ SiO ₃ 82 % Pellets 1 Li ₂ SiO ₃ 75 % Pellets	1 Li ₂ SiO ₃ 82 % Pellets 1 Li ₂ SiO ₃ 75 % Pellets 1 Li ₂ ZrO ₃ 80 % Pellets	10 2
KfK Karlsruhe	1 Li ₄ SiO ₄ 98 % Sph. 1 Li ₄ SiO ₄ 85 % Gran. 1 Li ₄ SiO ₄ 90 % Pellets 1 Li ₂ SiO ₃ 90 % Pellets	1 Li ₄ SiO ₄ 98 % Sph. 1 Li ₄ SiO ₄ 85 % Gran. 1 Li ₄ SiO ₄ 90 % Pellets 1 Li ₂ SiO ₃ 90 % Pellets	1 Li ₄ SiO ₄ 98 % Sph. 1 Li ₄ SiO ₄ 85 % Gran. 1 Li ₄ SiO ₄ 90 % Pellets 1 Li ₂ SiO ₃ 90 % Pellets	1 Li ₄ SiO ₄ 98 % Sph. 1 Li ₄ SiO ₄ 85 % Gran. 1 Li ₄ SiO ₄ 90 % Pellets 1 Li ₂ SiO ₃ 90 % Pellets	4 4 4 4
Total	18	18	18	18	72

*) % Theoretical Density

Sph. = Molten Spheres

Gran. = Sintered Granulate

Sample size 5 mm Ø x 40 mm length

Table 6: Sample Matrix of the Comparative Irradiation ELIMA 2/DELICE 03 B15.3

M1 The Large Coil Task

The Large Coil Task is an experiment of the International Energy Agency with contributions of four nations. The goal of the experiment is to make the superconducting magnet technology available for Tokamaks. The European Community contributes to this experiment with one superconducting coil. The coil was designed, developed and constructed on behalf of Euratom by KfK-Karlsruhe together with two German companies: Vacuumschmelze, Hanau (conductor) and Siemens AG, Erlangen (coil). The test program is running since January 1986 at Oak Ridge Nat. Lab., USA. The Euratom coil passed successfully all "Standard Tests" and entered in April 86 the series of the "Extended Tests". The whole test program was successfully completed in September with outstanding results for the Euratom LCT coil.

In the series of Extended Tests the coils should demonstrate their capabilities beyond the rated design values as a single coil and in a toroidal configuration. In a five coil array the coils were exposed to high out-of-plane forces. These tests demonstrated the performance of the coils in a failure mode if one coil of the toroidal configuration is without current.

As addition to the original test program a safety test program was approved by the Executive Committee in which some aspects of the safety of superconducting magnets could be experimentally explored. Relevant tests were proposed by KfK. Test procedures were worked out by the LCT staff on site which considered the existing instrumentation of the coils, the risks for the coils, the relevance for future magnet technology and the time needed to perform the task. As high priority items were identified "hot spot" measurements and the loss of flow for forced flow cooled coils. The Westinghouse coil was selected for "hot spot" and the Euratom coil for both types of investigations.

In the single coil tests, the Euratom LCT reached 9 T at 140% of the rated current (Fig. 13). This was the highest overload that could be achieved in the various tests. The coil was operated stably 18 minutes at this point without any indication of resistive voltages within an accuracy of $\pm 40 \mu\text{V}$. Current and field values agreed with those derived by short sample measurements of the single cable strands /1/.

In a series of experiments helium slugs were injected in one cooling circuit of the outermost double pancake. The slugs were heated up well controlled to the current sharing temperature at the location of the conductor inlet. At four current levels the "take-off" voltages were measured (Fig. 14) for a series of heater shots with 4 s pulse duration each. Voltages down to several μV were measurable with a suitable signal conditioning. Exact field calculations at the location of the inlet, measurement of the temperature profile of the helium and the measurement of the appearance of the resistive voltage were used to determine the current sharing temperature. In Fig. 15 a nearly straight line is drawn in a B-

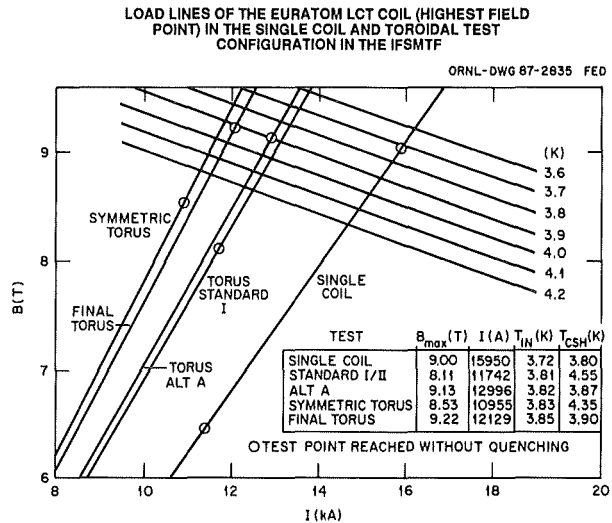


Fig. 13: Load lines of the Euratom LCT-coil in its single and toroidal test configuration in the Int. Fus. Superc. Magn. Test Facility (IFSMTF).

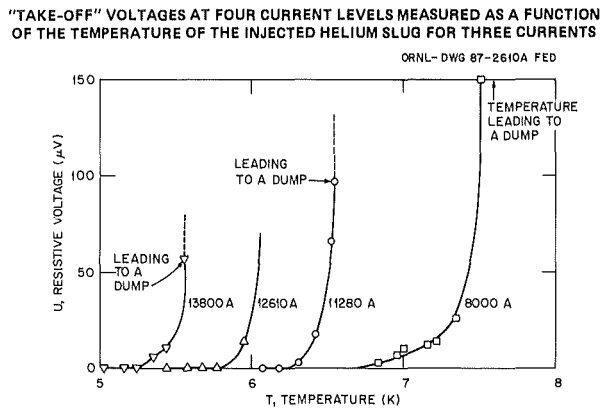


Fig. 14: "Take-off" voltages for different current levels measured by the injection of heated helium gaseous slugs.

T_r diagram derived from short sample measurements. From Fig. 14 transition points for 0 μV and 10 μV were taken and linearly extrapolated up to 9 T. Taking into account all extrapolation and measuring accuracies the agreement with the expected value, the 9 T point obtained and the current sharing temperature measurements is fairly good.

The coil was intentionally quenched three times during the current-sharing measurements. Based on the resistive voltage and the fact that the temperature was below 20 K

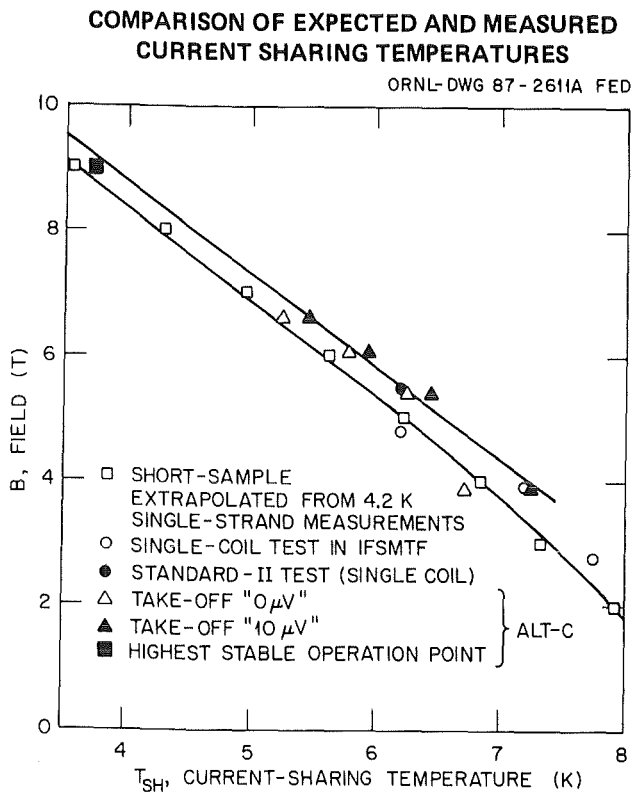


Fig. 15: Comparison of measured current-sharing temperatures with those extrapolated from the short-sample strand measurements.

before the dump, the propagation velocity was calculated. The propagation velocity increases more weakly than with I^2 .

The temperature profile of the expelled gas was measured too. Analysis of the data showed that this temperature represents the hot spot temperature of the conductor.

The results are summarized in Fig. 16. The small flow rate contributes considerably to reduction of the hot spot temperature, which can be determined by measuring the temperature of the expelled gas. The measured and calculated values are in agreement within 5 K.

Mechanical properties were investigated by using strain gauge rosettes on the coil case surface and displacement transducers, which measure the gap between the winding and the coil case. The equivalent stresses, especially at the test in the IFSMTF, are in fair agreement with finite element calculations. For the single coil at 100% and 140% rated current, the stresses increase by a factor of 2 as expected (Fig. 17). Similar to the TOSKA test, some deviations occurred in the straight section. Nonlinearities were not observed.

The coil experienced its highest central force of 54 MN in the toroidal configuration in the ALT A test (highest field). The winding was compressed in such a way that gap between

COMPARISON OF MEASURED AND CALCULATED "HOT SPOT" TEMPERATURES BY THE EXPELLED HELIUM GAS vs CURRENT SQUARED

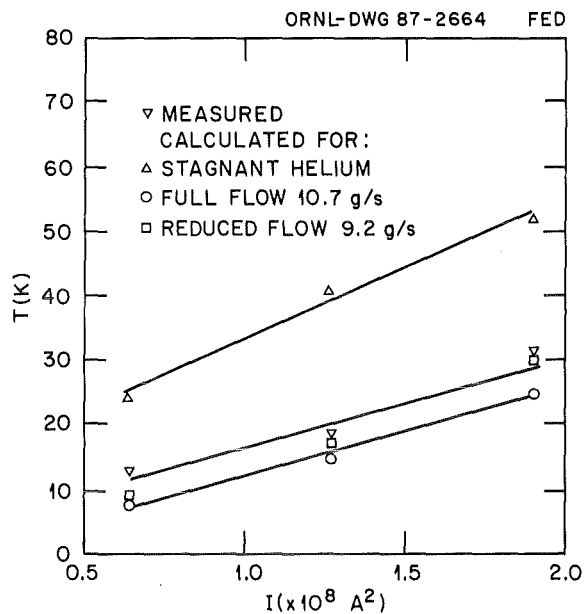


Fig. 16: Measured and calculated hot spot temperatures for the Euratom LCT conductor with flowing and stagnant helium.

COMPARISON OF THE EQUIVALENT STRESSES OF THE EURATOM LCT

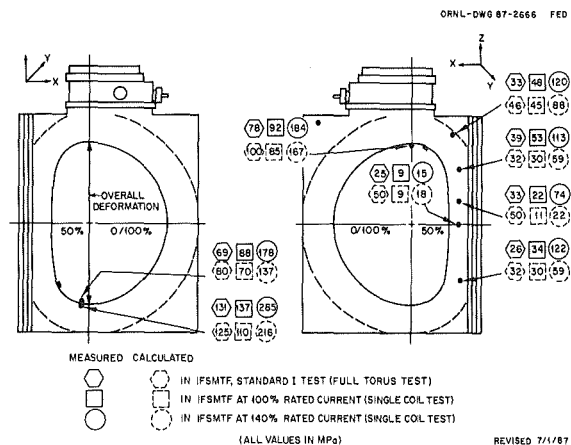


Fig. 17: Equivalent stresses measured on the coil case surface in comparison with predictions from the finite element calculations.

winding and coil case reached 2.52 mm. Finally in the last torus test the field was increased to 9.1 T at the reference point and 9.2 T maximum field in the smallest curvature. These values were obtained by the Euratom-LCT-coil with 56% of the design mass flow rate of 150 g/s and 11 MN out-of-

plane force. Much higher out-of-plane force experienced the coil in the ALT B test series where one coil of the toroidal configuration was uncharged. The Euratom-LCT-coil experienced an out-of-plane force from both sides. When the Westinghouse coil was at zero current 23 MN overall out-of-plane force acted on the coil front side. An out-of-plane force of 26.6 MN was obtained when the CH-coil was without current. This was the highest out-of-plane force in the test series at all which a coil was loaded with. The first evaluation showed that highest equivalent stresses were measured at locations as expected. This were 138 MPa in the first load case and 165 MPa in the second one. Both values were lower than expected according to the calculations. In the frame of Safety Tests "hot spot" measurements on the Euratom coil were performed for a lower mass flow rate and a delayed dump according to the same evaluation procedure used in ALT C test (Fig. 16). The evaluation of the obtained results is being in progress. The loss of the forced flow cooling was investigated by valving off and on the mass flow in steps of increasing duration in time. This procedure was performed without current as well as at two current levels (8030 A and 11 400 A). Temperature profiles were measured first for the mass flow rate valving off in one cooling circuit and then for the whole coil. No critical items were found for mass flow rate stoppage in one cooling circuit. All temperatures remain far below the current sharing temperature at this location (joints, current feedthrough). The most critical item for valving off the total flow was the warming up of the stagnant helium in the supply piping. At the 8030 A current level the valving off and on of the flow was practised up to 20 minutes without any problem. The helium slug injected had a temperature which was every time below the current sharing temperature at this current level. The interruption of the total mass flow through the coil was performed at the 11 400 A level in the following way. The coil was held 10 minutes at full current. Afterward it was ramped down to zero without any forced flow cooling. The coil stayed superconducting. No signs of a normal region were observed. In this experiment the coil was 1 hour without active cooling. It was successfully demonstrated that for the Euratom coil design the loss of the forced flow cooling is no critical item.

The experimental operation of the Large Coil Task was successfully finished on September 3, 87. The facility is now being warmed up to room temperature. It was demonstrated that such a large system can be kept cold and operable over 20 months. The system had enough redundancy that the most of the arising problems were handled and overcome. The EU-coil demonstrated by its excellent performance that the applied technology has the maturity for systems like NET.

Staff:

G. Friesinger
S. Gauss
W. Herz
W. Maurer
L. Siewerdt
A. Ulbricht
F. Wüchner
G. Zahn

References

- /1/ G. Friesinger et al., Testing of the Euratom LCT Coil in the Toroidal Arrangement of International Fusion Superconducting Magnet Facility without External Pulsed Field and with them and an Extended Single - Coil Test
Proc. MT-10, Boston Sept. 25-29, 1987 USA
- /2/ W. Herz et al., Results of the Test of the European LCT Coil in the TOSKA facility.
IEE Trans. Magn. MAG 21, pp. 249-252, 1985

M3 Development of High Field Composite Conductors

Effect of Transverse Compressive Stresses on J_c of Nb_3Sn Wires

The effect of transverse compressive stresses on Nb_3Sn wires has been studied for the first time in connection with their use in toroidal fusion coils. A new test rig was built where the sample is submitted to both, electrical current and transverse compression. The lower part of the rig with the dimensions of $68 \times 8 \text{ mm}^2$ fits into the magnet gap and is shown in Fig. 18. The transverse force, F_t , which acts symmetrically on both flat sides of the conductor (0.85 mm) by a pair of pressure blocks, is oriented perpendicularly to the field, B , and the current, I . The actively compressed length of the sample amounts to 10 mm and is located in the midplane of the magnet. The transverse compressive stress on the sample is calculated from the transverse force, F_t , and the compressed cross section of the sample. The latter amounts to $10 \times 0.85 \text{ mm}^2$, where 0.85 mm is the width of the sample. F_t was measured directly between the pressure blocks, replacing the sample by a quartz miniature force transducer at low temperature. Simultaneously the axial force, F_a , was measured with a load cell on the pull rod at the top of the test rig at room temperature (not shown in Fig. 18) and compared with F_t . The limits for F_a and I for this test rig are 1.2 kN and 200 A, respectively.

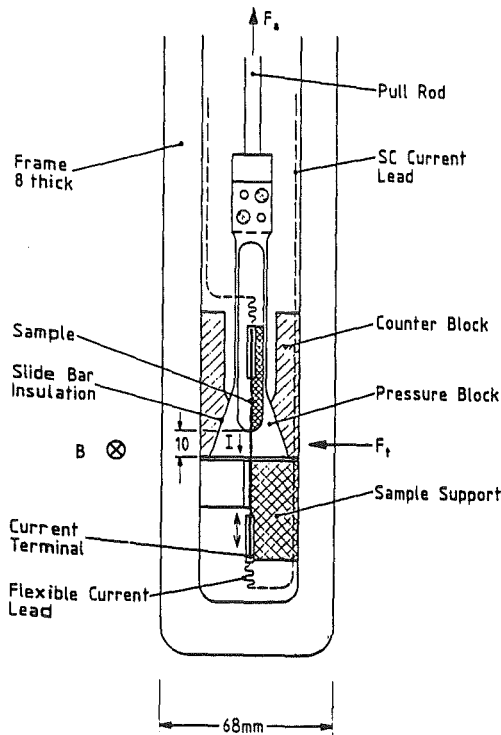


Fig. 18: Lower part of test rig for applying transverse compression on a wire.

The normalized critical current, I_c/I_{cm} , versus applied transverse compression, σ_t , for the flattened Nb_3Sn wire is illustrated in Fig. 2. I_c/I_{cm} exhibits a slight maximum at σ_{tm}

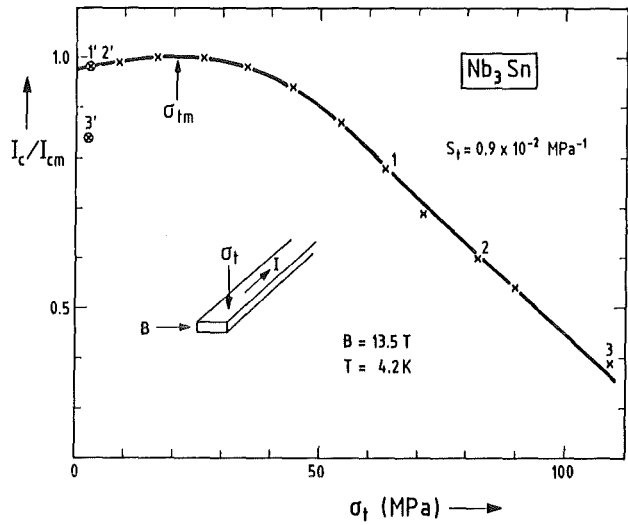


Fig. 19: Normalized critical current I_c/I_{cm} , versus transverse compression, σ_t , for a binary Nb_3Sn wire at 13.5 T and 4.2 K. Complete reversibility is observed up to point 2 ($\sigma_t = 80 \text{ MPa}$).

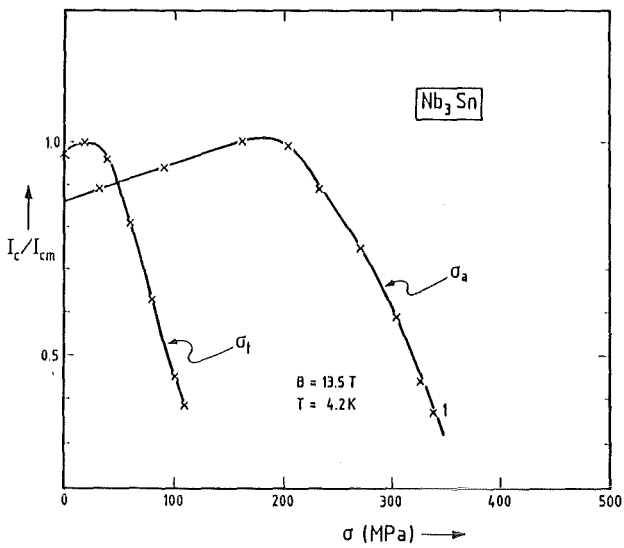
= 21 MPa and decreases drastically to 0.5 at 100 MPa. In order to check the irreversible behaviour the pressure on the sample was removed three times, at the points 1, 2 and 3 in Fig. 19. From point 1 and 2 I_c/I_{cm} recovers completely to point 1' and 2', respectively, but after releasing from point 3 one observes at 3' a 15% degradation of I_c . An irreversible characteristic of I_c thus occurs between point 2 and 3, at a compressive stress of $\sigma_{t, irr} > 80 \text{ MPa}$ for this sample.

The effect of transverse compressive stress appears to be much stronger than that of tensile axial stresses. As illustrated by Fig. 20., the degradation of J_c after transverse compression is even effective at small stresses. At 50 MPa, it is of the order of 20%. The present results are of primary importance for the application of Nb_3Sn wires in toroidal fusion magnets. In particular the conductor concept has to be chosen in order to reduce peak transverse stresses.

Experiments in the HOMER Test Facility

In HOMER a background field of up to 19 T in a bore of ~ 2 cm can be obtained. This background field is applied to measure the superconducting properties of various Nb_3Sn conductors. Thus, the potential of obtaining field strengths far in excess of the limit of $NbTi$ (~ 11 T) shall be explored.

In particular a $(NbTa)_3Sn$ conductor in the bronze route technique and a $(NbTi)_3Sn$ conductor in a Nb tube technique with internal tin diffusion were tested. Both conductors have very specific properties: The $(NbTa)_3Sn$ conductor has a smaller critical current density but a steeper resistive



Staff:

W. Barth
M. Beckenbach
M. Br nner
P. Duelli
U. Fath
R. Fl kiger
S. F rster
F. Gauland
S. Gauss
W. Goldacker
A. Kling
B. Lott
G. N ther
A. Nyilas
H. Orschulko
H. Raber
T. Schneider
W. Specking
S. Stumpf
P. Turowski

Fig. 20: Normalized critical current I_c/I_{cm} , versus transverse compression, σ_t , and axial tension, σ_a , for a binary Nb_3Sn wire at 13.5 T and 4.2 K.

transition at the critical current value whereas the $(NbTi)_3Sn$ conductor has a high critical current density but a low resistive transition expressed in a n-value of about 20 compared to 40 of the first conductor. With overall current densities in commercial available conductors between $1 \times 10^4 A/cm^2$ and $1.5 \times 10^4 A/cm^2$ at 18 T and 4.2 K both conductors are useful for high field magnets. Specific requirements as copper content, resistivity ratio, n-value or mechanical properties may favour the one or other conductor configuration.

The influence of tensile stresses due to the Lorentz forces on the performance of the above conductors was studied. For this investigation the conductors were tested in single layer coils of 40, 80 and 150 mm diameter up to a field of 12.5 T. The high field test facility was modified with a sacrifice in magnetic field to get a larger bore diameter. The results showed that at a stress level of 120-130 MPa training effects limit the performance of the conductors.

M 4 Superconducting Poloidal Field Coil Development

The aim of task M 4 is to develop and test a model coil Tore Supra and NET to simulate load conditions. The model coil of 3 m ϕ is under design to be operated in the KfK-Toska test facility in 1988. Both tasks M 4 and M 8 are joint efforts of KfK and CEA.

Conductor Fabrication

The industrial contract for the fabrication of the conductor has been placed to Vakuumschmelze, Hanau. Two different types of conductors are foreseen. Half of the length will have a CuNi strip wrapped around the subcables, the other half will have a glass/Kapton/glass tape instead of the CuNi-strip filled and covered with epoxy resin in order to glue the subcables to each other. The production length will be 2x25 m to assure the fabrication procedure and 4x145 m final production. Difficulties in the development and fabrication of the quarter section have caused an overall delay of the conductor fabrication of 6 months.

The cable production will start as soon as the outer steel section production has been successfully completed. So far the required lengths of the quarter sections have been produced with the exception of a final drawing step. This step still requires an additional adjustment of the last drawing die.

Stability Experiment

A round cable out of the sample production with CuNi strips around the subcable has been successfully bent to the needed geometry. It will be inserted into a pulsed dipole magnet. A transport current will be induced by the transformer principle using a small superconducting solenoid (Fig. 21). The stability of the cable will be investigated at transport currents up to 24 kA in pulsed dipole fields as soon as the connections of the conductor ends have been manufactured.

2-Phase Flow Experiment

A fourth test run was made. This test was done to gain experience with the operation of a LHe pump. For a first test the Linde pump was successfully used.

The test arrangement proved satisfactory. It will therefore be also applied for the model coil.

The void measuring cell and the heating section made by CEA were successfully operated, too. Volume related against mass related vapor content were measured over a range of massflow between 1 and 5 g/s. In the same variation range of mass flow the temperature difference between wall and fluid was determined in the heating section with a heat load of up to 500 W/cm². The use of the pump showed a considerably reduced pressure drop during a heat pulse as compared to the

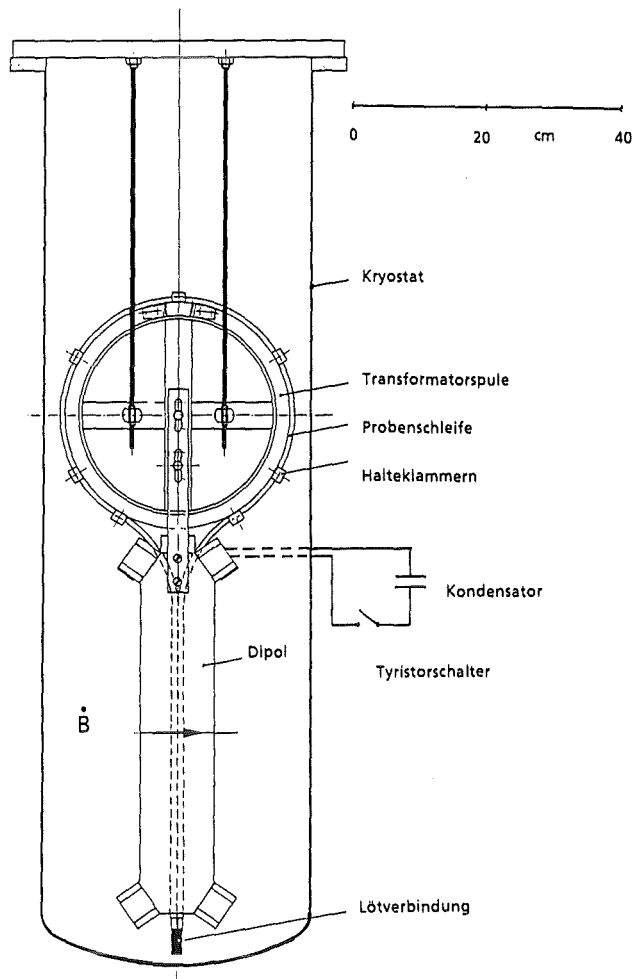


Fig. 21: Polo cable loop inside the stability test facility

experiments with no pump. A pump will therefore be used during the model coil experiment.

In agreement with CERN, we have started to build a pump, the type of which is used successfully since several years and for which CERN has delivered the drawings to KfK. Despite the clear separation of gas and liquid in the tube the temperature difference between wall and fluid is very low along the circumference of the tube in all our load cases and needs therefore no specific consideration for the operation of the model coil.

The two phase flow experiment has been successfully terminated. A good understanding of the two phase flow in the operation regime of the model coil and for thermal loads far above has been gained.

Material Investigation

In a joint effort of KfK and Alstom shear tests of the coil insulation materials have been performed to compare pure glass/glass with glass/Kapton/glass insulations at cryogenic temperature. In order to gain more insight into the reasons for the different levels of shear strength when using different types of test specimen finite element calculations have been performed in parallel. We now can clearly state, that only

three point bending shear specimens can give a realistic picture of the material strength in our case. With that type of specimen, we reached more than 50 MPa shear strength at LHe-temperature as it was aimed at with the pure glass/glass insulation which we prefer.

Measurements of the electrical insulation properties showed, that partial discharges start above the nominal voltage of 5.7 kV, which is a very satisfactory result. Potential calculations of the various electrode geometries and optimisation of the high voltage components both for the model coil and for testing purposes is an ongoing activity together with the University of Karlsruhe.

Electrical Power Switch and Test Circuit

The 23 kV/30 kA test circuit including all switches has been installed. Due to the requested high flexibility and safety of the circuit, the acceptance test is a very cumbersome and ongoing activity which still poses a lot of problems to the supplier.

Data Acquisition, Instrumentation and Test Procedure

For instrumentation and signal conditioning of the model coil it must be distinguished between sensors at high voltage (23 kV rated voltage) and at low voltage potential. The isolated amplifier and signal transmission lines must be suitably designed. According to the test procedure of the coil, three scanrates (micro-seconds, milliseconds, seconds) due to the signal rise time at the different operation modes will be required. For each operation mode a fixed amount of transient channels is assigned. The operation modes include

- charge up and down, inverter mode
- safety discharge
- stability investigation, 10 Hz current pulsing, high voltage discharge into the short circuit ring (full and half coil discharge).

For that rather complex scenario the data acquisition system has been designed. The programming of the scanning operations, the data storage and data manipulations, like graphic displays, live display, are started for the application on a VAX computer. The signal amplifiers and transmission lines are under development.

Staff:

H. Bayer
F. Beckenbach

I. Donner
P. Duelli

S. Förster
P. Gruber

W. Heep

U. Jeske

H. Katheder

J. Lühning

G. Nöther

A. Nyilas

U. Padligur

R. Rietzschel

L. Schappals

G. Schenk

C. Schmidt

K. Schweickert

E. Specht

H.-J. Spiegel

F. Süß

M. Süßer

A. Ulbricht

R. Wagner

D. Weigert

F. Wüchner

G. Würz

M 8 Design and Construction of a Poloidal Field
Coil for TORE Supra as NET-Prototype Coil

The objective of the task is the development and test of an Equilibrium Field Coil (EF Coil) with parameters relevant for NET. The reliable operation of a superconducting PF-coil shall be demonstrated in a real tokamak environment with the rapid field variations due to start up, plasma position control and disruptions. The development has to confirm the coil construction process proposed for NET on a fairly large scale

For this purpose, the upper ring coil "E_h" of TORE SUPRA will be replaced by a superconducting coil "EHS". Design and construction will be based on the results of the already running task M 4.

Design of the TORE SUPRA Coil "EHS"

Design proposals have been worked out for

- the coil winding including the connection area with the LHe supply tubes, the pancake connections and potential breaks.
- the cable terminations in a vertical dome of the vacuum vessel
- the vacuum vessel including supports to the iron yoke and insulating sections to limit the eddy currents.

Eddy current calculations have been carried out by the University of Graz.

Staff:

F. Beckenbach

S. Förster

U. Jeske

H. Katheder

L. Schappals

G. Schenk

M9 Structural Materials Fatigue Characteri-
zation at 4 K

Joining of structural materials

Best consumables for optimized weldments of the preferred steel types should be selected by weldment tests. All hot cracking tests with the delivered five different consumable welding wires were completed. Impact tests (ISO-V notch) carried out at 77 K with the weld metal indicate a reasonable correlation between the impact values and hot cracking susceptibility. The evaluation of these test results is ongoing. Preliminary evaluations show that only three wires out of five are suited for further use. These wires of the three different vendors together with three different heats were the starting point for the production of 30 mm thick weld seams. Variation of the joint configuration showed a V-opening of 60° as an optimum value. Weldings with 45° openings gave poor results. Weld seams of 1000 mm length were produced with the already supplied three types of austenitic stainless steel plate material. The overall dimension of each welded plate was ~ 1000x500x30 mm³ with the butt weld in the midsection. The weldments were released by plasma jet cutting for further machining of different specimens such as tensile, fracture and fatigue specimen.

Bulk materials characterization

For the 4 K bulk materials characterization fracture toughness and tensile specimens were already machined from the first delivered plate material, type 1.4429. This plate material was also supplied to NBS (Boulder) for the Round Robin testing by different laboratories.

Cryogenic test facility

The flow cryostat with the integrated 50 kN load frame was delivered. The cool down tests carried out with liquid helium showed a liquid helium consumption of ~ 20 liters per cool down to 4 K. At He temperatures, an evaporation rate of 3 l/h was found. First mechanical tests will be carried out after delivery of the 25 kN servohydraulic unit.

Staff:

S. Fischer

H.P. Raber

A. Nyilas

M 12 Low Electrical Conductivity Structures
Development

Thick walled plate materials

The development of a 40 mm thick glass fiber reinforced plastic material was started. Materials specification were E-glass fibers in form of glass fabric with a suitable epoxy resin for low temperature application. This plate material is already delivered and machining of test specimens is ongoing. Tests will be carried out with respect to the flexural and shear properties.

Advanced fiber reinforced materials

Three hybrid materials with different glass/carbon fiber contents were industrially manufactured. These plates were 4 mm thick and were developed with the purpose of using the potentials of carbon fibers high modulus and the high straining capacity of the glass fibers. The matrix used was manufacturer related for a specified use at low temperatures. The carbon ply was placed in all three cases in mid section and the thicknesses were varied between 2 mm and 0.5 mm. These plates are now delivered and the machining of test specimens was started. Specimens will be prepared for flexural and shear testings at 77 K and 4 K. Tests will be carried out in the next future.

Staff:

S. Fischer

H.P. Raber

A. Nyilas

MAT 1.6 Development and Qualification of Type 1.4914
Base metal Properties

After the procurement of the NET-heat (Nr. 53645) of Type 1.4914, the composition of which is given in Table 7, semifinished rods and plates with dimensions requested by the different EC laboratories have been manufactured. Most of the EC labs and industrial partners associated with the research programs on Type 1.4914 material have in the meantime been supplied with material.

In order to recommend a final heat treatment for this fully martensitic steel investigations have been started in which the influence of austenitizing temperature (varied between 1050 and 1175°C) and the follow on tempering treatment (680-780°C) on microstructure and toughness are studied. Especially δ - ferrite formation, prior austenite grain size and structural homogeneity are investigated. The results indicate, that in addition to the above heat treatment parameters, also the fabrication steps such as rolling, drawing, forging, and tempering used for the production of plates and rods with variable thicknesses and diameters can influence the microstructure and the δ - ferrite formation.

For the material in all dimensions the following final heat-treatment procedure 950°C/2h + 1075°C/30min + 750°C/2h produces a homogeneous, δ -ferrite free and fully martensitic structure. Therefore this heat treatment should be used in further experimental investigations as a reference heat-treatment for steel 1.4914. The entire heat-treatment procedure is given in Table 8.

1.NET	
Charge.Nr. 53645	
C	0.14
Si	0.37
Mn	0.76
P	0.005
S	0.004
Cr	10.5
Ni	0.92
Mo	0.77
Fe	Rest
V	0.20
Nb	0.16
Al	0.054
B	0.0085
N	0.020
Co	0.01
Cu	0.015
Zr	0.059

Table 7: Chemical composition of 1.4914 steel

I. Grain Refining Heat Treatment

Annealing Temperature 1)	950°C
Annealing Time 2)	2h
Cooling Rate 3)	> 30K/min.
Cooling down to Room Temperature (RT)	

II. Austenitizing Heat Treatment

Austenitizing Temperature 1)	1075°C
Austenitizing Time 2)	1/2h
Cooling Rate 3)	> 30K/min.
Cooling down to Room Temperature (RT)	

III. Tempering Heat Treatment

Tempering Temperature 1)	750°C
Tempering Time 2)	2h
Cooling Rate 4)	< 15K/min.
Cooling down to Room Temperature (RT)	

Table 8: Instructions for the Final Heat Treatment of 1.4914 Martensitic Cr-Steel

- 1) - the heat treatment have to be done in vacuum or reducing atmosphere.
- 2) - As a rule the performance times for sheets with a thickness above 10 mm and for rods with a diameter above 15 mm increase about 1-2 minutes per mm increase in thickness or diameter, respectively.
- 3) - Cooling in normal atmosphere, blowing if necessary.
- 4) - Furnace cooling.

Staff:

B. Dafferner

C. Wassilew

MAT 1.9 Pre- and Post-Irradiation Fatigue Properties
of 1.4914 Martensitic Steel

Thermal cycling of large components is a serious problem for the designer. The structure considered in the present case is the first wall of a fusion reactor. Its surface, in the present design concept, will be subjected to radiation heating from the plasma facing graphite tiles which may lead to severe thermal stresses. Due to the discontinuous operational mode thermal cycling will generate oscillating temperature gradients. These, depending on the loading conditions, will cause elastic or elasto-plastic reversed deformation giving rise to thermal fatigue which at present is considered as the most detrimental lifetime limiting phenomenon for the structure considered. The investigations of MAT 1.9 are devoted to this problem.

In the absence of stress gradients (idealized case) the so-called mechanical loading equivalent for thermal cycling can be obtained from calculations. Such investigations, in which calculated strain cycles are imposed to test specimens at a constant temperature in MAT 1.9, precede the proper thermal cycling fatigue tests. These were already reported in the previous Semianual Report. In reality, however, the loading of the first wall is very complex. Beside the thermal gradients the structure is additionally loaded by irradiation. The simulation of the combined influence of irradiation and thermo-mechanical loading and its influence upon the lifetime is the aim of investigations conducted within the Programs MAT 2.2 and MAT 9.2. The actual studies to be performed within MAT 1.9 are:

- Development of appropriate test specimens and test methods respectively
- The results therefrom should provide the data basis for:
 - a) design calculations and b) for MAT 9.2; and finally
- they should contribute to the understanding of the physical mechanisms involved.

Tubular specimens made from the martensitic steel Type 1.4914

The tubular so-called H-GRIM specimens (see Fig. 22) to be used in Mat 1.9 were derived from the original solid GRIM specimens. Till now several dozens of H-GRIM specimens made from the austenitic steels (mainly Type AISI 316) were successfully tested. Their advantages are:

- a) Geometrical stability during cyclic push-pull loading.
- b) Plastic deformation is restricted to a small "active deformation volume" which assures a very good reproducibility of the plastic quantities examined.
- c) Convenient stress distribution, which in the active part corresponds to that of ideally cylindrical thin-walled tubes.
- d) Transparency for high energy protons.

- e) Good coolability in irradiation and thermal cycling experiments.

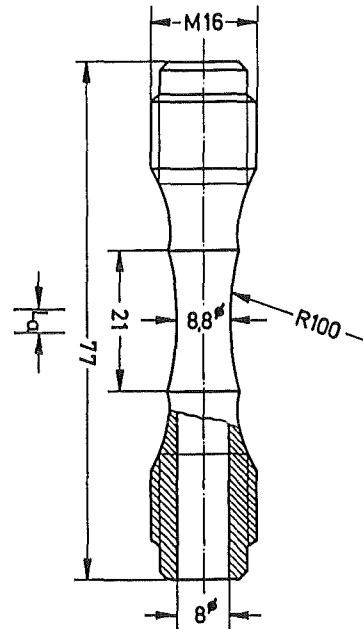


Fig. 22: H-GRIM (Hollow-GRIM) specimen

At present, within the NET Project a modification of the martensitic 12% Cr steel W.Nr. 1.4914 is being considered as a potential structural material. Because special thermo-mechanical treatments are involved in the fabrication process of H-GRIM specimens it was necessary to check whether these treatments can be carried out without affecting neither the sample quality (i.e. the high precision requirements) nor the original material properties. The procedure applied has proven successful, leading essentially to the same quality of samples as achieved with H-GRIM specimens fabricated from AISI 316L. However, as compared to these, the number of cycles to failure N_f is for the martensitic H-GRIM specimens much less than for the AISI 316L H-GRIM specimens, although for the same conditions (temperature, total strain amplitude and strain rate) the N_f -values for the solid specimens fabricated from both the materials are approximately the same. However, irrespective of the type of specimen the cyclic work hardening behaviour for both the materials is different. Further systematic examinations on this subject seem necessary.

Strain cycling of H-GRIM specimens under azimuthal temperature gradients

The factor which restricts the applicability of H-GRIM specimens in dual-beam irradiation experiments is connected with the different effective wall thickness of the H-GRIM specimens for the penetrating proton beam. This leads to an anisotropy of radiation damage which is associated with

anisotropic heat generation. As a consequence azimuthal temperature gradients are built up in the active zone of these specimens. Because the geometric stability of strain cycled H-GRIM specimens is of principal importance in in-beam experiments the influence of azimuthal temperature gradients upon the stability of cycled specimens against buckling was examined in the present investigation.

The experiments, conducted in a closed loop testing machine, were performed on AISI 316L H-GRIM specimens by means of a radiation furnace additionally equipped with a light spot heating. Azimuthal gradients up to $50\text{ }^{\circ}\text{C} / 180\text{ }^{\circ}\Delta$ could be achieved at different temperatures. Several experiments were conducted at 350 and 550 $^{\circ}\text{C}$ with a total strain amplitude of 0.6% and gradients between 40 to 50%

$180\text{ }^{\circ}\Delta$. Under these conditions in all the tests the T-gradients did not affect the geometric stability of the H-GRIM specimen. There are indications, however, that as compared to specimens with a homogeneous azimuthal T-distribution, depending on test temperature, T-gradients may increase the lifetime of strain cycled specimens. Further experiments are needed to clarify this indication.

Preliminary tests conducted with martensitic H-GRIM specimens have shown good stability in push-pull testing. In a next series of experiments the behaviour of SH-GRIM specimens (see below) subjected to thermal gradients up to $120\text{ }^{\circ}\text{C} / 180\text{ }^{\circ}\Delta$ will be examined. The investigations will be accomplished by tests with martensitic H- and SH-GRIM specimens.

Temperature cycling experiments

For given goals the choice of the thermal cycling procedure will mainly depend of the geometry of the test specimens. In the present investigations H-GRIM specimens will be used. The geometry of this specimen triggers the plastic deformation which, as already mentioned, takes place in the middle section of the specimen (active zone).

The geometry of the specimen considered is appropriate to heat them "ohmically" by a.c. current. Both ends of the specimen are rigidly attached to the loading frame. Accordingly the specimen is constrained for tension as well as for compression. The upper end of the specimen is connected to the force measuring device (load cell). During the test the mutual distance of specimen's ends remains constant. The scheme of the test facility is shown in Fig. 23.

For the "fixed end" condition the net axial strain ϵ_n associated with thermally cyclic loading is zero, independent of time. For the analysis ϵ_n is separated into three components: the thermal strain ϵ_T , the elastic strain ϵ_e and the plastic strain ϵ_p . According to the above it is

$$\epsilon_T + \epsilon_e + \epsilon_p = \epsilon_n = 0$$

and therefore

$$\epsilon_T = \alpha\Delta T - (\epsilon_e + \epsilon_p)$$

where α is the linear thermal expansion coefficient. In order to register the cyclic stress/strain curves the stress σ is

calculated from the force F . The corresponding strain $\epsilon_e + \epsilon_p$

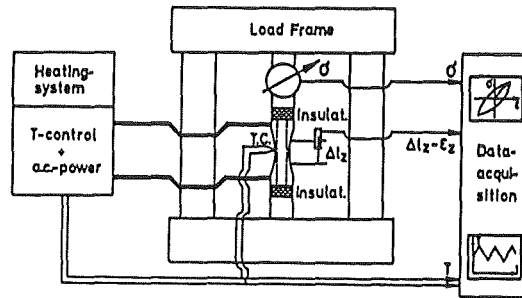


Fig.23: Sketch of test facility

will be measured by means of an extensometer attached to the shoulders of the specimen. In order to improve the precision of the axial strain value $\epsilon_z = \epsilon_e + \epsilon_p$ the active length L_n must be estimated as good as possible. This will be done by means of the functional relationship between the circumferential strain ϵ_c and the (unknown) axial strain ϵ_z . The data acquisition system is a computer controlled real time device which automatically records the temperature T , the force F and the axial displacement of the extensometer. The system contains the feeding electronics and amplifiers for the load cell as well as for the extensometer. These data can be read out during the test and analysed by an already available program.

Within the time reported:

- The heating devices were delivered and checked.
- The loading frame was designed and is now under construction in the workshops. The selection of load and extension measuring devices is accomplished and will be ordered.
- Calculations of the axial temperature distribution were performed and compared with experimental measurements conducted with a heating device incorporated into a closed loop testing machine serving as a pilot thermal cycling test rig. The agreement between calculations and measurements is very satisfactory.

The first test rig is expected to operate at the end of this year. The remaining 9 test rigs will be installed successively during the next year.

Considerations on an alternative test specimen

As already mentioned above the applicability of H-GRIM specimens in the Dual Beam Experiment is limited, by some anisotropy in radiation damage, heat deposition and He-implantation. Because from the usual experimental set-ups only data are available about the integral mechanical behaviour, the question arises how to analyze and interpret this integral data which finally should give information about the in-situ influence of irradiation upon particular plastic properties.

Considerations have therefore been made on a new type of specimen which is derived from the H-GRIM specimen by

cutting out shell-like segments. Accordingly, the so called SH-GRIM (Segmented Hollow-GRIM) specimen consists of two tubular parts connected by shell-like segments, the remainder of the tube.

In order to provide an analysis of integral deformation data, calculations have been carried out for SH-GRIM specimens subjected to different deformation procedures. Assuming adequate homogeneity plastic quantities of the individual segments can be calculated from the integral value (the only one measurable on the SH-GRIM specimen) provided the corresponding value of one of the segments is known. This may be achieved by differential testing when - in one experiment - under otherwise known loading conditions only one of the segments e.g. is irradiated.

A strain cycling performance test has successfully been carried out with an AISI 316 L SH-GRIM specimen up to now. Some slight improvements of the fabrication process seem necessary. In order to compare calculations with experimental results a series of different deformation tests would be required, in particular with the 1.4914 martensitic steel. Some other technical problems (e.g. cooling) would have to be solved before this new type of specimen could be introduced in the Dual Beam testing programme.

Staff:

W. Baumgärtner

M. Bocek

C. Petersen

D. Rodrian

W. Scheibe

R. Schmitt

H. Schneider

W. Schweiger

MAT 1.11 Post-Irradiation Fracture Toughness of
Type 1.4914 Martensitic Steel

The target of the MAT 1.11 activities is to study the influence of fission neutron irradiations on the impact properties of 1.4914 material. Emphasis is given to the problem of DBT-temperature shift and to an eventual change of impact energy as a function of irradiation temperature and neutron fluence. In addition, radiation hardening and post irradiation annealing behaviour are studied by tensile and hardness tests.

In accordance with the planning schedule 90 minaturized Charpy-V-samples from the NET-heat 1.4914 have been prepared for the common JRC-ECN-KfK irradiation SIENA-E-198-14. In this experiment samples with the reference heat treatment as well as other metallurgical treatments, in which the tempering temperature has been varied between 600 and 750°C, are included. Also samples taken in different orientation to the rolling direction of the ingot material have been put into this experiment. Tensile samples with the reference treatment have been manufactured by our ECN colleagues and have also been loaded into the irradiation rig. The irradiation has started. The unloading of low-dose irradiated samples (3 dpa) is expected early 88.

Staff:

B. Dafferner

K. Ehrlich

C. Wassilew

MAT 2.2 In-Pile Creep-Fatigue Testing of Type 316 and 1.4914 Steels

It is intended to study the in-reactor deformation and fracture behaviour of the two candidate structural materials for NET under load cycling in tension. The irradiations will be performed in the central position of KNK II.

The test device shown in Fig. 24 consists of eight tubes which can individually be pressurised and temperature-controlled. It is intended to run the samples at 450 and 500°C resp. with a variation of the inner pressure between 10 and max. 450 bar. For the martensitic steel 1.4914 such a sample geometry was selected ($\phi = 7,6\text{mm}$, $s = 0,5\text{mm}$) that an equivalent maximal tangential stress of 260 MPa can be generated.

During that last year the concept for a suitable pressure supply device was elaborated and the device has been ordered in the meantime. The critical parts which determine the shortest achievable cycle length and the characteristic time for the pressure increase or decrease are the compressor and the throttle tubes of the pressure supply circuit. The throttles are necessary from safety reasons. For the pressure supply a multistep membrane compressor has been selected, which allows cycles of a minimum length of 65 s in case that all eight test samples are operated in parallel in the same mode. During the pressureless phase a minimum hold time of 25 s is necessary due to the limited capacity of the compressor system. In Fig. 25 the characteristic time dependence of such a pressure transient is given for this device. Of course additional hold-times of variable length can be added at maximum and minimum pressure levels. These parameters allow a very good simulation of the stress-cycling in a Takamak-type First Wall.

The manufacturing of the heatable, pressurized capsules made from 1.4914 material needs the development of a joining technique which connects the austenitic tubes from the pressure supply system with the martensitic samples. These joints have to withstand high pressures and temperatures. Up to now good results were achieved by brazing with high Ni-materials. The fixing of the tiny thermocouples at the sample surfaces has not been solved satisfactorily.

It is expected that the open technical problems which are connected with the fabrication of the pressurized tubes made from 1.4914 material can be solved by early 1988. The time schedule foreseen for the delivery of the pressure supply unit is May 1988, so that the parallel out-of-pile tests can start at that date. Irradiation start is then expected by early 89.

Staff:

- K. Ehrlich
- G. Reimann
- L. Schmidt

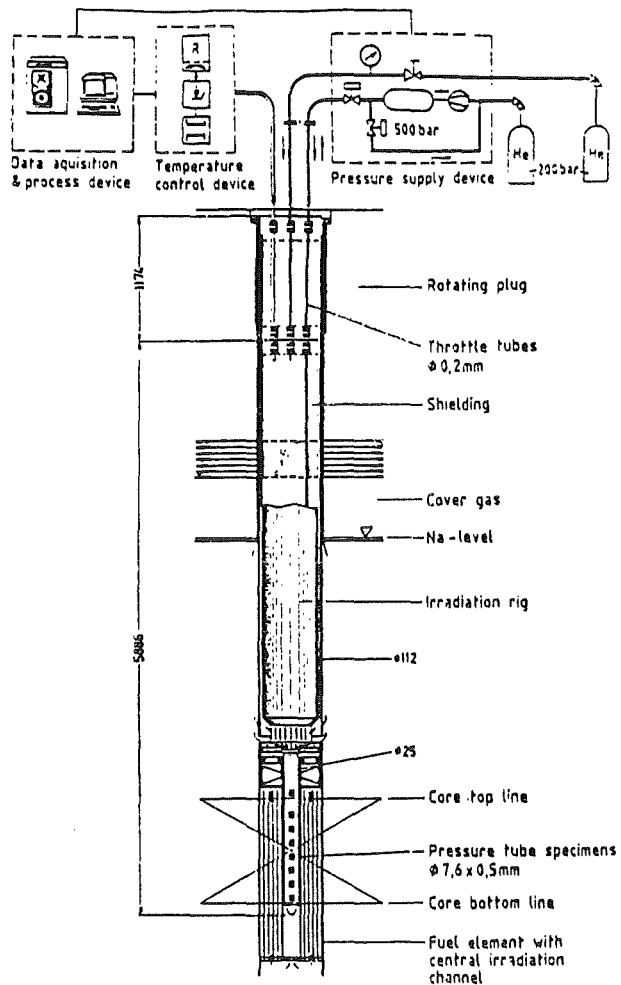


Fig. 24: KNK II Test device for pressurised tube specimens

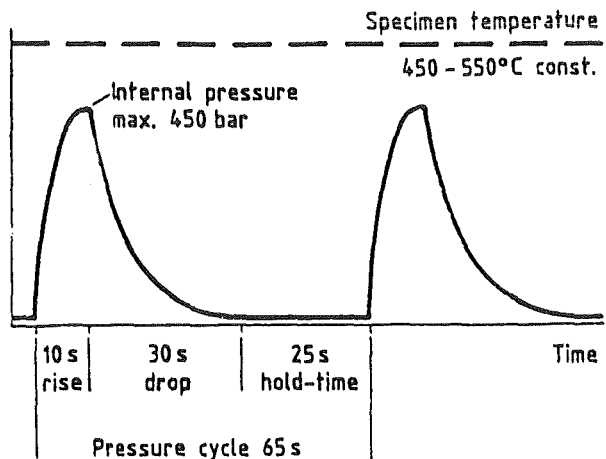


Fig. 25: Characteristic time dependence of achievable pressure transient

MAT 6/MAT 13 Ceramics for First-Wall Protection and for RF Windows

SiC qualities of industrial manufacturers are to be tested concerning the durability of tiles to protect the first wall against plasma instabilities and disruptions. Insulator materials (like Al_2O_3 , $MgAl_2O_4$, AlN) are to be selected with regard to their resistance to thermal crack formation by dielectric loss in RF-windows. These windows shall be applied to separate wave guides for ECR heating from the plasma vacuum.

Concerning the thermal operation conditions of protective tiles on the first wall, a critical temperature limitation may be given by the evaporation behaviour of SiC. Therefore evaporation experiments have been conducted with various hot-pressed and sintered SiC grades under high vacuum. The results are shown in Fig. 26. There was no considerable variation for the different SiC grades. In long-time experiments at 1700 °C (up to 600 h) the sublimation rate approached the lower limit of the scattering band. Qualitative electron microprobe analysis indicated that the evaporation of silicon is dominant. But the sublimation rate given (in mm/year) was estimated from the weight change of the samples assuming simultaneous loss of Si and C.

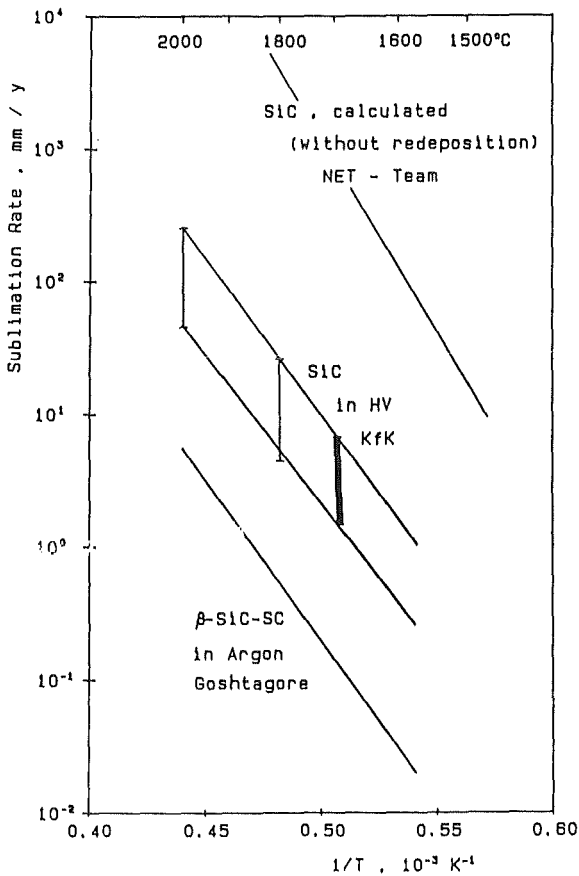


Fig. 26: Evaporation behaviour of SiC

Bending tests were continued on new batches of sintered SiC and HIP-SiC. The mean bend strength and the Weibull modulus were found to be 320 MPa and 4.7 for SSiC, and 490 MPa and 4.7 for HIP-SiC. Considerably higher Weibull moduli

had been measured on bending samples cut from small SiC tiles, and the question remains, whether the Weibull modulus depends on the pressed piece dimensions or on the specific cutting procedure. A systematic examination of the microstructure of different SiC types has been started.

Concerning the investigation of ceramic insulator materials for RF windows, the OSIRIS irradiation ($1 \cdot 10^{22}$ n/cm², 550 °C) of about 40 Al_2O_3 samples for measurements of bend strength, thermal conductivity and thermal shock resistance was finished in April 1987. The transport of the samples to KfK is being prepared.

Measurements of dielectric properties of candidate materials for RF windows were continued at 30 - 40 GHz, and were newly started at 52 MHz and 140 GHz. At 52 MHz dielectric loss was much lower than at 30 - 40 GHz, and particularly low for single crystal Al_2O_3 . Together with measurements at about 10 and 380 GHz in other laboratories, a set of AL23 samples (99.5 % Al_2O_3 , polycrystalline) exhibited a distinct increase of dielectric loss with frequency.

Measurements on neutron-irradiated Al_2O_3 samples after HFR irradiation to $2.6 \cdot 10^{20}$ n/cm² at ≤ 215 °C showed that at 30 - 40 GHz dielectric loss had increased by a factor of 3 - 4 in AL23, but not in sapphire. Strong annealing effects are observed up to 500 °C (Fig. 27), but not below 800 °C at 52 MHz.

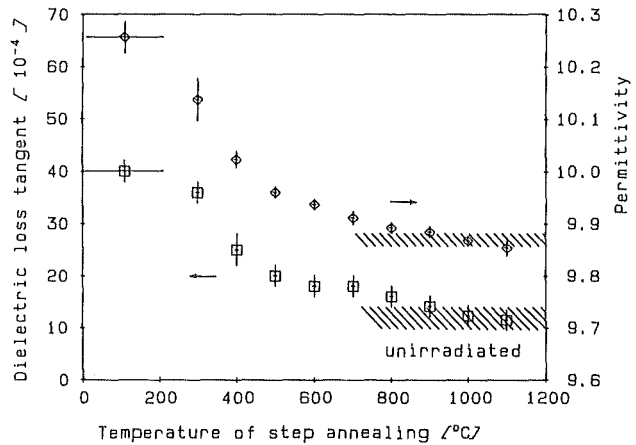


Fig. 27: Post-irradiation recovery of dielectric properties of AL23 (10 h annealing periods).

Staff:
 M. Blumhofer
 W. Dienst
 G. Gausmann
 R. Heidinger
 K.-H. Kurz

Multiphase Materials and Coatings

A separate project, which has not yet been formally introduced into the MAT-programme was started for the development of multiphase ceramic materials in order to improve some relevant mechanical properties like tensile strength, fracture toughness and thermal shock resistance. The conception is based on the strain energy dissipation by introducing high amounts of phase boundaries in an optimized microstructure of ceramic materials in general. It can be applied with special advantage on transition metal carbides, nitrides and borides, and it seems feasible for bulk materials as well as for coatings.

As a first step, the combination TiC/TiB₂ was inspected. It appeared that the coexisting compounds, the microstructure and the constitution of the interfaces have an important effect. Eutectic systems like the TiC-TiB₂ system are apparently favourable for the formation of an optimized microstructure with high atom mobility at the grain boundaries.

Bulk samples were prepared from commercial powders (grain size ~ 3 μm) by ball milling to 1.5 μm, cold isostatic pressing at 300 MPa, presintering (2 h/1000 °C/Ar) and subsequent sintering (6 h/1700 °C/Ar). After presintering they can be treated with tools to get their final shape (Fig. 28). This procedure results in a highly dense material. The shrinkage by sintering is much higher compared to the single phase materials (Fig. 29). The phase boundaries between TiC and

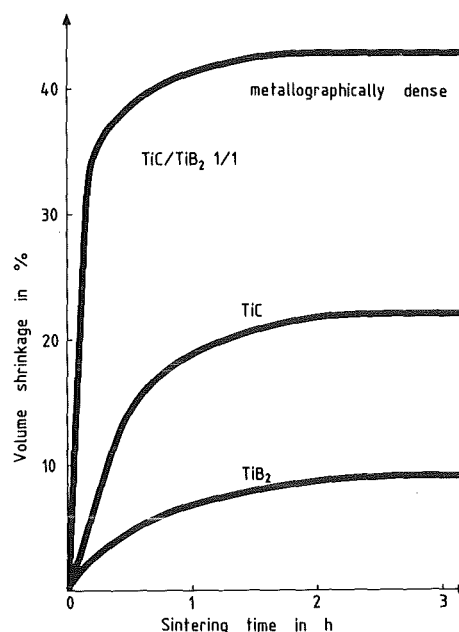


Fig. 29: Sintering behaviour of TiC, TiB₂ and TiC/TiB₂

in the excellent sintering behaviour and the favourable microstructure. First tests show improved thermal shock resistance (quenching from 1000 °C in water) and fracture toughness compared to the single phase materials.

The same material was used for the fabrication of PVD coatings. Multilayer coatings were produced by direct magnetron sputtering with rotating sample holder below the TiC and TiB₂ targets onto stainless steel substrates (AISI 316L and DIN 1.4914). The resistance to crack propagation was measured and found to have a maximum for a single layer thickness of 20 - 50 nm (250 - 100 layers, 5 μm coating).

Staff:

K. Biemüller
 H. Holleck
 H. Janzer
 H. Leiste
 E. Nold
 G. Schlickeiser
 H. Schulz
A. Skokan

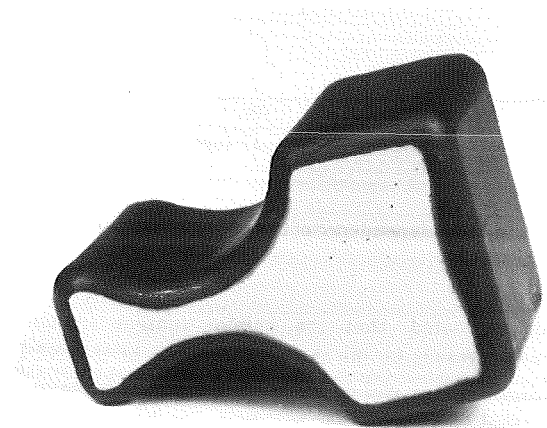


Fig. 28: TiC/TiB₂ tile

TiB₂ grains were analyzed by transmission electron microscopy and Auger electron spectroscopy. The grains of different phases are partly oriented forming coherent phase boundaries. Interfacial layers with Ti, C and B were observed that are not consistent with equilibrium relations. These layers are probably the reason for the high atom mobility resulting

Mat 9.2 Investigation of Fatigue Under Dual Beam Irradiation

The Dual Beam Facility of KfK was developed as a research tool for materials within the European Technology Programme. The Dual Beam Technique allows the production both of damage and helium in thick specimens by simultaneous irradiation with high energy protons (≤ 40 MeV) and alpha particles (≤ 104 MeV) produced by KfK cyclotrons. One of the objectives is to investigate the influence of helium on the mechanical properties of first wall materials.

Tensile specimens of martensitic steel 1.4914 with a gauge size $7.2 \cdot 0.2 \text{ mm}^3$ were homogeneously He-implanted after a heat treatment at $1075^\circ\text{C}/30' + 750^\circ\text{C}/2\text{h}$. A high He-to-damage ratio of 1850 appm/dpa was chosen to separate a possible He-effect from displacement damage. This ratio is far beyond the predicted one for NET (7.7 appm He/dpa). The defect production rate, however, was very similar to the predicted one for NET ($3 \cdot 10^{-7}$ dpa/s). This experimental condition made the irradiations rather time consuming. The experimental conditions are shown in table 9.

Fig. 30 shows the temperature behaviour and Fig. 31 the He-dose dependence of the ultimate tensile strength. Thermal aging at implantation conditions has no visible effects on material ductility and tensile strength. Short time irradiations, with He- concentrations below about 100 appm do not change the tensile behaviour significantly over the whole temperature region investigated.

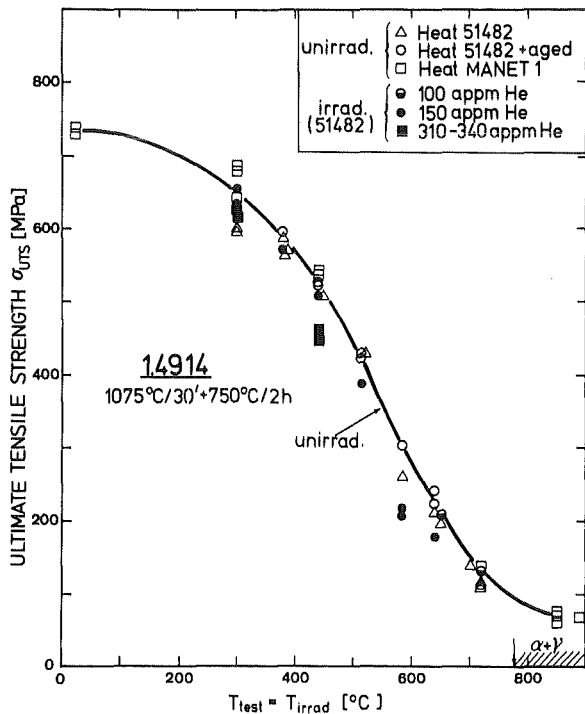


Fig. 30 Ultimate tensile strength of He - implanted and aged control samples

Irradiations beyond this limit with higher He- contents (150-350 appm), reduced the ultimate tensile strength above $\sim 380^\circ\text{C}$ remarkably, whereas the yield strength $\sigma_{0.2}$ is only marginally influenced by the irradiation. This irradiation induced softening is more pronounced with increasing temperature and irradiation time. Tensile tests done at temperatures T_{test} , which deviate from the irradiation temperature T_{irrad} (Fig. 31), show clearly that the extent of the softening is given by T_{irrad} .

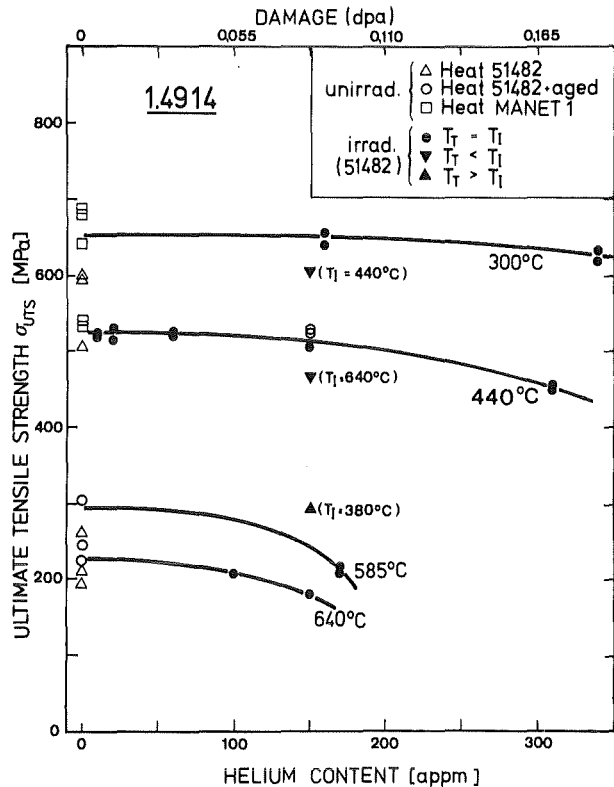


Fig. 31: He - dose dependence of the ultimate tensile strength

It should be noted, that the helium content in this experiments exceeds by far the predicted one of the NET specifications. By the end of phase III (fluence 0.8 MWa/m^2) the estimated helium content will have reached about 80 appm in ferritic/ martensitic steels. From the tensile behaviour we therefore conclude, that even at very high He/dpa-ratios and He-contents up to several hundred appm the predicted hardening- effect of He is completely covered by radiation induced softening. This strength decrease appears obviously already at low damage rates (Fig. 31) and probably reflects a vacancy assisted recovery of dislocations within the lattice.

Microstructural investigations of the tensile tested specimens including transmission and scanning electron microscopy as well as metallographic methods are in progress Fig. 32 shows a SEM fractography of the fracture surface

($T_{\text{test}} = T_{\text{irrad}} = 440^{\circ}\text{C}$, 150 appm He). The observed dimple formation is the same as that of unimplanted control samples and is characteristic for a ductile and transgranular fracture mechanism.

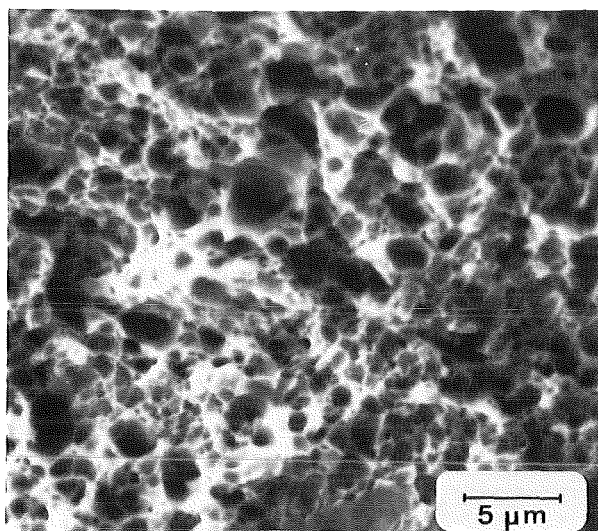


Fig. 32: SEM fractography of steel 1.4914 irradiated (150 appm He) and tested at 440°C.

Temperature range	300 - 720°
implantation rate	$(6 - 9) \cdot 10^{-4}$ appm He s ⁻¹
damage rate	$(3 - 5) \cdot 10^{-7}$ dpa/s
He / damage ratio	1850 appm He / dpa
implanted dose	≤ 340 appm He
irradiation time	< 160h
strain rate $\dot{\epsilon}$	$1.2 \cdot 10^{-4}$ s ⁻¹

Table 9: Conditions of implantation / tensile test

Staff:

G. Bürkle

R. Lindau

A. Möslang

D. Preininger

G. Przykutta

MAT 18

Development of Low Activation Ferritic-Martensitic Steels

First wall and blanket structures of fusion machines will get activated during operation by the high neutron fluxes, giving rise to problems in reprocessing or waste disposal. To overcome these problems, it is necessary to avoid the presence of certain alloying elements (or some isotopes therefrom) and to minimize impurity elements exhibiting unfavourable activation properties. A literature survey has shown that in recent years 9-12% ferritic/martensitic steels have been analyzed in which mainly Mo and Nb have been replaced by additions of W or enhanced levels of V or Mn. The results obtained show that for the modified materials the standard of commercial alloys, like 1.4914, FV 448 or HT9, has not been reached, especially with regard to an adequate balance of tensile and impact properties. Research efforts underway at KfK/JEN to improve this situation have been described in the semi-annual report 4/86-8/86 (KfK-report 4165).

a) Investigation of the effect of Ce-, Ta-, Hf-additions:

Two melts, No. 857 and 858, have been produced (Fa. Saarstahl, Völklingen) which are now available as forged, 25 mm square rods.

These are Ce and Ta, and Ta and Hf bearing alloys, respectively. The hardening temperature response is shown in Fig. 33. At and above a hardening temperature of 950°C the level HV \geq 400 of commercial 9-12% Cr alloys is obtained. The microstructure (grain size) and tensile properties determinations are in progress.

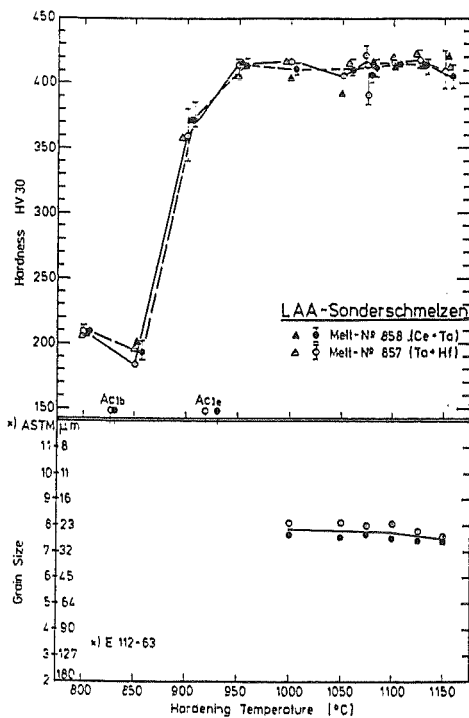


Fig. 33: Hardening temperature response of the two alloys No. 857 and 858

b) Variation of the δ -ferrite content.

6 alloys with δ -ferrite contents varying between 0 and 25% have been made up. After hardening from 1075°C their 2h-annealing (tempering) response in the temperature range 300-950°C has been determined. The results are shown in Fig. 34.

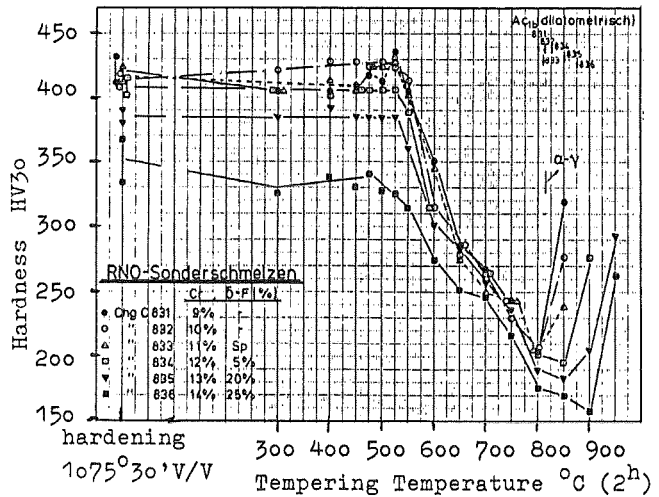


Fig. 34: Effect of tempering temperature on hardness

Up to tempering temperatures of 550°C the room temperature hardness decreases clearly with increasing δ -ferrite content. Between 550 and 800°C the harder alloys soften more so that the hardness differences are diminished.

Staff:

K. Anderko
M. Schirra

N1 Design Study of Plasma Facing Components

This task comprises design studies concerning first wall and first wall protection and the investigation of divertor concepts for NET.

First Wall Design with Radiatively Cooled Protection Tiles

First wall protection against impact of particles and mainly against plasma disruptions is considered necessary for at least the first operation phase of NET. Graphite is a short term candidate protection material. Since direct coatings can probably not be made thick enough to reach a sufficient life time, protection tiles and attachment methods are being developed. Cooling of the tiles by radiation to the first wall steel structure is probably the most reliable heat transfer mechanism and stresses in the tiles are minimized by loosely fitting the tiles between cooling tubes acting as support rails.

Even with the massive protection tiles as heat buffer the first wall steel structure is subjected to considerable thermal fatigue loads during the burn cycle. In order to verify prediction models for thermal fatigue failure of the actual geometry and to investigate phenomenologically the behavior of the composite first wall under relevant thermal conditions a high temperature thermal fatigue test program is being planned. A test apparatus is under consideration that will be capable of conducting thermal fatigue tests with maximum tile temperatures of 1800 °C and cyclically active heat fluxes of up to 50 W/cm² in a vacuum atmosphere; the test apparatus will be designed to house specimens up to the size of a reasonable length portion of a full width NET-segment.

Staff:

G. Hofmann

K. Rust

The respective thermomechanical sample tests for the NET divertor are planned to be performed at KfK by using an existing plasma spray device as a heat source. In several series of pretests it was demonstrated that the device can satisfy the requirements for the cyclic sample tests. In particular the heat flux and the radial heat flux distribution at the probe as a function of the operating parameters (i.e. target distance, electrical heating current, vacuum vessel pressure, feed gas flow rate, and target surface temperature) have been quantified.

The major results are that the measured peak heat flux reached 15 MW/m² at the assumed reference device parameters and are extrapolated to be close to 30 MW/m² at the device limits. The radial heat flux profile exerted by the plasma flame onto a flat target is nearly Gaussian and axisymmetric. The profile width, where the power is above 50% of the peak value, is about 3 cm in diameter and is nearly independent of the target distance. Distance and arc current are the most suitable parameters to control the heat flux in a wide range. The influence of the surface temperature on the deposited heat flux is substantial. These results will be used in planning and precalculating the sample tests.

Before entering the sample tests, the plasma spray device needs to be upgraded by providing a sample cooling circuit, additional instrumentation, computerized process control, and a moveable sample holder. Planning and procurement of several components of the equipment have been initiated.

Staff:

G. Class

K. Kleefeldt

K. Schramm

E. Stratmanns

Divertor Design

The main thermomechanical issues for the NET divertor are the high heat flux, the physical and chemical sputtering rates, and the surface erosion from plasma disruptions. Most of the divertor walls proposed so far consist of a metallic heat sink structure protected by a heat and erosion resistant surface material. In this duplex structure material compatibility, perfect bonding, temperature limits, and cycling shear stresses due to differential thermal expansion are the major features of concern.

As a first computational approach the heat flux potential was compared for several candidate material combinations in terms of stress and temperature limits. The results, which were briefly reported in the last semi-annual report, have been documented and evidenced the need for experimental support.

N2

Shield Design Studies

The KfK design of a movable shield segment which can be placed on a blanket segment position is optimized from the point of view of fabricability, reliability, and simplicity. In the reporting period emphasis was put on the water cooled version. It consists of a large steel container with an internal steel structure. Fig. 35 shows a cross section through the equatorial torus plane of an outboard segment. In contrast

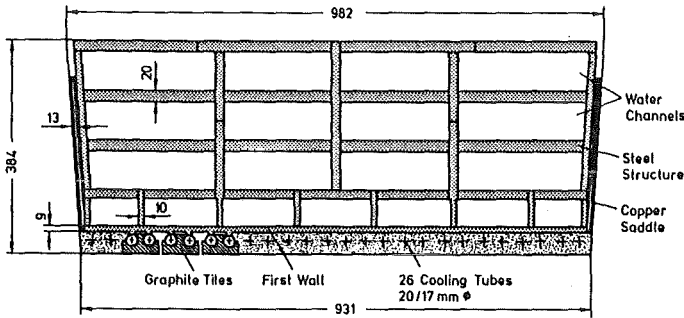


Fig. 35 radial-toroidal cross section of a water cooled outboard shield blanket (dimensions in mm).

to the previous version the separate first wall box is now abandoned. Box and canister had to be joined together and would be replaced jointly anyway. With the first wall being the most critical component there is also no safety advantage of the separate box solution. The one unit design has the advantage that the first wall is now cooled from both sides, which allows to reduce the first wall to 9 mm and reduces the stresses considerably. Moreover the design is much simpler.

Cooling water flows downwards in the front channels, then upwards in the second row, then down and up again in the last row. The top and bottom parts with flow reversal and redistribution were designed. First wall cooling is separate at the inlet but back flow is jointly with the shield structure coolant. If one cooling system fails the other one acts as emergency cooling. A more detailed engineering design with stress analysis, fabricability assessments, and cost estimate is now being done at Sulzer Company.

The emphasis on fabricability and reliability led to a low steel fraction of about 30 vol %. Optimum shielding efficiency is achieved with 80% steel. However, neutronics calculations showed that shielding effectiveness is adequate and that the dose rate in the superconducting magnets is only 24% higher than for the optimum composition. This difference is small when compared with the uncertainties of dose limits and corresponds to a difference in shield thickness of 18 mm (see Fig. 36).

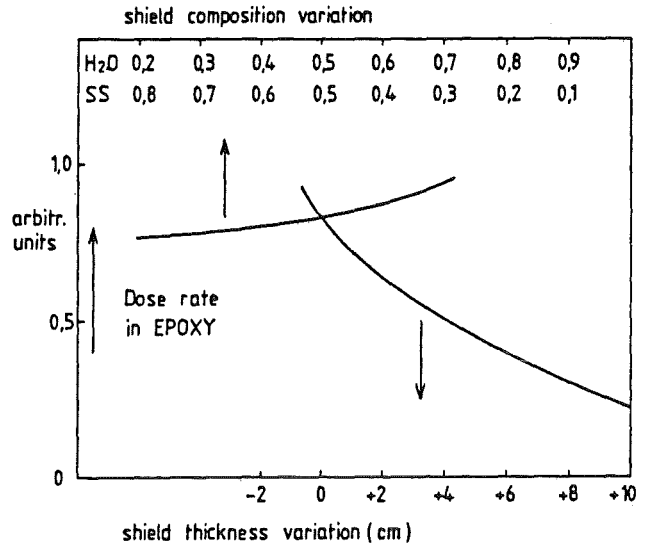


Fig. 36 Variation of dose rate in the superconducting magnet with shield thickness and shield composition, results of 1d neutron transport calculations

The larger water volume fraction is beneficial when a Li-salt solution is used for tritium production (see /1/ and previous progressreport KfK4276).

Neutronics calculations revealed that there is only little gain when tungsten is used in the movable shield as a partial replacement of water. Significant improvements of about order of magnitude in shielding effectiveness are obtainable however with tungsten in the permanent shield.

Most critical is the inboard shield for the extended plasma version. Calculations with a simplified representation of the present permanent shield version indicated that an operation time of 0.5 full power years would lead to the Epoxy dose limit. The results were obtained by Monte Carlo calculations using a continuous energy representation of the nuclear data. Comparisons to usual multigroup neutron transport calculations showed that the latter overestimate the shielding effectiveness considerably (see B2 of this report).

Staff:

E. Bojarksy

U. Fischer

M. Küchle

H. Reiser

Publications

1. M. Küchle et al. "Potential and Problems of an Aqueous Lithium Salt Solution Blanket for NET" KfK 4271 (1987)

N 3 Development of Procedures and Tools for Structural Design Evaluation

The plasma-facing components in a fusion reactor are loaded by high heat fluxes. These thermal loads cause thermal stresses and strains of an extent which is outside the validity range of linear materials models, i.e. elastically calculated stresses and strains exceed the yield strength.

Design of components operated in the high-temperature regime can be made by codes, e.g. ASME, which make use of elastic stress distributions, or by inelastic calculation.

The inelastic analysis requires the application of sophisticated materials models, the so-called unified models, comprising all kinds of inelastic behaviour such as plasticity, creep, relaxation. A large number of such constitutive models are applicable to special materials or groups of materials in a limited temperature range. Usually they are given by a system of coupled, nonlinear differential equations.

Inelastic Analysis of First-Wall Components

Part of the work is to provide computational tools for inelastic structural analysis within Finite Element (FE) codes. Within these codes unified models have not yet been available. Viscoplastic material models describing metallic components at high temperatures have been implemented into ABAQUS. One of them, the Robinson model, has been tested - using different forms of integration methods - with respect to convergence, stability and CPU-time. (Investigations to determine the internal parameters in the Robinson model for the stainless steel 316 L have been started.)

In the mean time calculations are based on the internal variables which were determined for some other steel. On the other hand the ORNL model which is implemented in ABAQUS has been used to perform computations for an austenitic 316 L plate under thermoshock conditions in order to have a reference model for further comparison of results.

The code will be extended to include irradiation creep and swelling in combination with the Chaboche plasticity model.

Evaluation of Procedures to Describe Constitutive Equations and Methods to Measure their Parameters

Design of First-Wall and blanket components which are currently under discussion use radiation-cooled graphitic protection tiles. During plasma operation

thermal loads cause high temperatures in these tiles. Typical values are of the order of 1200°C up to 1800°C.

Failure modes are subcritical crack growth and creep crack growth. Lifetime predictions require the knowledge of stresses for all locations of the loaded structure. Therefore knowledge of creep behaviour of ceramic materials is important.

A general procedure was evaluated to determine the parameters of constitutive equations for ceramics only from outer fibre strain measurements. The improvement of this method is that the creep behaviour of ceramics may be determined only by using bending tests.

Improvement of Lifetime Prediction of Fatigue Crack Growth

An important problem in fatigue lifetime prediction for fusion reactors is the knowledge of the best appropriated stress intensity factor solutions for surface cracks considering the complex stress distributions in the First Wall.

Application of the weight function method for calculating averaged weighted stress intensity factors requires that both the stress intensity factors and the crack opening displacements are known for a reference load case, mostly chosen as a constant stress. Whilst the stress intensity factors are known for many crack geometries and load cases, the displacements are available for a few special cases only. Therefore an approximative crack opening displacement field was developed. Similar to the treatment of straight-through cracks the reference crack opening displacements in the reference loading case are expressed by a power series. The coefficients can be determined from geometrical conditions and from the self-consistency condition of the weighted stress intensity factors. Using these weighted stress intensity factors crack growth under arbitrary stress distributions $\alpha(x,y)$ can be calculated.

Staff:

E. Diegele

T. Fett

D. Munz

H. Stamm

N 5 Development of Theory and Tools for Evaluation of Magnetic Field Effects on Liquid-Metal Breeder Blankets

Investigations of MHD in Liquid Metals

The governing problems in developing a selfcooled liquid-metal breeder blanket for NET are pressure drop and flow distribution of the liquid metal circulating in the high magnetic field of a fusion machine. The proof that this pressure drop can be kept low by appropriately guiding the flow will decide on the feasibility of such a concept. To overcome the lack of reliable experimental data the program MEKKA was initiated at KfK in 1985. It is described in the last semi-annual report.

The Sodium-Potassium liquid-metal loop NaK-1 designed and built up at KfK in the frame of the MEKKA program has been made available. First test runs with cold NaK showed that the canned motor pump which circulates the liquid metal produces the foreseen pressure peak of 9 bar at a flow rate of 25 m³/h.

Using a positioning device with stepping motors the three-dimensional magnetic field distribution of the normal-conducting dipole magnet which is to be used for the first step of MEKKA has been measured at the maximum field strength of 2 Tesla. In the supporting theoretical program the MHD flow has been simulated numerically in simple geometries.

As an example Fig. 37 shows the calculated velocity distribution and the corresponding current densities in the cross section of a straight channel at a Hartmann number of 100, a wall conduction ratio of 10⁻¹ for the top and bottom wall and 5 · 10⁻³ for the side-wall.

To prove the principle of flow tailoring as described in the semi-annual report April 1986 - September 1986 a joint experiment is undertaken by Argonne National Laboratory (ANL) and Kernforschungszentrum Karlsruhe (KfK).

A photograph of the test section designed and built by KfK is given in Fig. 38. The photograph shows the duct with the expansions and contractions to produce the flow tailoring, the pressure taps, the flanges for the installation of the velocity measurement instrumentation and the voltage probes.

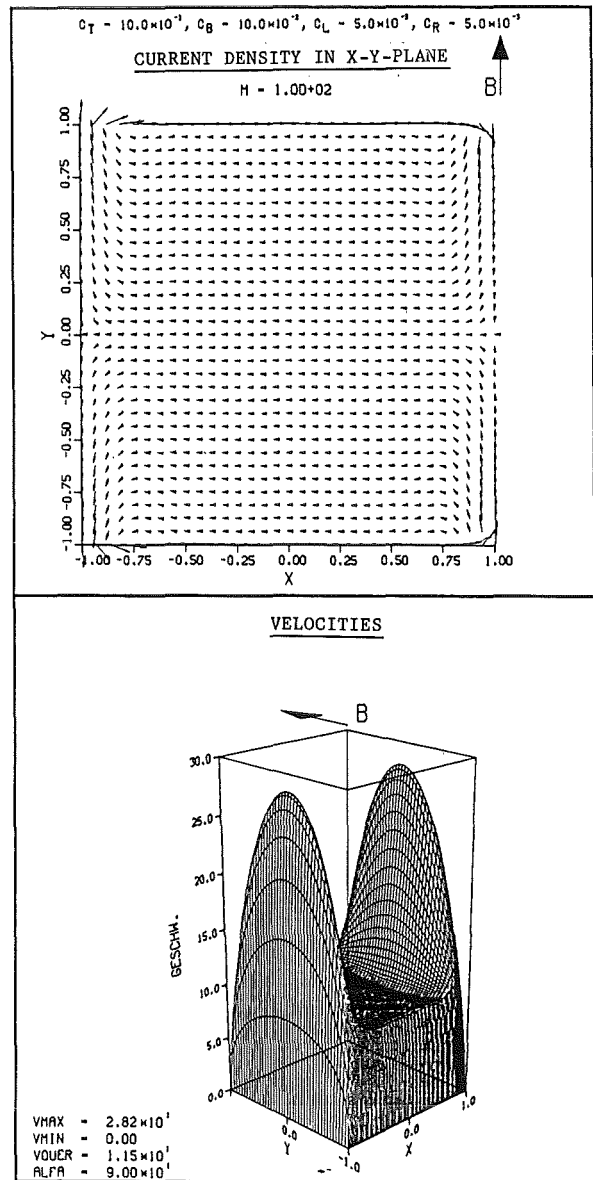


Fig. 37: Velocity distribution and current densities in the cross section of the straight channel

Development of a Velocity Meter

A velocity meter for local measurement is being developed. At the location of measurement the propagation of artificially induced temperature pulses are used to determine the fluid velocity. Within the period to be reported measurements were carried out in flowing sodium. Test facility TEFLU, which is part of the sodium circuit WÜP II, was used. In a vertically arranged tube 110 mm i.d.) sodium is flowing upwards.

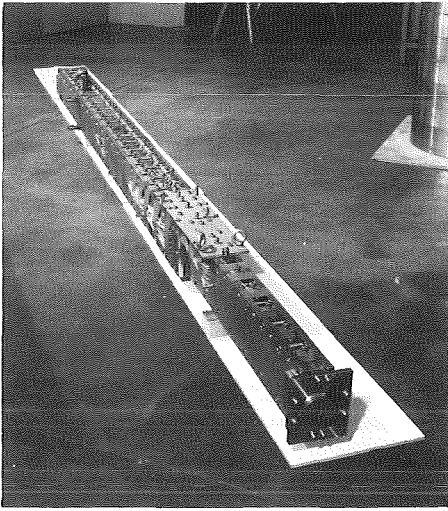


Fig. 38: Photograph of flow tailoring test section

A measuring head with a mineral-insulated heater (0.5 mm o.d.) for pulse creation and 4 mineral insulated thermocouples (0.25 mm o.d. with boron-nitride insulator) were used; the heat could be moved during operation along the radius of the flow channel and could be turned around its axis. Upstream from the measuring head a block with nozzles was installed for flow equalization. This distance amounted to $L/d = 5$. Fig. 39 shows as an example a temperature-time signal,

the temperature-time signals. The disturbance near the wall ($r/R_0 \approx 1$) is caused by a flow disturbance effected by the penetration of the measuring head through the flow channel housing.

The results obtained until now demonstrate the accuracy of the measuring device. Additional work has to be performed for optimization of measuring head geometry and for some improvement in the data evaluation system.

Staff:

- G. Arnold
- L. Barleon
- V. Casal
- R. Kirchner
- H. Kreuzinger
- H. Kußmaul
- K.J. Mack
- A. Sterl
- K. Thomauske

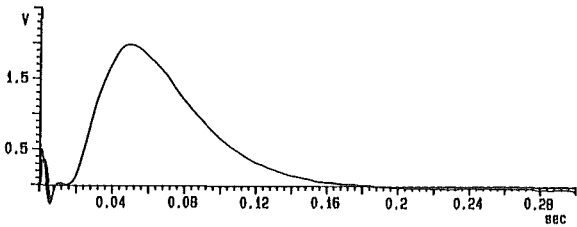


Fig. 39: Temperature-time signal

calculated in a computer. Fig. 40 shows a radial velocity profile in the tube computed on the basis of

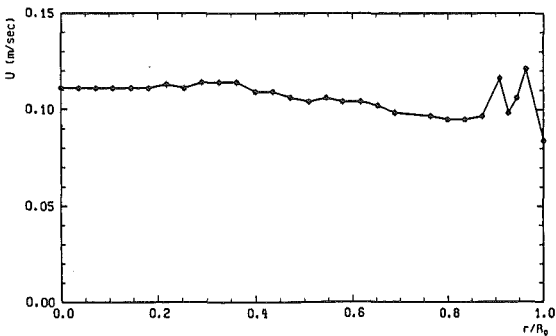


Fig. 40: Velocity profile as function of radius r/R_0

N6 Studies of Pebble Beds of Ceramic
Compounds

The results of the studies of pebble beds are included in the report on B1 Blanket Design Studies chapter Helium-Cooled Ceramic Breeder Blanket.

RM1 Background Studies on Remote Maintenance

This task concentrates on the investigation of pipe connectors (for water cooling, liquid metal breeder fuelling, gas cooling, and gas purging systems), electrical connectors, and cutting and welding techniques for fusion reactors.

The work includes:

- identification of development needs,
- recommendation of a pre-testing programme,
- performance of pre-tests, identification of necessary improvements and modifications,
- design and fabrication of prototypes,
- performance of a manual for licensing and standardization.

Based on the results of the NET studies "Pipe and Vacuum Duct Connections" and "Vacuum Tight Connections and Closures, Lip Welding and Cutting" efforts have been going into the further development of remotely handleable pipe connectors and welding units for fusion reactors.

During the period under review the work was concentrated on

- definition of a test programme for NET relevant connecting techniques
- performance of pretests with a selection of JET and KFK types of pipe connectors
- construction of a test loop for the investigation of the corrosion rate of stainless steel flanges and gaskets in contact with liquid Pb-17Li
- design of a test facility for integral tests of pipe connectors and lip welding units
- design and construction of sub-components for a test rig for basic tests of welding and cutting equipment.

Performance of pretests

At KfK there are 3 different test facilities available for basic tests of pipe connectors.

Tightness tests under normal and elevated stress conditions will be performed in the test facility PAULA. Tests have been started with three JET water and vacuum connectors and with all the different KfK-type connectors up to 100 mm diameter.

The remote handling capability of the different configurations of pipe jumpers can be demonstrated in the test rig FUTE (Fig. 41) and in the test rig JUTTA which was originally designed for the investigation of the FEMO-connecting technique (Fig. 42).

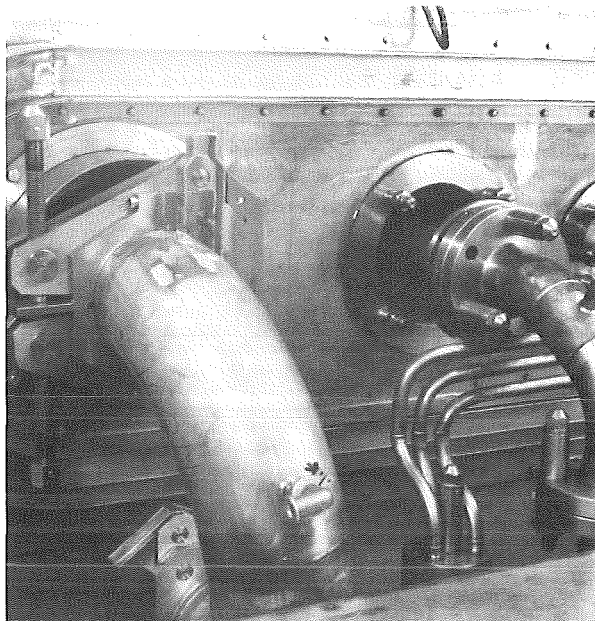


Fig. 41: Test rig FUTE

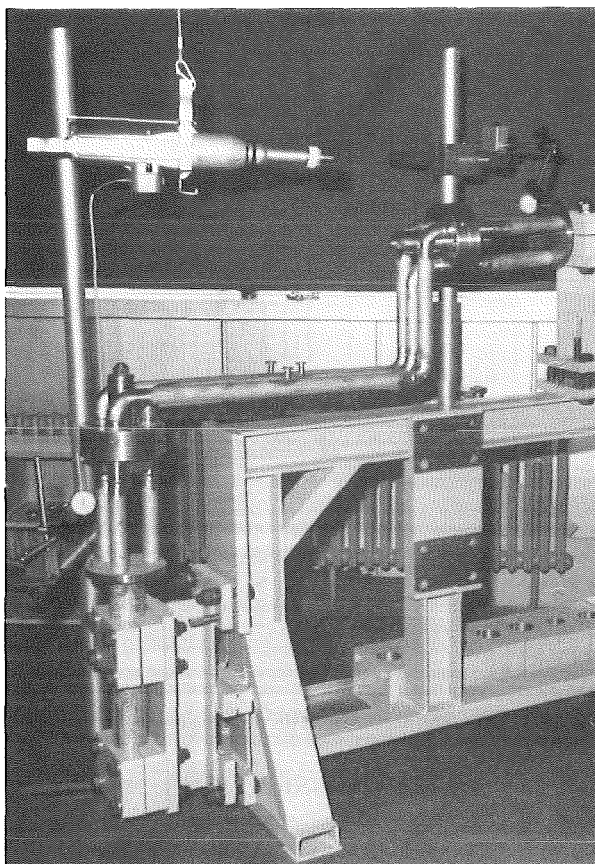


Fig. 42: Test rig JUTTA

Corrosion tests

Investigations have shown that one can expect a relatively high corrosion rate of stainless steel in contact with liquid Pb-17Li. This can reduce the lifetime of flanges and gaskets significantly. To obtain proven results for further development of pipe connections and gaskets respectively, KfK has designed and constructed a test rig for the determination of tightness and corrosion rates of pipe flanges and gaskets.

The test rig consists of a loop in which the heated LiPb flows in free convection through the connection to be tested. (Fig. 43)

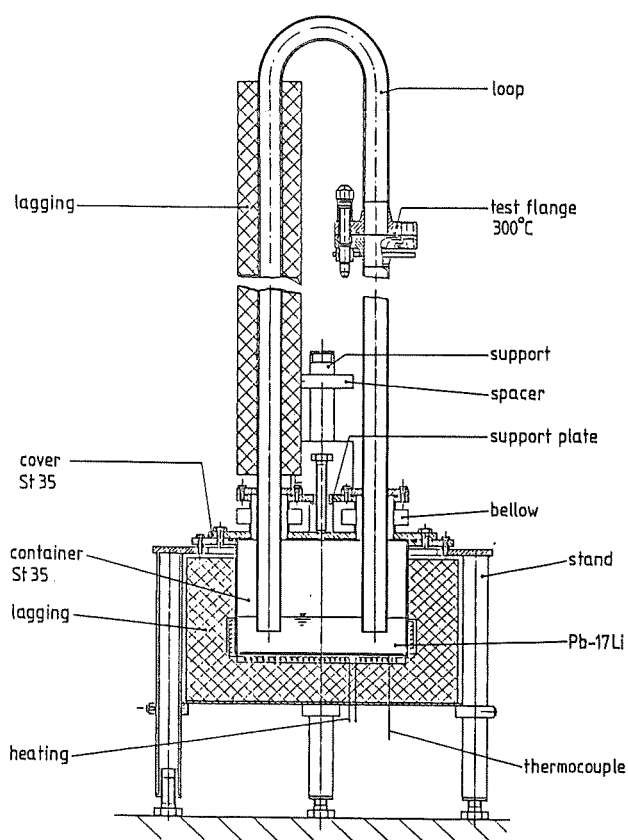


Fig. 43: Test rig FLATEST

Integral tests of pipe connectors and lip welding equipment

The basic test programme with selected prototypes has to be performed under NET typical geometrical conditions and, if possible, with NET typical handling tools in an integral test facility. This test facility will simulate the upper part of a prototype blanket segment including its auxiliary coolant make up and supply systems. The preliminary draft worked out provides connections for the different types of blankets under investigation. The sealing lip connections of blanket segments can be tested using the lip welding units currently being developed at KfK.

Work has been concentrated on the design of the general arrangement, the configuration of the pipe jumper and the segmentation of the blanket modul.

Development of welding and cutting equipment

The design of the prototype lip welding unit has been completed. The fabrication drawings for the most important sub-components have been given to the workshop.

Basic tests of the different cutting and welding units under design or construction will be performed in another test rig. To meet the NET requirement as much as possible this rig will be equipped with a computer control system for parallel operation of different units. The computer control system and the remote handling equipment have been designed. The first system components have already been ordered.

Staff:

L. Gumb
U. Kirchenbauer
A. Schäf
M. Selig
M. Trettin
R. Ullrich

RM2 Mechanical Components Assembly

In order to provide designers and contractors with information NET launched the preparation of a Remote Handling Manual (RHM). It contains a set of General Rules and Design Standards, adapted by NET for components and units of the NET device which require remote handling, and settles guidelines for handling equipment design.

Work within the frame of the RM2 contract was based on a first draft of the NET-RHM and concentrated on

- the review of design guidelines for remote handling, in particular modularization, assembly/disassembly and transport of machine components,
- the definition of standard components for remote handling in close connection with the RM1 Task "Background Studies",
- proposals for remote handling equipment to perform maintenance tasks inside and outside of the NET device, and
- proposals for remote handling assurance procedures.

With the progress of machine design, the investigation and standardization of components, and the development of remote handling equipment the Remote Handling Manual will be completed according to the time schedule of NET with the beginning of the Detailed Design Phase in 1990.

Staff:

G.. Böhme

W. Köhler

M. Selig

A. Suppan

RM3 Handling Equipment for In-Vessel Components

The investigation of an In-Vessel Handling Unit (IVHU) for inspection, repair and replacement of NET in-vessel components was continued. CEA, CEN/SCK, ENEA, JET and KfK cooperate in the development of such equipment. It consists of

- a contained transfer unit (CTU)
- a transport unit based on an articulated boom or an in-vessel vehicle movable on telescopically inserted rails
- various work units with end-effectors attachable to the transporter
- the control system

Out of the 9 sub-items of the RM3 technology programme the following tasks were carried out:

SUB-TASK 1: Development of a Conceptual Design

According to the RM3 workshop in November 1986 the development of the IVHU was split between the Associated Laboratories mentioned above. In agreement with the NET team the KfK activities were mainly based on the investigation of an articulated boom as a transport unit with a reach envelope of 180° of the torus. The work was continued during the period to be reported. Main emphasis was given to

- predesign the transporter and its components, e.g. links and joints of the boom. Out of various options and with respect to boom stiffness, minimum number of joints and drives, the selected system is based on scissor links. The boom is mounted on a driven carriage movable horizontally and radially to the torus (Fig. 44). Its first link located at the carriage has a combined yaw and rotation joint. The latter one controls the access through the relatively small torus entry ports which are arranged symmetrically with an angle of 90° to each other. The transporter ends with an end-frame at which the different work units are attachable. To orientate the end-frame in working position the deflection originating from bending moments and torsion is compensated by means of a combined pitch and rotation joint ($\pm 5^\circ$ to the vertical axis). Additional vertical compensation is required for the work units to replace divertor plates and RF-antennae. It will be performed by means of telescopes installed at the work units. A promising solution for actuating the yaw joints are ball screw spindles driven by DC brushless motors. But other solutions are also under investigation.

perform structure mechanics calculations. Cross sections of the boom links are limited by the size of the entry ports. Structure mechanics calculations of links and joints resulted for the 180° boom in relatively high stresses. Improvements are possible by application of weight-

saving construction (change from austenitic steel to titanium for the front links) and/or framework construction. Corresponding calculations are ongoing.

investigate the influence on machine design, ex-vessel components and plant layout. The IVHU works at the midplane level of the torus. To prevent contamination from the reactor hall the use of CTUs and/or transport flasks was investigated. On the basis of trade-off considerations and time estimations for typical maintenance tasks a possible compromise might be a solution with two permanently installed CTUs and temporarily installed transport flasks for the transfer of components. This compromise does not exclude a later change to another solution, e.g. during the technology phase of NET to a 3-ante-chamber option.

Although the 180° boom was chosen as a reference solution an alternative option with a 90° boom was also investigated. The solution is of some interest with respect to minimize the boom size and to reduce the structure mechanics requirements.

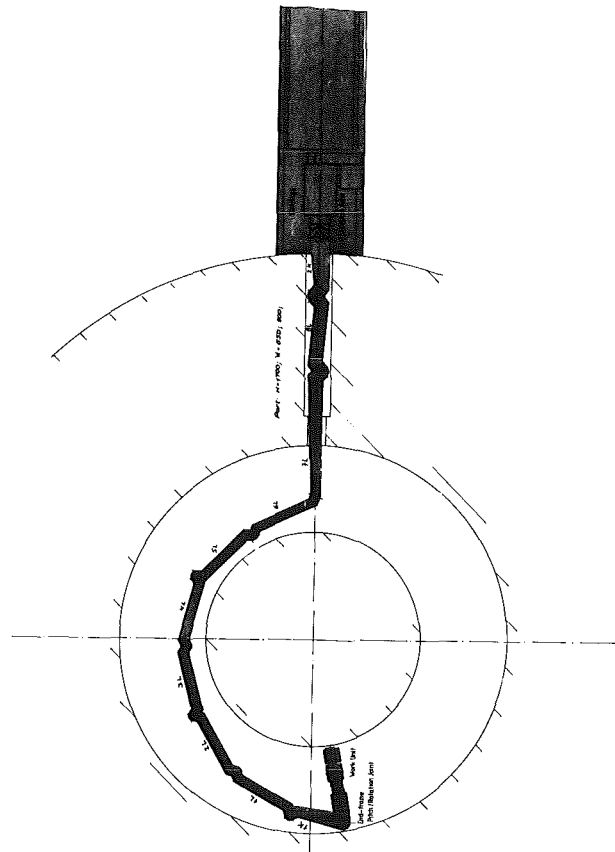


Fig. 44: In-Vessel Handling unit - 180° Reach Envelope: Cross section in equatorial plane

SUB-TASK 2: Overall Geometry Measurement

The implementation of the prototype system for out-of-vessel geometry measurements is going on as planned. The following modules are running:

- postprocessor for interpretation of CAD data (points to be measured and their environment) in IGES data format,
- interactive tele-control of the theodolite, automatic measuring, triangulation computations for resection,
- preparation and output of results.

For realistic tests a metallic model was designed on a CAD system and manufactured. This model with marked measuring points was transferred to the GMSYS (Geometry Measurement SYStem) prototype and measured. The tests showed, that automatic levelling will be a remarkable enhancement of the system. The development of a suited equipment was started. To improve the tele-control, the theodolite will be equipped with an integrated CCD-camera and motorized focus.

For in-vessel measurement a concept of theodolite-periscope was worked out, which is based on triangulation using controllable mirrors in the measuring path.

Alternative measuring principles like photogrammetry will be investigated for both areas of geometry measurement.

SUB-TASK 3: Boom Position Monitoring

The concept of the control system for the NET boom was worked out.

The basic goal for the remote handling system is assumed to be the minimization of maintenance times by high speed and safety of operations. The proposed approach for a control system supports to obtain this goals by several general concepts suited to facilitate complex tasks like plant maintenance. It is anticipated that the control system may be implemented in steps with increasing degree of capabilities. It is important, however, to consider the final stages to be achieved in some years time. Otherwise design decisions based on short-term goals may make future enhancements difficult or even impossible. This applies particularly to mechanical hardware. The control systems is organized as a **supervisory system**, separating task level work from executing or motion control work. This structure supports safety of work by a clear separation of simple subtasks and a clear distribution of responsibilities. The supervisory control is a control structure suited for a combination of manual work and automated subtasks. A high **functional modularity** allows to automate subtasks step by step with an evolving state of the art. The separation of the whole boom task in functional building blocks like transport, referencing, positioning, and working is mirrored in the control system as well as in the kinematic structure of the boom. This is the reason for two extra joints in the transporter part. The modularity and the supervisory organisation serve for a smooth transition from teleoperation to telerobotics. The first subtask which should be partly automated is the transport task. A central part of the control system is a **real time simulator** used for a problem suited synthetic scene presentation and for off-line simulation and programming of subtasks (teaching). The JET-KfK boom simulator is the reference implementation. **Collision detection** is based on the simulators gometric model and the joint angles and on ultrasonic sensors placed at a group of transporter links.

For the special problem of assembly and disassembly of heavy components, especially the pick and place operations,

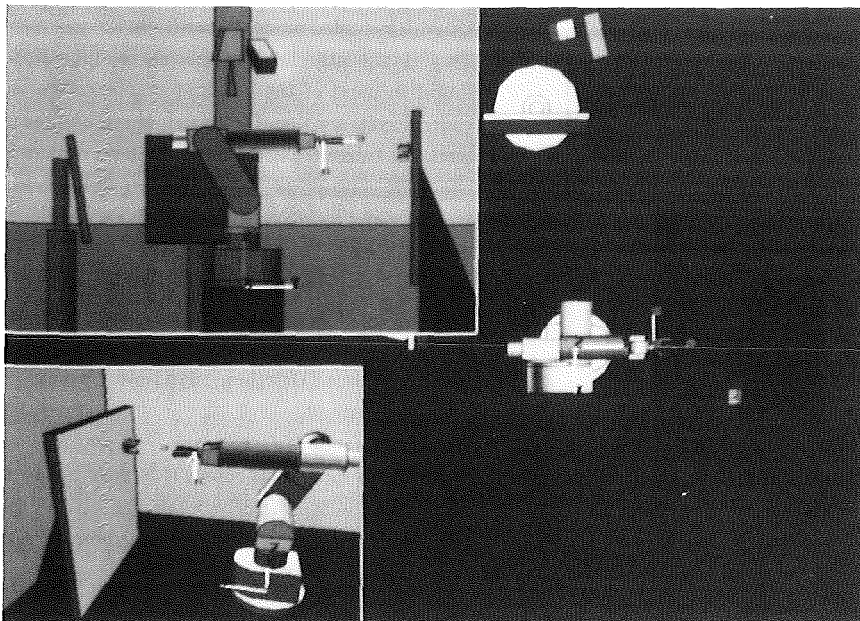


Fig. 45: Model of Laboratory Environment for Remote Handling Experiments: Top, side and camera view

investigations are started by a first conceptual study which is planned to result in experiments with a NET mock-up.

The work on the JET graphics boom simulator GBsim proceeds as planned, new features were implemented and are being tested at the JET site.

The GBsim kernel was adapted to the CATROB (Computer Aided Telemanipulation with ROBoTs) requirements (RBSim: RoBot SIMulator) to test manipulator control techniques relevant for NET boom control like integration of autonomous preprogrammed subtasks, simulation, and offline programming into a remote handling control system. To be able to control and simulate related out-of-vessel remote handling activities too, a concept for a problem suited data structure was developed.

The software package ROBOT running on the Applicon CAD system was completed and tested. This software supports interactive generation of remote handling equipment models for simulation of maintenance procedures and for down loading onto the realtime simulators GBsim and RBSim. The tests were done with a NET boom design (Figure 46) and a model of a laboratory environment with roboter and camera system (Figure 45). In order to provide for the possibility to perform dynamic analyses with the CAD model of the NET boom, the procurement of appropriate software (ADAMS) was initiated. ADAMS will run in conjunction with the Applicon CAD system.

The survey of sensors for boom position monitoring was extended on all types discussed in the control system concept.

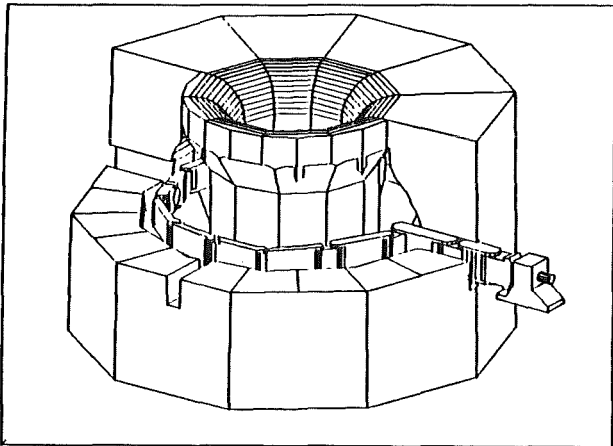


Fig. 46: ROBOT Simulation of NET

SUB-TASK 4: Conceptual Design of Work Units

In order to perform the various maintenance tasks inside the torus the transporter can be equipped with different kinds of work units attachable to the end-frame of the transporter, i.e. one manipulator unit, suitable for inspection, protection tile

replacement and performance of preparatory work for divertor and antenna replacement, one work unit to replace antennae and another one to replace divertors. Comparing

the work units, the one to replace divertors is the most crucial one with respect to the requirements, e.g. payload of 10 kN, reach envelope and working capability. Therefore, a conceptual design was defined and the feasibility checked. The unit consists of a device for withdrawal and insertion of the plates supported by an electrical force reflecting manipulator and viewing systems. It combines rotation joints, yaw and pitch joints and a vertically arranged telescope (Figure 47).

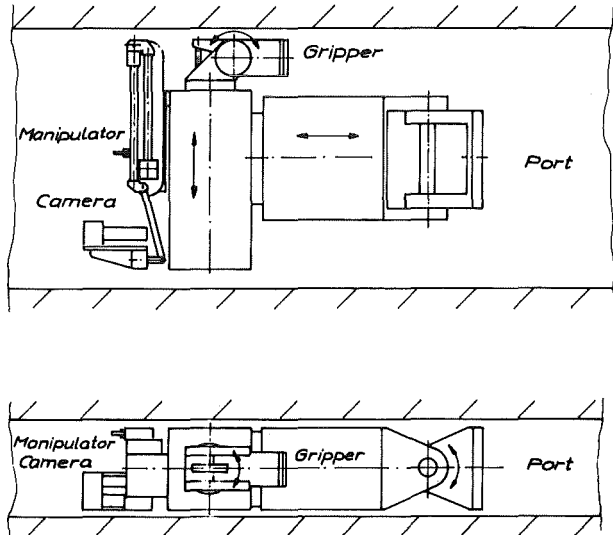


Fig. 47: Work Unit To Replace Divertor Plates

Master/Slave Manipulator Control System Development

A concept for the master/slave manipulator control system has been developed, which combines some unique features (c.f. Fig. 48) as far as the possible modes of operation are concerned:

- Operator-guided mode of operation:

This is the standard master/slave operation, which is found in most of the existing master/slave manipulator control systems, usually implemented by means of analog circuitry. In contrast to those implementations, however, the KfK-concept is not based on "bilateral reversible position and velocity control", which uses the positional error signal to compute the forces to be reflected to the master manipulator (force reflection). A precise calculation of forces and torques, using the inverse model of the master and slave arm for determining the necessary compensations (friction, dynamic forces, weight) is provided instead.
- Automatic mode of operation:

As with an industrial robot, it is possible to operate the slave arm automatically following either synthetically generated paths or trajectories being generated by teaching (playback).

- Teaching:
Teaching of arbitrary trajectories is accomplished via the master manipulator (including force reflection), or by means of operating the slave manipulator via the sensor ball (see below). Recorded trajectories are cataloged and stored in the trajectory data base.
- Mode switching:
While in automatic mode of operation, the system operator is able to switch to manual (direct) manipulation at any point in time by means of simply touching the handle of the master manipulator.
Return is possible either to the aborted trajectory or to a new one selected via menu at the graphic display.
- Alternate master device:
As a part of the man-machine interface, a sensor ball is provided, which can be used instead of the master manipulator in cases where less dexterity is required and as a backup device.
The sensor ball uses a torque/force sensor to generate six mutually independent signals according to the forces and torques exercised with the ball. Thus position and gripper orientation of the slave arm can be controlled.

To investigate the generic aspects of a manipulator control system showing the above functionality, a first version of the system has been implemented on a multiprocessor multibus microcomputer and adapted to an EMSM-2 electrical master/slave manipulator. The test site is in operation since April 1987 with basically all of the functions being available.

Version 2 is in preparation; it will offer improved compensations and force reflection together with a conceptual redesign of the man-machine interface.

SUB-TASKS 8 and 9: Radiation and Temperature Hardening

The market survey on sensors showed the necessity of radiation experiments with selected sensors and cable materials. The performance of these experiments is planned to be done in cooperation with CEN/SCK

Staff:

K. Becker	W. Link
G. Böhme	A. Ludwig
H. Breitwieser	G. Müller
B. Haferkamp	S. Müller
<u>E. Holler</u>	H. A. Rohrbacher
J. Hübener	<u>E.G. Schlechtendahl</u>
H. Köhler	K. Schleisieck
W. Köhler	P. Schultheiß
R. Krieg	<u>A. Suppan</u>
U. Kühnapfel	E. Wehner
K. Leinemann	

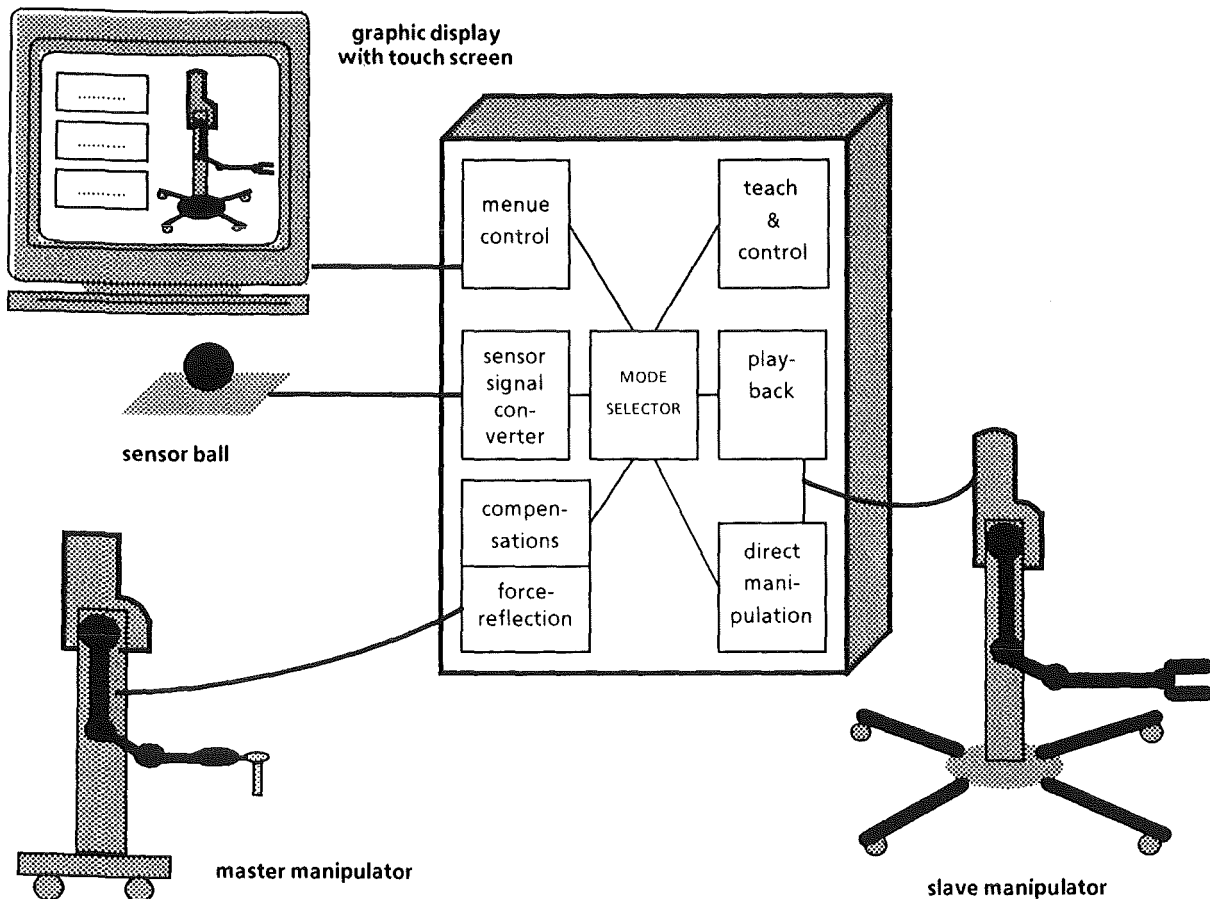


Figure 48: Architecture of the microprocessor based master/slave manipulator control system developed at KfK

S + E 4.1.2 Safety Aspects of the Cryosystem

Under this task safety aspects of the cryostat of NET are investigated. The cryostat is a shell structure surrounding the torus and all coils. It has to maintain high vacuum conditions. To guarantee the integrity of this outer pressure loaded vessel the complicated buckling behaviour has to be studied for normal and accident conditions.

In order to investigate the buckling behaviour for different accident situations a simplified strategy to calculate the buckling loads is under development. Experiments are or will be performed in order to assess the calculational results. Another goal is to develop a nondestructive buckling detection device for cryostat experiments. Furthermore the study of the buckling behaviour should give a feedback to optimal cryostat design.

During the last period the development of the simplified procedure for buckling analysis has been continued. As reported earlier, the simplification partly has to be paid by the introduction of some knowledge about the buckling shape functions into the calculation. For many cases this is not very restrictive as the shapes often are known by experience and as good buckling load results can be obtained knowing the buckling shape only approximatively. Even, if this knowledge is not available, it has been shown that a few iterations may help to find the critical buckling form using again only linear calculations. This is an important progress, e.g. for treating imperfection sensitive structures with arbitrary local imperfections. These studies are going on.

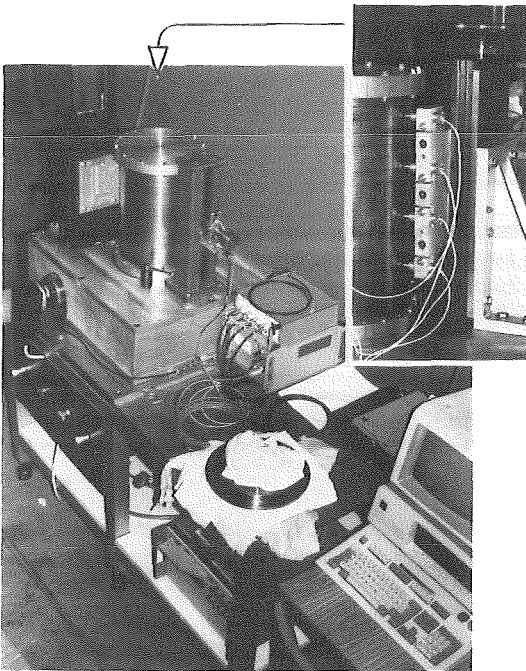


Fig. 49: Test rig for buckling experiments

The experimental investigations for code assessment and nondestructive buckling load measurements have been started. Fig. 49 shows the test rig with the data equipment. The test sample is a thin-walled milled steel cylinder (255 mm in diameter, 350 mm in length, 0.4 mm wallthickness). It is loaded by an inner vacuum. The actual geometry of the surface of the cylinder has been measured by four transducers of a non-contact measuring system. To get the actual geometry of the surface and the displacements under loading in high resolution, the cylinder is mounted on a motor driven

turning table and the transducers can be shifted in axial direction on a carriage. For chosen angles the computer controlled device measures the displacements. Fig. 50 shows the relief of the initial imperfections of the unloaded cylinder. Its maximum amplitudes are about 40 % of the wallthickness. These are important informations for the precalculations. Measurements under load will be performed subsequently.

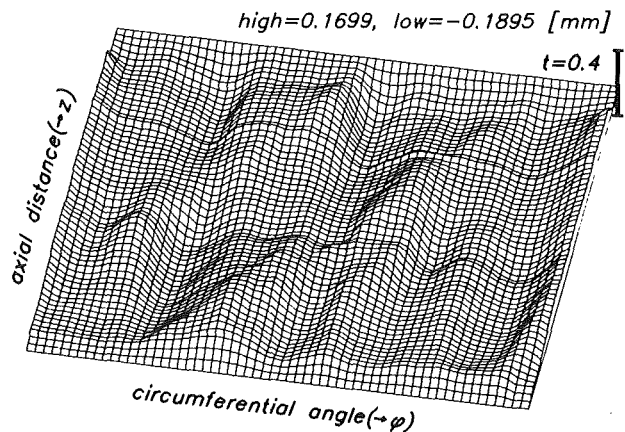
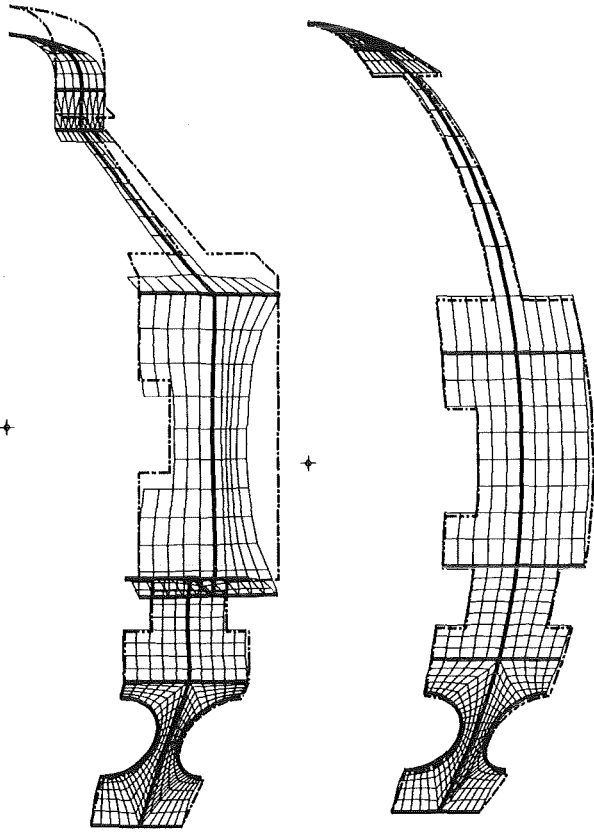


Fig. 50: Measured initial imperfection shape of a cylindrical shell

On the righthand side of the cylinder of Fig. 49 there is a stiffness measurement device for nondestructive buckling load detection. These measurements will be performed in parallel to the displacement measurements under load.

Whereas the first measurements at the "ideal" cylinder serve as a reference point, the following samples with cutouts and load imperfections will give interesting cryostat relevant results.



a.) reference design b.) spherical shape

Fig. 51: Linear displacement of the cryostat under atmospheric outer pressure load (result scale 100)

To support the cryostat design a study has been started, where a proper geometry accordant to the cryostat loading is searched for. Fig. 51a represents a 22.5° section of the actual cryostat geometry with the different ports. In Fig. 51b a spherical cryostat variant is shown. Calculation of the displacements under outer pressure load for both geometries using the same shell and stiffener dimensions and properties reveals, that a spherical geometry would have some advantage concerning the displacements at the ports. The buckling properties will have to be studied further on.

Staff:

B. Dolensky
R. Krieg
T. Malmberg
S. Raff
E. Wolf

Publication:

S. Raff, B. Dolensky, R. Krieg
"A simplified procedure for elastic buckling analysis"
Transactions of the 9th SMIRT, Vol. B, p. 569-574
Balkema Rotterdam, Boston 1987

S + E 4.1.3 Safety Aspects of Superconducting Magnets

During operation of superconducting magnet systems disturbances are conceivable which could finally result in a destruction of a magnet. The energy discharged thereby into an electric arc may lead to damage of the surroundings of the magnet. Cause and course of the disturbances, their detection and identification as well as their possibly destructive consequences are to be investigated using the superconducting torus arrangement TESPE-S. Through development of codes and their verification on the TESPE-S experiment an attempt will be made to transform the results to other larger magnet systems.

In case of destruction by arcing a number of different faults may occur simultaneously, e.g. loss of cooling, loss of vacuum, conductor short circuits. In order to keep theory and experiment transparent, in our experiments such failures are first simulated and built-in in separate experiments, respectively, and initial non-destructive tests are performed. The work includes the faults mentioned above and the generation of electric arcs. At the end of the series of experiments an attempt will be made to demonstrate that a destructive arc in one coil can be mastered safely.

After having performed loss-of-coolant, loss-of-vacuum, and short-circuit experiments the next step on the way to destructive arcing was to study arcing across one coil outside of the cryostat. For this purpose a selected coil was equipped with an extra pair of current leads to room temperature surroundings. The warm ends are fed into a helium-gas filled spark chamber. The electrodes are movable and adjustable. After having started a discharge of the system, an arc was ignited across the electrodes. These electrodes could be easily exchanged when damaged. Three ways of occurrence of an arc are conceivable: First, by an overvoltage together with a defective insulation, second, by burning of a locally overheated conductor, and third, by breakage of a current carrying conductor. Therefore different methods of arc initiation were applied: First, by a high voltage pulse across one coil's terminals during discharge of the stored energy of the system, second, by explosion of a thin copper wire between the terminals, and third, by mechanical opening of a short-circuit mounted across the terminals. The arc burned in helium gas atmosphere at different low pressures. The maximum arc current up to now was 3140 A. In this experiment nearly 600 kJ were set free in the arc leading to heating of the electrodes and melting of 171 g copper (Fig. 52).

Typical voltage for a stationary arc was 20 V, but also values of more than 100 V were observed in case of moving or flickering arcs. In this respect also first experiments on the influence of metal and insulator pieces, evaporated when hit by the arc, were started.

For theoretical description of the electric behavior of the magnet system having a fault like a short or an arc, the

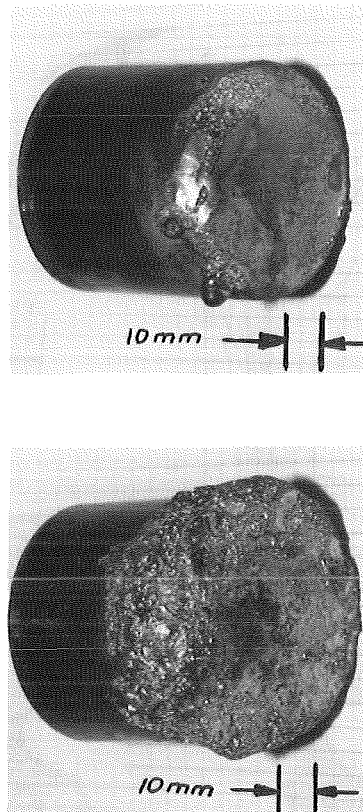


Fig. 52. Electrodes after 3140 A arcing (anode (top) and cathode)

program MSCAP (Magnetic System Circuitry Analysis Program) of EG & G, Idaho, was introduced in KfK within a collaboration with INEL, Idaho. First test runs were performed successfully.

The safety analysis of components of superconducting magnet systems was continued with the analysis of the fast discharge system of the Large Coil Test Facility. This step was taken before studying the corresponding NET component as there are experimental and hardware data available. Based on an analysis for the TOP event "No current interrupt upon demand", the fault trees were constructed and a first calculation was performed for the Boolean function.

Staff:

- P. Duelli
- J.S. Herring
- L. Hütten
- K.P. Jüngst
- H. Kiesel
- H. Kronhardt
- G. Obermaier
- M. Oehmann
- H. Schnauder
- J. Seibert
- E. Süß
- A. Wickenhäuser

S + E 5.2.2. Behaviour of Gaseous Tritium in the System Plant/Soil

Molecular tritium (HT) released to the atmosphere will be converted to the more radiotoxic tritiated water (HTO) and organically bound tritium (OBT) after contact with soil and vegetation. Studies are concentrated on the formation of OBT by plants and its fate in the food chain.

A closed chamber simulating environmental conditions is used for the exposure of different kinds of agriculturally used plants to HT. After each experiment HT and its oxidation product HTO have to be removed from the chamber as fast as possible. It has been proved that for the purification of the exhaust air from HT a tritium adsorption system of large scale is needed because of the big volume of the exposure chamber (about 18 m³). A commercially manufactured device for this purpose was offered by a firm but very expensive. So it was decided to propose a permission for the release of HT to the atmosphere. The supposition for this permission is the construction of a 10 m stack which will be built in the next two months. HTO produced during the experiment can be retained by molecular sieve.

HT to be introduced into the chamber will be stored under pressure in a 10 l aluminum cylinder as a mixture with nitrogen. From the cylinder a definite quantity of HT can be injected into the chamber using a flow controller. Because tritium in molecular form is supplied in glass vials a transfer from the vial to the aluminum cylinder has to be performed utilizing a vacuum system with special precautions. The procedure of this gas transfer has been tested and will be performed in the next week.

Concerning the problem of watering the plants automatically during the HT exposure and isolation of the soil in which they grow from the atmosphere several possibilities were discussed and tested. But only the results after the first HT exposure will show the best way.

A new contamination of wheat grass with HTO has been performed in order to test and improve the biochemical methods for separation of plants into different fractions and to compare with the results to be obtained after exposure of the same plants to HT. Preliminary results are:

- Specific H-3-concentrations of protein, fat, cellulose, nucleic acid and water soluble fractions are different.
- Highest specific activity was found in the fat fraction, lowest in the nucleic acid fraction (about 4 times lower).

The results of the first French Tritium Release Experiment on October 15, 1986 are presented in the final report.

Perspectives for the Period October 1987 - March 1988

- Contamination of other kinds of plants (e.g. grass, beans, maize) with HTO and separation into the main components.
- Filling of HT into the climatic chamber without plants to test the leakage rate and the oxidation rate by the chamber walls.
- Exposure of a large number of agriculturally used plants to HT under optimal growth conditions.

Staff

S. Diabaté

D. Honig

H. Schüttelkopf

Publication:

H. Djerassi et al., "Environmental Tritium Behaviour - French Experiment", Final report - First Part, NET Contract N. 85-07 GSA (in preparation)

S + E 5.4 Overall Plant Accident Scenarios for NET

Besides the component related safety studies performed under the topic S + E 4 this work concentrates on the interactions of the different components and systems and the integral behaviour of the whole plant.

A first set of accident sequences for NET was set up based on engineering judgement and expressed in terms of tables. In discussions with component designers it turned out, that the way of presenting the sequences was not adequate. Therefore another representation was selected which is similar to event trees. First responses of the designers on this other representation so far are positive.

As an outcome of the investigation of the overall plant accident scenarios, component related safety studies were defined to be done at KfK. The points of interest are accident sequences with the TF coils. The most serious consequences of a coil accident is to be expected if the coil or parts of the coil move. Therefore in one scenario it is assumed that a coil leg is completely separated while the coil currents are constant. Since realistic times for such a separation are not yet known a very short time is assumed. The resulting displacement of the coil is the interesting result. Different locations and current levels will be investigated.

Whereas in the first scenario a short time is assumed for the separation of the coil leg in the second scenario thermodynamic investigations are initiated to get a more realistic idea on the time necessary to heat up a coil cross section up to temperatures at which the coil leg can be separated at the force levels given.

Staff:

R. Meyder

S+E 5.5 Development of Safety Guidelines for the Design of NET

Design measures of NET have to ensure public and workforce safety and investment protection. To support these objectives and to integrate safety considerations into the design at an early, cost saving stage a special working group with members from different associations is developing Design Safety Guidelines for NET. KfK is participating in this Design Safety Guidelines Working Group (DSGWG).

The task is divided into two main parts: General Design Safety Guidelines and Specific Design Safety Guidelines with more than 10 special topics. This structure is illustrated in Fig. 53.

The actual drafts of the General Design Safety Guidelines and of the topic External Hazards and Fire Safety within the Specific Guidelines are ready for discussion with the designers.

Staff:
W. Kramer
R. Krieg
R. Meyder

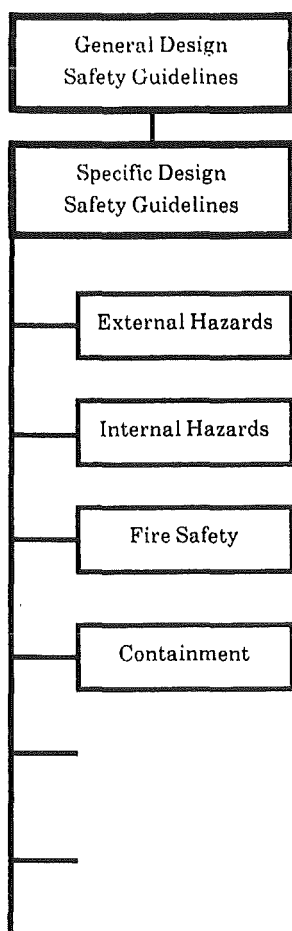


Fig. 53: Structure of the Design Safety Guidelines for NET

The general guidelines provide in particular general safety issues and radiological design objectives for normal operation and accident conditions. The specific guidelines will provide more detailed safety advice and recommendations to protect against different hazards.

During the time under review KfK has made essential contributions to the drafts of the General Design Safety Guidelines and to the topic of External Hazards. Additional work is under way to the topics Internal Hazards and Containment.

T6 Industrial Development of Large Components for Plasma Exhaust Pumping

On behalf of the Commission of the European Communities (CEC) a working group of CEA and KfK elaborates the specifications and conducts the development of large vacuum components for NET. Two alternative solutions for plasma exhaust gas pumping are pursued in parallel: mechanical pumps and cryopumps. The large components required (high vacuum pumps, roughing pumps, and valves) are not commercially available at present. It is planned to develop them within T6.

The results of the theoretical and experimental investigations conducted by the A.Pfeiffer company with a view to building a turbomolecular pump (TMP) for the NET plasma exhaust gas system have shown that such a pump can actually be built.

Based on a model of computation and tests performed on a 1:10 model scale it has been proved that the requirements made on the evacuation capacity of a pump can be fulfilled with a suction capacity of 50.000 l/s. The design data for the pump as well as the data of the individual rotor and stator stages have been entered in Tables 10 and 11.

The model of computation for one pump stage has been developed and compared with the data of previously built pumps. This results in a range of validity of the model of computation with the limits termed "expected" and "worst case". The corresponding values are contained in Table 11.

The mechanical design of the TMP including the magnetic bearing have been completed. The thermal load of the pump due to magnetic field induction, driving motor and magnetic bearings has been investigated. The coolability of the pump has been demonstrated.

The additional work needed for the development of TMPs has been specified and the proposals for implementation have been elaborated.

The order for a feasibility study of all-metal gate valves has been placed with an industrial firm. Work started by a search of valve types commercially available.

Bids have been invited for the feasibility study on the roughing pump. The deadline for bidding is late October 1987.

Work has been continued on the planning of a testing facility for prototypes of the large components.

Staff:

- H. Haas
- H. Lukitsch
- U. Kirchhof
- A. Mack
- D. Perinić

disk name	number of disks		disk-diameter	blade length	blade thickness		blade angle		volume flow rate S_0		compression ratio K_{max}		blade number	disk thickness
	rotor	stator			outer	inner	outer	inner	H ₂	He	H ₂	He		
Dim.			mm	mm	mm	mm	Deg.	Deg.	m ³ /s	m ³ /s				mm
HV2	1	-	1500	300	6	18	45	45	61,7	59,9	1,39	1,57	36	80
HV1	1	2	1500	250	7,5	17,5	27,6	44,1	52,7	51,0	1,47	1,70	36	60
MV2	2	2	1500	250	5	15	18,6	32,8	42,0	48,3	1,56	1,83	36	40
MV1	1	1	1500	185	3,75	11,25	16,1	25,1	30,0	36,2	1,63	1,95	36	35
VV	12	12	1500	120	2,5	7,5	11,6	16,2	16,0	19,0	1,65	1,98	36	25

Table 10: Vacuum data of the single disks of TMP 50.000

	Requirements	Expected case	Worst case
Volume flow rate for He in the free molecular range	50.000 l/s	57.000 l/s	
Compression ratio for H ₂ in the free molecular range	$> 5 \times 10^6$	$1,1 \times 10^7$	
Compression ratio for N ₂ in the free molecular range		$> 10^9$	
Volume flow rate for H ₂ in the free molecular range		56.000 l/s	
Compression ratio for He in the free molecular range		$> 10^9$	
He throughput at PHV = 4×10^{-3} mbar and outlet pressure of	165 mbar l/s 4×10^{-1} mbar	180 mbar l/s $4,4 \times 10^{-1}$ mbar	115 mbar l/s 3×10^{-1} mbar
He throughput at P _{HV} = 7×10^{-3} mbar and outlet pressure of	2 mbar l/s or 10 mbar l/s (new) 7×10^{-1} mbar	40 mbar l/s $1,5 \times 10^{-1}$ mbar	
Ultimate pressure at ultimate backing-pump-pressure of $\leq 10^{-4}$ mbar	$< 5 \times 10^{-10}$ mbar	$\leq 5 \times 10^{-10}$ mbar at residual degassing rate of $qr \leq 3 \times 10^{-8}$ mbar l/s m ²	

Table 11: Vacuum data of the TMP 50.000 for He and H₂

T 10 A Plasma Exhaust Purification by Means of Cryosorption on Molecular-Sieves or Alternative Adsorbents

For the installation of a cryostat (see Fig. 54) a glove box in the control area is being decontaminated, the existing equipment dismantled and the peripherals adapted to the requirements of low temperature

out in a flow system. The principal components of the flow apparatus are a moisture supplying device (5 - 5000 ppm), a reactor and a water monitor. The measurement principle of the monitor is based on the equilibrium between water in the gas phase and water electrolytically decomposed on a platinum sensor.

Staff:

U. Tank

H.E. Noppel

R.D. Penzhorn

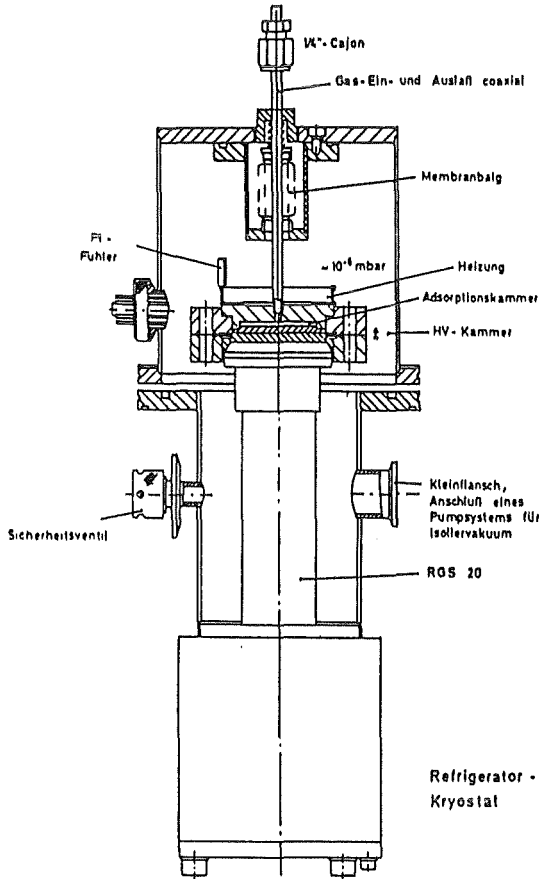


Fig. 54: Scheme of the cryostat

experiments. Calibration tests are in progress for the quantitative determination of hydrogen isotopes by a gas chromatographic technique. The separation is carried out on an alumina/ferric hydroxide column operated at $1N_2$ temperature.

Mainly with the objective of establishing the experimental technique, break-through curves for the retention of water on zeolite 5A have been obtained as a function of temperature and the partial pressure of water in the sweep gas. The experiments are carried

T 10 C Plasma Exhaust Gas Purification by Use of Hot-Metal Getters

The objective of this task is the investigation of hot-metal getters as a process option for the purification of the plasma exhaust gas of a fusion reactor. Metal getters are capable of liberating chemically bound tritium and removing C-O-N in a single process.

The main program steps are:

- A) Inactive tests with a He/H₂ carrier gas on various getter metals and alloys (e.g. Zr-Al, Zr-Fe-V) to study their absorption and desorption behavior with respect to gaseous impurities, i.e. N₂, CO, CO₂, CH₄, and H₂O;
- B) Active tests with tritium to demonstrate the purification efficiency under realistic operational conditions.

Current Progress

The assembly of the first stage of the PEGASUS facility (Plasma Exhaust Gas Purification System, former name TRIGA) which is under construction since February 1987 has been almost completed. In addition, several function tests have been carried out, the results of which are reported in the following along with a brief description of the main components of the facility.

Supply of test gases:

Eight gas-bottles containing the carrier gases (He, H₂), the impurity gases (CO, CO₂, CH₄, ...) and the gases for the operation of the gas chromatograph (GC) have been installed in a double-walled steel cabinet. Test gas mixtures can be prepared volumetrically by pVT-procedures in either a 10 ltr. or a 100 ltr. storage vessel into which known amounts of the gas components are introduced employing a dosing valve.

Test loop and manifold:

Prior to the test gas preparation, the storage vessel and the test loop are evacuated until the partial pressures of the residual gases are less than 10⁻⁵ mb. To determine the retention capability of the gas purifiers down to residual gas concentrations in the ppm-region the integral leakage of the facility must be maintained below 10⁻⁷ mbarltr/sec. Both

requirements have been accomplished (a) by using exclusively metallic gaskets (CF- and Cajon-fittings) for the flange connections and (b) by baking the walls of the tubes and the gas storage vessels at temperatures between 250 and 300°C, c.f. Fig. 55.

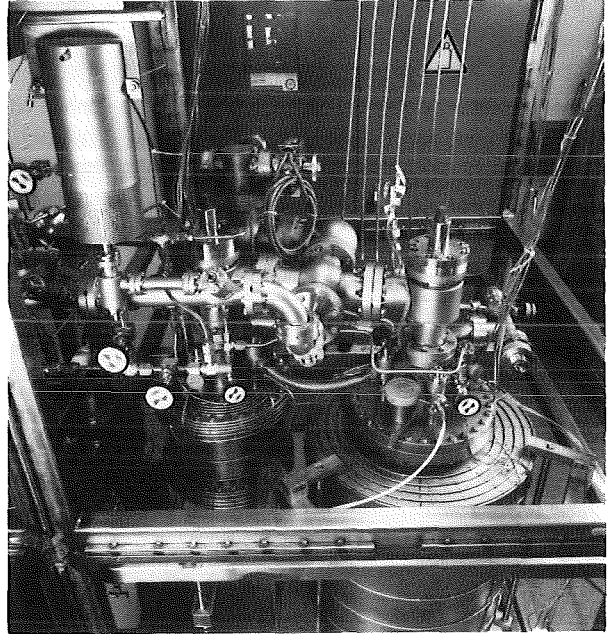


Fig. 55: Partial view of the PEGASUS facility; top left: SAES gas purifier, foreground: gas storage vessels with resistance heating wires

Instrumentation of the loop:

Two circulation pumps and automatic control systems for gas flow and pressure allow independent adjustment of these two parameters. Gas samples for the GC are taken in a bypass of the gas loop. Here, some additional devices are needed to establish reproducible conditions for pressure and gas flow at the GC entrance.

Gas purifiers:

The first test series will be carried out to investigate the commercial purifiers of SAES/Milano. Three of these purifiers have been installed in the facility. Each is filled with 700 g of getter material of the type ST-101 (Zr-Al), ST-707 (Zr-V-Fe), and ST-198 (Zr-Fe). The operation temperature will be in the range of 300 - 700°C.

Chemical analysis:

Quantitative analysis of the impurities in the carrier gas is achieved by use of a GC with a highly sensitive Helium-Ionisation-Detector (HID). After some scoping tests with various GC columns (Porapak QS/3m, molecular sieve 5A/4m and 2m, Porapak R/6m), first calibration measurements have been carried out. It was found that the range of detectable concentrations can be extended from 1 ppm up to about 5%, if the detector voltage is reduced for concentrations about 100 ppm. It will be possible, therefore, to use only one analytic method for measuring the impurity concentrations at the inlet and the outlet of the gas purifiers.

Plans for the Near Future

- Continue and complete GC tests for optimizing the gas analysis;
- complete installations for the non-radioactive tests, e.g. devices for water cooling and pressure control;
- start measurements on the H₂ absorption/desorption behavior of the SAES getters and on the gettering properties with respect to impurities;
- continue design, construction, and acquisition of additional equipment for tritium tracer experiments.

Staff:

H. Albrecht

T. Kastner

T 10 E Adsorption of DT on Heated Metal Beds other than Uranium

Metal hydrides acting as a reversible getter have been proposed for interim storage and transport of tritium. The most extensively investigated and most widely used getter is uranium. This nuclear material is however subject to restrictions and, in addition, its high chemical reactivity makes precautionary safety measures mandatory. Therefore, alternative getter metals and alloys which are chemically resistant to the impact of air and water are presently under investigation.

ZrCo alloy may be cited among the metals proposed for use as a reversible tritium getter. Hydrogenation and dehydrogenation pressure/composition isotherms were determined for the hydrogen ZrCo system in the temperature range 200 - 300°C employing a volumetric procedure. The results obtained were found to be in essential agreement with the data of Nagasaki et al. (Fusion Technology 9, 506 (1986)). The equilibrium pressure of hydrogen over $ZrCoH_{0.8}$ can be described by the eqn.

$$\log p_{H_2}/Pa = \frac{4751 \pm 183}{T} + (12.74 \pm 0.35)$$

which yields a hydrogen dissociation pressure of 6×10^{-4} Pa (6×10^{-6} mbar) at room temperature. As the temperature is reduced the composition of the ZrCo-H₂ system approaches the stoichiometry of the compound ZrCoH₃. This ternary compound does not ignite in air.

Methane is slowly cracked on ZrCo alloy at 304°C with liberation of molecular hydrogen. The effect of the decomposition of 2.12×10^{-3} mol of methane over 3.65×10^{-2} mol of getter on the pressure composition isotherms is illustrated in Fig. 56. As apparent from the results, after reaction with methane a raise in dissociation pressure of ZrCoH_x is observed, which may be caused by the formation of carbide. The rate of hydrogen absorption was not significantly influenced by the presence of carbon on the ZrCo alloy. Carbon deposited on ZrCo will not react with molecular hydrogen at 304°C. Auger and XPS analysis of the carbonized getter shows only ZrO₂ on the surface of the alloy.

Staff:

R.D. Penzhorn

M. Sirch

E. Willin

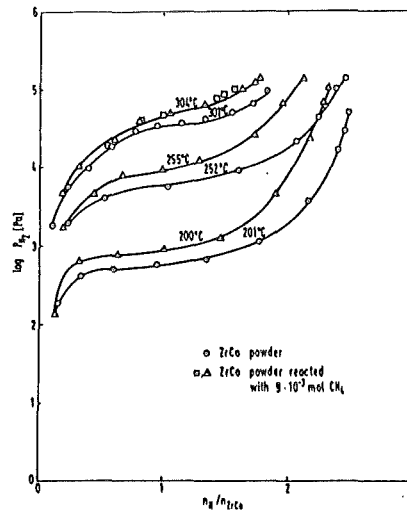


Fig. 56: Pressure composition isotherms of ZrCoH_x before (o) and after (Δ) cracking of methane at the getter surface

T 10 H Catalyst Development Exhaust Purification Process

Impurities such as helium, tritiated hydrocarbons, tritiated water, carbon monoxide, carbon dioxide and tritiated ammonia must be removed from the plasma exhaust of a fusion reactor to avoid (i) plasma cooling by radiation losses, (ii) freeze-out of condensable gases in the cryogenic isotope separation system and (iii) poisoning of the deuterium/tritium storage beds. In addition, D,T associated to impurities should be recovered for reuse in the fuel cycle and the effluent gas decontaminated to a high degree prior to its discharge into the tritiated-waste treatment system. To accomplish this task a three step process concept based on experimental laboratory results is proposed. Tritium recovery is carried out catalytically to minimize solid waste.

The main purification step consists of an array of Pd/Ag alloy membrane diffusers, which operated with a relatively small tritium inventory and delivers a high purity D,T fraction (99.9 mol % hydrogen) as well as an impurity stream. Tritiated ammonia, if present, will decompose quantitatively into the elements on the Pd/Ag metal surface; the produced hydrogen permeates together with the main fuel stream. In the bleed stream of the diffuser very low D,T partial pressures can be attained.

The permeation rate of hydrogen through a Pd/Ag alloy diffuser was studied in a closed-loop apparatus employing gas chromatographic and mass spectrometric analysis. The rate was found to be essentially independent of the type of hydrogen carrier gas employed, i.e. helium, nitrogen or methane. In a series of runs the influence of carbon monoxide on the rate of permeation of hydrogen (initial partial pressure 300 mbar) diluted in helium (total pressure 1 bar) through a commercial Pd/Ag alloy diffuser was studied, having a surface area of 289 m² and operated at 450°C. Within the experimental uncertainty, the permeation coefficient of hydrogen diluted in helium is not influenced by carbon monoxide partial pressures of up to 200 mbar (see Table 12). These observations are in line with a previous study carried out at CEA with much lower CO contaminant concentration.

In a second step the Pd/Ag alloy permeator effluent gas is passed over a CuO/Cr₂O₃/ZnO catalytic reduction bed kept at 150 - 200°C. On this bed tritiated water reacts with carbon monoxide to yield tritiated hydrogen and carbon dioxide. In the presence of an excess CO the reaction is quantitative. As expected

from thermodynamics, the addition of methane to a helium carrier gas containing the reactants CO and H₂O was found to have no effect of on the chemical equilibrium. The reaction rate is not influenced by methane.

P _{H₂} mbar	P _{He} mbar	P _{CO} mbar	R mol*cm/cm ² *min kPa ^{1/2}	No.of runs
200	800	---	(3.17 ± 0.27)	3
200	780	20	(3.20 ± 0.10)	2
200	700	100	(2.71 ± 0.05)	2
200	600	200	(3.27 ± 0.31)	5

Table 12: Influence of CO on the rate of hydrogen permeating through a commercial Pd/Ag permeator

The third and final step of the proposed catalytic purification system consists of a second Pd/Ag alloy diffuser in close contact with a Ni catalyst. Tritiated methane is cracked on this catalyst into carbon and tritiated hydrogen; the latter permeating through the Pd/Ag diffuser into the clean D,T stream from the main diffuser. The cracking reaction has been investigated using helium/methane mixtures at about 1 bar total pressure and methane partial pressures in the range 100 - 420 mbar. The reversibility of the reaction was demonstrated by passing hydrogen over the catalyst with a carbon deposit from the cracking of methane. In 18 cracking/regeneration cycles a total of 2.1 mol methane were cracked on 10 g catalyst. Preliminary results indicate that within the employed pressure range the cracking reaction is first order in methane. 0.25 mol of methane can be cracked quantitatively on 10 g catalyst with a half-life of 4 min. Beyond that amount of cracked methane an increase in half-life is observed. Up to a temperature of 520°C the apparent activation energy of the reaction is estimated to be 13 kJ/mol. Above that temperature the reaction proceeds with a negative activation energy.

Staff:

M. Glugla
K. Günther
R.-D. Penzhorn
R. Rodriguez

Development of ECRH Power Sources at 150 GHz*)

The KfK gyrotron has been producing microwaves since October 1986. During this first year the gyrotron was operated using the slightly tapered 19 mm resonator. This setup yielded a typical power output of 100 to 120 kW at various modes in the 150 GHz frequency range. Several improvements have been introduced during this period.

A steering system has been added to adjust the position of the beam during operation. The steering magnets placed at the entrance of the compression region are able to displace the beam within the resonator by up to about 0.7 mm. Without steering the electron-beam was off axis by about 0.5 mm, which was concluded from the asymmetry of the beam observed by X-ray photography on the collector surface.

The output waveguide of the KfK gyrotron is highly oversized, e.g. a diameter of 70 mm is used to reduce the thermal stress on the waveguide window during long-pulse operation. A low average power octanol calorimeter simply fits the oversized waveguide. With its small volume a quick response is obtained. By some improvements on the thermal insulation of the calorimeter and on the calibration procedure an accuracy of $\pm 5\%$ for the power measurements as been obtained.

The high-voltage system was improved to allow a more stable operation with a pulse length up to 5 ms.

After these modifications of the experimental set-up, the rf output power and the frequency of the gyrotron have been measured in several runs as a function of the magnetic field strength with constant beam current.

From the frequency measurement it is obvious that the TE23, TE03 and TE52 modes are excited. The power curve shows a broad maximum around the magnetic field of 5.8 T, which corresponds to the TE03 mode. Theoretically for each mode there should be a separate maximum in the power curve. This discrepancy has to be studied in more detail.

The maximum of rf output power of 120 kW at 149.5 GHz and $B=5.8$ T with a pulse length of 1 ms has been observed at $B=5.8$ T. This magnetic field is too small for the TE031 mode to be excited, even though thermal paper measurements show a TE03 pattern. Frequency

measurements allow to conclude that the TE03 mode oscillates at 149.0 GHz, 149.5 GHz and 150.0 GHz, corresponding to the TE031, TE032 and TE033 mode, respectively. The power maximum was reached in the TE032 mode.

Axial mode competition inhibits the high-power and high-efficiency oscillation theoretically expected with the TE031 mode for this parameter set. Nevertheless an essential reduction of the power density at the wall could be obtained in higher axial mode operation.

After these test runs the modular gyrotron was disassembled for exchange of the gun and resonator sections.

Staff:

W. Baumgärtner
E. Borie
H. Budig
G. Dammertz
U. Feißt
P. Grundel
G. Haubrich
R. Hietschold
G. Hochschild
A. Hornung
B. Jödicke
M. Kuntze
R. Lehm
A. Möbius
N. Münch
H. Oppermann
B. Piosczyk
G. Redemann
H. Stickel
R. Vincon
H. Wenzelburger

*) Contribution within the Plasma Physics Program of the European Community

NET Study Contracts

Availability of the LCT Plant

The availability of the LCT plant in the final phase of the test program was mainly determined by a bearing seal problem of one of the screw compressors on subatmospheric side of the helium circuit. This led to air contamination of the helium in the system. The time needed for trouble shooting, repairment purification and recooldown of the system was about 2 month.

During the extended pulse field tests of the Japanese coil a considerable leak, probably nitrogen, opened with a inleakage of 0,4 kg/h. It was successfully demonstrated that the effect of cryojumping was sufficient to keep the vessel vacuum pressure in the 10^{-5} mbar range while was needed to get sufficient thermal insulation. The remaining part of the extended tests were successfully settled under this boundary condition as already described in task M 1.

Staff:

A. Ulbricht

Study on the NET Pancake Test

The NET Pancake study was continued with a comparison of, the cluster configuration C3 and solenoid configuration S1. A preliminary estimation of the required conductor length, manufacturing costs of the model coils and modification costs of the facility was performed.

In order to reduce the required amount of conductor for the model coils and the modification costs for the facility the minimum bending radius was reduced from 1.2 m to 1 m.

The solenoid and cluster configuration were redesigned taking in the account the reduced bending radius and the new target test values. Due to this modification and an enlargement of the LN₂-shield, an installation of the cluster configuration into the existing vacuum vessel in possible without a removal of the vessel and LN₂-shield wall as shown in Fig. 57.

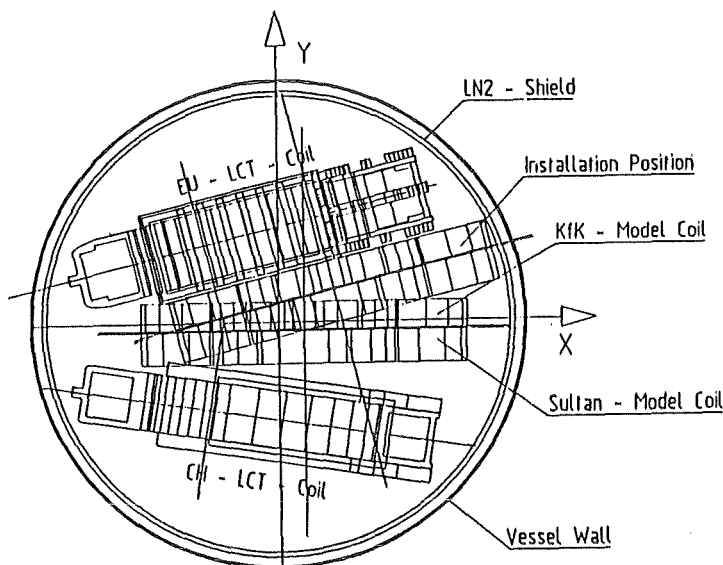


Fig. 57: Top view of the cluster configuration C6

For both configurations the magnetic field, forces, stresses were calculated and compared with the target values. The flow schemes for the cooling circuits of the coils and current leads were also redesigned and the cooling power were estimated.

A model coil test programme and a time schedule were worked out and the costs and man power requirements were estimated for the new configurations C6 and S3.

A final study report was worked out in collaboration with the laboratories of ECS, SIN and the NET-team and will be published soon.

Staff:

G. Zahn

Investigation of the Vacuum and Exhaust Performance of NET

The present work focusses on the study of the conditions which determine dwell-time pumping. The objective is the quantitative simulation of the vacuum performance during dwell-time. For this purpose, the VAKMAP1 code, which was developed under a previous NET-study contract, will be extended. The modifications in the design of the plasma chamber internals, especially the introduction of graphite first wall protection tiles, and a new vacuum duct configuration will be taken into account.

However, at temperatures of interest for fusion plants, the hydrogen-solids interaction processes are much more complex with graphite than in case of metals, e.g. stainless steel. At temperatures up to 1000 K the surface diffusion of hydrogen along internal pore surfaces plays the leading role. The hydrogen retention of these surfaces may rise to monolayer coverage. At higher temperatures transgranular diffusion of hydrogen in the graphite lattice increases in importance. Considerable amounts of hydrogen get deposited also in trap sites. Because of the very high trapping energies involved (~ 4 eV) it is almost impossible to remove the trapped hydrogen again, unless the graphite is brought to very high temperatures. The operation of JET has shown in addition that when the plasma contacts the inner graphite bumper limiter large amounts of hydrogen are adsorbed /1/. According to laboratory experiments made by W.L. Hsu and R.A. Causey it seems that this mechanism is practically unsaturable /2/.

The whole data base describing the numerical values of these hydrogen-graphite interaction processes for the various kinds of graphite envisaged for use within the plasma chamber is still very small at present.

In view of the extremely complex situation arising if graphite is used, a stepwise procedure is applied in the development of the new version of the VAKMAP code towards dwell-time pumping. For first test purposes, graphite is excluded as material; instead, metallic surfaces are assumed to exist throughout the vacuum chamber. Furthermore, analytical approximation formulae developed in the course of the INTOR-project and relying on tabulated values of the error function complement and the error function integrated, respectively, are used to calculate the space-time dependent distribution of hydrogen concentration and temperature within the wall material and the corresponding re-emission flux into the plasma chamber. In conformity with the growing data base for graphite these analytical approximation formulae will be replaced later-on by appropriate subroutines for graphite.

For the main part-processes the sub-programmes based on the analytical approximation formulae were programmed and tested. The vacuum relevant properties of the vacuum chamber were defined in the course of the NET-DN design review.

The literature survey on the hydrogen-solid interaction phenomenon was continued and the results stored in data banks on a personal computer. The numerical results of some empirical formulae describing the hydrogen retention and outgassing behaviour of graphite were studied.

Staff:

R.A. Müller
F. Engelhardt

References:

. Huguët, J.A. Booth, G. Cetentano, E. Deksnis, K.J. Dietz, P.H. Rebut, R. Shaw, K. Sonnenberg: "Limiters and First Wall on JET"; 11th Symposium on Fusion Engineering, Austin, Texas, USA 18 to 22 Nov. 1985.

W.L. Hsu and R.A. Causey: "Pumping of Hydrogen During Plasma-Graphite Interaction"; Proc.33rd. Nat. Symp. Am. Vac. Soc., Baltimore, Maryland, USA, October 1986.

Development of Helium Cryopumping Materials and Preliminary Design Concept of Cryocompound Pumps for NET

Experimental investigations are under way at KfK with the aim to develop and optimize porous active cryosorption surfaces for helium pumping from the plasma exhaust gas. In these investigations a multitude of combinations of materials are tested for the sorbent, bond and cold wall and the bonding techniques are investigated with a view to select the best suited candidates.

Experimental investigations have been reported on the thermal cycling of the sorbent/substrate bonding on 50 mm diameter specimens. Each specimen has been loaded up to 100 times alternately at 78 K and 300°C at the maximum. The specimens which withstood thermal cycling tests are subjected to sorption capacity screening tests to compare them with the cryosorption capacity of helium gas at 4,2 K.

The HELENE test facility for sorption capacity tests was assembled and tested. The layout of HELENE test facility is shown in Fig.58

After its installation in the specimen holder (18) the specimen to be examined (19) is placed into the analyzing tube (20) together with the radiation shield (17) and the electric connections.

As a preparation to the sorption measurements the analyzing tube (20) is heated in a furnace to 300°C at the maximum and then evacuated in a turbomolecular pump bench. Then the corner valve (40) is closed and the rig is transferred from the furnace into the cryostat (1) where the specimen is cooled down to $\sim 4,2$ K using LHe. After this temperature has been attained the analyzing tube is flooded to 1 bar pressure using GHe. The specimen is saturated with helium during this

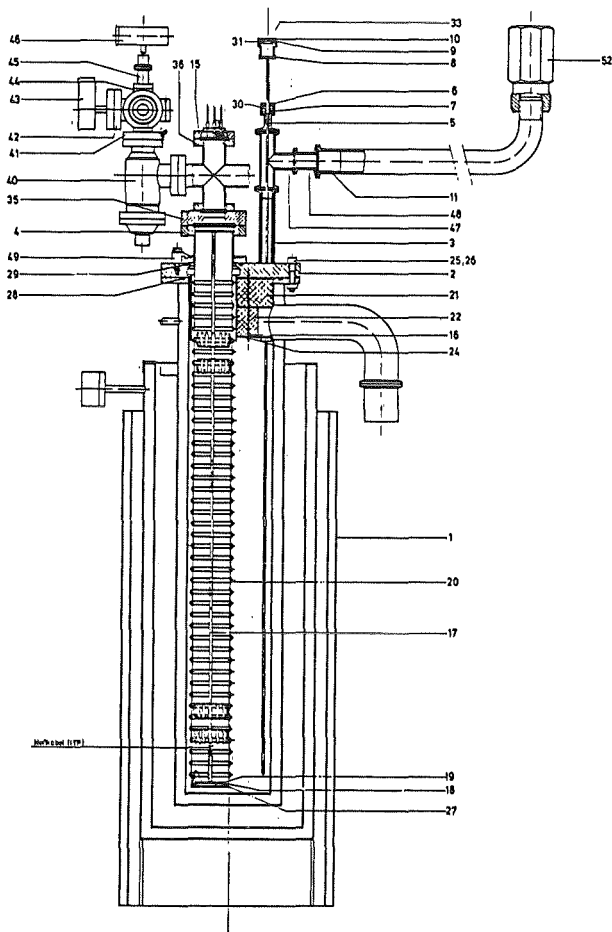


Fig. 58: HELENE test facility

process. In order to improve the accuracy of measurement the pressure in the analyzing tube is lowered by a roughing pump to a level between 10^{-2} and 10^{-3} mbar. The saturation pressure which is established in this way is considered as the reference pressure at 4.2 K.

After the hermetically sealed analyzing tube has been heated to room temperature pressure measurements are again performed. The difference of the two measured values is used to determine the pumping capacity of the specimens with respect to GHe at 4.2 K.

Trial operation of the HELENE facility started in September 1987.

The subsequent cryopumping tests on a technical scale (sorption panels with 400 mm diameter) will be carried out at the TITAN facility, which was ordered in 1986.

The design computations have been completed for the TITAN test facility. The drawings have been completed. On account of the possibility of an oxyhydrogen gas explosion after inflow of air the recipient is designed for a maximum admissible overpressure during operation of 10 bar and secured by a bursting protection. The recipient is presently being manufactured at KfK.

Staff:

H. Haas
J. Hanauer
W. Höhn
B. Kammerer
U. Kirchhof
H. Lukitsch
A. Mack
D. Perinić
D. Zimmerlin

Engineering Problems of NET Blanket Testing and Blanket Insertion Strategy

This task was done in the frame of a first pre NET contract. The investigations were focused on the question, what are the requisites necessary on the NET plant and which solutions seem to be attractive to supply the plant with different types of shield and blanket segments during the plant life. A high degree of flexibility is desired to shift the decisions of coolant choice, of the design details of the blanket segments, and of the cooling and supplying circuits to the end of a test phase.

Following the proposals of the NET-team /1/, in a first operation phase the NET reactor will be equipped mainly with shielding segments. The performance of these elements seems to be predictable, and therefore the optimum of reliability will be reached. Due to the increasing experience during the early operation phases one can expect hints at necessary or desirable design improvements for these elements. Also the tritium breeding, the economy, the reliability and the handling will get some increasing weight in the later operating phase. Therefore advanced blanket types must be developed and tested in the future. For this no testing facility will be available except the NET reactor itself, which operates at relevant load conditions with respect to a tokamak fusion reactor. As a result, the NET reactor itself has to serve as a test bed for the advanced breeding blankets of the NET plant and of e.g. a later DEMO fusion reactor.

Already in the first operation phase of NET the simultaneous use of shield segments and of some test segments is envisaged. Up to now, the insertion of both, a water cooled and a helium cooled test segment is expected. Also a self-cooled LiPb segment should be useable in place of an other test segment.

Our study is based on the following types of blanket and shield elements: a watercooled shield segment, which is under development by KfK IMF, a watercooled LiPb blanket segment, designed by IRC-Ispra and the NET-Team, a helium cooled blanket, designed by KfK INR and IMF, and a selfcooled liquid metal blanket, on which KfK IRB is working on. The design of all these segments is still in an early phase of development. Therefore many design problems are still unsolved. For these open questions we made assumptions, which must be reviewed later again. This type of assumptions are e.g. emergency cooling systems, usable also for the

transport cooling, the allowance of an emergency coolant flow in the inboard and outboard elements in parallel, the possibility to use pipes for helium as a coolant, which were previously filled with water, and so on.

In the near past it was proposed to use the water cooled shield blankets in later operation stages as a breeding blanket. This will be performed by adding some water soluble Li-salts to the coolant. It is expected, that the resulting breeding process satisfies the supply of NET with tritium. The necessity of the use of the NET reactor as a test bed for advanced blanket types basically will not be changed due to this option.

This aim of the use of the NET reactor as a test bed is accepted by the NET Team. Only two torus sectors must be prepared for such test positions. But this preparation surely cannot be valid for any kind of coolants or blankets because of space and geometrical restrictions on one hand, and the necessity of availability of some infrastructure (different coolants, tritium extraction, handling devices and so on) on the other hand. That means, that a boundary must be prepared, which is compatible with those of the blanket types, which should be tested in NET. For both test position it is to be decided, which coolants have to be available there. Also the handling devices are to be prepared with respect to the types of blankets and their coolants. This all has to result in a type of strategy, which ensures the use of NET as a test bed for advanced blankets.

The development of this strategy implies a high degree of prospection of technological potentials in a field of physical, chemical and technological basics and of operational demands, which are up to now still very diffuse and need future development. This is clearly the main difficulty of our task. Due to the partial lack of knowledge on partially undefined boundary conditions, one runs the risk of designing technical solutions, which cannot survive in the future. The design goal is still a moving target and changing nearly monthly, resulting in a fulness of problems, demands and design variants. In this sense the way forward will be a way of trial and error, we fix some assumptions and search for the consequences.

Our design is characterized by a set of ring pipe coolant headers, which surrounds the reactor torus at the level of the "blanket access ports". Each access port is connected with one intermediate coolant header cell. In each of these 16 cells some intermediate coolant headers are located, which are branch lines of the coolant ring pipes. The intermediate headers are branching to different coolant pipes, supplying the attached blanket and shield segments. Also valves and connections for measuring devices are located in these cells. The intermediate header cells and the cells for the ring pipes are separated from each other. Therefore the location of an arising leak will be located easily.

The external components of the cooling circuits and the coolant supply and make-up systems are located in separated

compartments of the reactor building. These systems supply the ring pipes by main interconnecting pipes.

The coolant supply system for the test segments differ from those of the shield segments. The test segments are supplied directly by pipes, which lead to the related external circuit components located in separate compartments of the reactor building. Special containers enclose these compartments to prevent tritium contamination of other cells and to simplify the exchange of the complete systems if desired. In both test sectors one or several test segments may be installed, depending on the test goals. Also inboard elements and the divertors, which are integrated in these elements, may be tested. Self cooled LiPb segments are also applicable in the test sectors. In this case they replace the other water or helium cooled test segments of this test sector. The related interface units are then placed above the reactor torus.

The plant is prepared to replace all shield segments by breeder segments in a later phase. In this case the breeder segments are supplied through the ring pipes. The pipes initially used for the test segments remain unused or can be dismantled.

In our design proposal the details and dimensions of the external components of the cooling and supplying systems are not fixed, because we want to avoid premature limitations in the future design of the blanket segments. It seems that the recently proposed reactor building layout includes compartments, which are big enough for this purpose. In contrast the space for the ring pipes is really tight up to now. In a future plant layout this should be improved.

In comparison to standard shielding and blanket elements the use of test elements requires certain additional equipment. Up to now we did not fix the extend of such equipment, because this can be done only on the basis of an exact specification of the components to be tested.

The results of our study are of preliminary character and may help in the definition of the related work to be done in an advanced NET design study.

Staff:

G. Class

K. Schramm

References:

M. Chazalon and B. Libin: Strategy of breeding blanket introduction in NET and testing requirements. 14th SOFT Meeting, Avignon, France, 1986.

Evaluation of Crack Growth Delay in Multilayer Sheets

For the first wall (FW) design multilayer structures are proposed which are composed of materials of different mechanical properties and in particular different crack growth behaviour. Two types of multilayer structures are of particular interest:

- (a) Brazed connections between FW plates and cooling tubes made of steel or between double tubes in order to provide a second containment of the coolant.
- (b) Multilayer construction for pressurized wall components with a soft layer between the structural material. It can be conjectured that a crack tip will blunt as soon as the soft layer is reached. As a consequence the crack may be delayed or changed in its direction or stopped totally.

Plates consisting of two layers made of SS 316 L and different types of brazing have been fabricated. First tests with straight through cracks in pulsating bending tests have been performed to evaluate the fatigue behaviour of multilayer structures as described in (a).

Staff:

E. Diegele

T. Fett

Design Study of Plasma Facing Components

The results of the Design Study of Plasma Facing Components are included in the report on N1.

CAD Data Exchange Between NET and KfK

As the work on NET becomes more detailed the exchange of the machine design data (i.e. two-dimensional drawings) between NET and KfK will become increasingly important. Such cooperative work would be much more efficient if the drawing data could be exchanged directly between the two design systems involved. NET and KfK will internally use computer aided design systems to produce these drawings for work performed by KfK under NET contracts of association.

Although a standard (Initial Graphics Exchange Specification, IGES) exists for such exchange, and both the CV-MEDUSA (used by NET) and the Applicon BRAVO! (used by KfK) systems have IGES processors, the use of these processors is not free of bugs. This is particularly true for complex drawings such as those which will be required for NET. The objective of the contract is to determine the limitations of IGES as regards MEDUSA - BRAVO! drawing exchange and to produce a reliable method for regularly exchanging CAD-data, either by the production of a pre-IGES processor for the systems or later by modifying the processors provided by the CAD supplier.

In this step the data transfer via IGES from the CAD system CV MEDUSA to the CAD system Applicon BRAVO! has been checked. Therefore a MEDUSA testmatrix has been created containing all relevant elements. The MEDUSA IGES preprocessor has been analyzed sufficiently except for the use of the IGES entities 216 (linear dimension) and 218 (ordinate dimension) which require additional checking. The BRAVO! IGES postprocessor has been analyzed in so far as the processing of the IGES entities comprised in the testmatrix has been checked. These entities are the most important entities for data transfer between NET and KfK.

In the next step the way back, data transfer via IGES from Applicon BRAVO! to CV MEDUSA, has to be analyzed. Therefore a BRAVO! testmatrix, similar to the MEDUSA testmatrix has to be created considering the internal data structure of the BRAVO! system, which is very different from the internal data structure of the MEDUSA system. The BRAVO! IGES preprocessor and the MEDUSA IGES postprocessor will be analyzed and first considerations will start to debug and enhance the analyzed IGES processors.

Staff:

U. Gengenbach

S. Haas

Appendix I: Table of Fusion Technology Contracts

Task Code No.	Title	KfK Departments
B 1	Blanket Design Studies	IMF III, INR, IRB, IT
B 2	Development of Computational Tools for Neutronics	INR
B 6	Corrosion of Structural Materials in Flowing Pb-17Li	IMF I, IMF II
B 6.3	Fatigue of Structural Steel in Pb-17Li	IMF I, IMF II
B 9	Tritium Extraction from Liquid Pb-17Li by the Use of Solid Getters	IT
B 11-16	Development of Ceramic Breeder Materials	IMF I, IMF III, INR, IRCH
B 15.3	End of Life of Solid Breeding Materials in Fast Neutron Flux	IMF I, IMF III, INR
M 1	The Large Coil Task (LCT)	ITP
M 3	Development of High Field Composite Conductors	ITP
M 4	Superconducting Poloidal Field Coil Development	ITP
M 8	Design and Construction of a Poloidal Field Coil for TORE SUPRA as NET-Prototype Coil	ITP
M 9	Structural Materials Fatigue Characterization at 4 K	ITP
M 12	Low Electrical Conductivity Structures Development	IMF IV, ITP
MAT 1.6	Development and Qualification of Type 1.4914 Base Metal Properties	IMF II
MAT 1.9	Pre- and Post-Irradiation Fatigue Properties of 1.4914 Martensitic Steel	IMF II
MAT 1.11	Post Irradiation Fracture Toughness of Type 1.4914 Martensitic Steel	IMF II
MAT 2.2	In-Pile Creep-Fatigue Testing of Type 316 and 1.4914 Steels	IMF II, IMF III
MAT 6/ MAT 13	Ceramics for First Wall Protection and for rf Windows	IMF I
MAT 9.2	Investigation of Fatigue under Dual Beam Irradiation	IMF II
MAT 18	Development of Low Activation Ferritic-Martensitic Steels	IMF II

N 1	Design Study of Plasma Facing Components	INR, IRB, IRE
N 2	Shield Design Studies	IMF III
N 3	Development of Procedures and Tools for Structural Design Evaluation	IMF IV
N 5	Development of Theory and Tools for Evaluation of Magnetic Field Effects on Liquid Breeder Blankets	IRB
N 6	Studies of Pepple Beds of Ceramics Compounds	INR
RM 1	Background Studies on Remote Maintenance	IT
RM 2	Mechanical Components Assembly	IT
RM 3	Handling Equipment for In-vessel Components	IDT, IRE, IT
S+E 4.1.2	Safety Aspects of the Cryosystem	IRE
S+E 4.1.3	Safety Aspects of Superconducting Magnets	IDT, IRE, ITP
S+E 5.2.2	Behavior of Gaseous Tritium in the System Plant/Soil	HS
S+E 5.4	Overall Plant Accident Scenarios for NET	IRE
S+E 5.5	Development of Safety Guidelines for the Design of NET	IRE
S+E 6	Licensing Activities	PKF-PL
S+E 7	Long Term Studies	AFAS, INR
T 6	Industrial Development of Large Components for Plasma Exhaust Pumping	IT
T 10 A	Plasma Exhaust Purification by Means of Cryosorption on Molecular Sieves or Alternative Adsorbents	IRCH
T 10 C	Plasma Exhaust Gas Purification by Use of Hot Metal Getters	IRCH
T 10 E	Adsorption of DT on Heated Metal Beds other than Uranium	IRCH
T 10 H	Catalyst Development Exhaust Purification Process	IRCH
Development of ECRH Power Sources at 150 GHz (This task is part of the Fusion Physics Programme of the EC.)		IDT, IK

Appendix II: Table of NET Contracts

Theme	Contract No.	Working Period
Study about the NET TF Pancake Tests	240/86-6/FU-D/NET	5/86 - 4/87
Engineering Problems of NET Blanket Testing and Blanket Insertion Strategy	243/86-6/FU-D/NET	7/86 - 7/87
Evaluation of Crack Growth Delay in Multilayer Sheets	253/86-11/FU-D/NET	11/86 - 12/87
Simulation of the Vacuum Performance of NET-DN	254/86-11/FU-D/NET	10/86 - 12/87
CAD Data Exchange Between NET and KfK	265/87-3/FU-D/NET	3/87 - 9/88

Appendix III: KfK Departments contributing to the Fusion Project

Kernforschungszentrum Karlsruhe GmbH
 Postfach 3640
 D-7500 Karlsruhe 1
 Federal Republic of Germany

Telephone (07247) 82-1
 Telex 7 826 484
 Telefax/Telecopies (0)07247/82 5070

KfK Department	KfK Institut/Abteilung	Director	Ext.
Applied Systems Analyses Department	Abteilung für Angewandte Systemanalyse (AFAS)	Dr. H. Paschen	2500
Central Safety and Security Department	Hauptabteilung Sicherheit (HS)	Prof. Dr. H. Kiefer	2660
Institute for Data Processing in Technology	Institut für Datenverarbeitung in der Technik (IDT)	Prof. Dr. H. Trauboth	5700
Institute for Nuclear Physics	Institut für Kernphysik II (IK)	Prof. Dr. A. Citron	3502
Institute for Materials and Solid State Research	Institut für Material- und Festkörperforschung (IMF)	I. Prof. Dr. W. Dienst	2887
		II. Dr. K. Anderko	2902
		III. Prof. Dr. K. Kummerer	2518
		IV. Prof. Dr. D. Munz	4815
Institute for Neutron Physics and Reactor Engineering	Institut für Neutronenphysik und Reaktortechnik (INR)	Prof. Dr. G. Keßler	2440
Institute for Reactor Components	Institut für Reaktorbau-elemente (IRB)	Prof. Dr. U. Müller	3450
Institute for Radiochemistry	Institut für Radiochemie (IRCH)	Prof. Dr. H.J. Ache	3200
Institute for Reactor Development	Institut für Reaktor-entwicklung (IRE)	Prof. Dr. D. Smidt	2550
Central Engineering Department	Hauptabteilung Ingenieur-technik (IT)	Dr. H. Rininsland	3000
Institute for Technical Physics	Institut für Technische Physik (ITP)	Prof. Dr. P. Komarek	3500

Appendix IV: Fusion Project Management Staff (PKF-PL)

Nuclear Fusion Project - Project Management Group	Project Manager	Dr. J.E. Vetter	ext. 5460
	Secretariate	I. Sickinger, I. Pleli	5461/5466
	Project Administration, Documentation	BW. G. Kast	5462
	International Affairs	Dr. F.W.A. Habermann	5520
	Studies, NET Contacts	Dr. J.E. Vetter	5460
	Blanket Development, Test Facilities	DI. H. Sebening	5464
	Superconducting Magnets, Gyrotron Development	N.N. (Dr. J.E. Vetter)	5460
	Tritium Technology, Structural Materials	Dr. H.D. Röhrig	5463
	Safety and Environmental Impact, Remote Handling	DI. A. Fiege	2668/5465